Transport Effects on the MHD ~~Magnetohydrodynamic~~ Stability of Pinches

by

Peter Michael Cox
of
Imperial College of Science, Technology and Medicine

A thesis submitted for the degree of Doctor of Philosophy of the
University of London
October, 1990

Abstract

A theoretical study is made of the stability of plasmas in the class of magnetic confinement devices known as pinches. The stability problem is treated by solving the linearised fluid equations of magnetohydrodynamics (MHD). However, unlike many previous studies, the model is not simplified to Ideal or Resistive MHD. Instead, many of the transport terms in the Braginskii equations are retained in order to model the stability of current and future pinch experiments more accurately. The complexity of the resulting system of equations, requires in most cases, a numerical treatment. This has been possible using the linear initial-value code, ODRIC, which was made available to Culham Laboratory by Lawrence Livermore Laboratory. This code includes the Hall terms, ion and electron thermal conductivity tensors, the ion stress tensor, the parallel thermal force and Ohmic heating, in addition to the familiar equations of Resistive MHD. Amendments have been made to the code, notably the correction of linear growth-rates for finite timestep, which allows more efficient convergence, and the inclusion of equilibrium density gradient terms.

ODRIC has been used to address some important questions on the stability of both Reversed Field Pinches (RFP's) and Z-pinches. In the former case resistive-g and η_i-modes have been studied, while in the latter the combined effect of resistivity and viscosity on sausage and kink instabilities is reported.

In addition to the numerical work, an analysis of the effect of finite pressure on the stability of a plasma surrounded by a resistive shell has been carried out. This appears to be of relevance to many current and most future RFP's, which will have pulse lengths much longer than the resistive diffusion time of the wall.

Symbols

All variables are in c.g.s. units unless otherwise stated, except for the electron and ion temperatures which are in eV
(i.e. Boltzmann's constant $k_B = 1.6 \times 10^{-12}\, ergs\, eV^{-1}$).

a	the pinch minor radius.
R_0	the RFP major radius.
$\vec{B} = (0, B_\theta, B_z)$	the equilibrium magnetic field.
$\vec{b} = (b_r, b_\theta, b_z)$	the perturbed magnetic field.
$\vec{v} = (v_r, v_\theta, v_z)$	the perturbed centre of mass velocity.
$\vec{\xi} = (\xi_r, \xi_\theta, \xi_z)$	the plasma displacement.
T_e	the equilibrium electron temperature.
T_{e1}	the perturbed electron temperature.
T_i	the equilibrium ion temperature.
T_{i1}	the perturbed ion temperature.
$n = n_e = n_i$	the equilibrium number density of electrons or ions.
$p = nk_B(T_e + T_i)$	the equilibrium pressure.
p_1	the perturbed pressure.
$\rho = n\, m_i$	the equilibrium mass density.
ρ_1	the perturbed mass density.
$\vec{J_0}$	the equilibrium current density.
$\vec{J_1}$	the perturbed current density.
I	the equilibrium plasma current.
γ	the mode growth-rate.
$\omega = \omega_R - i\gamma$	the mode frequency.
m	the poloidal mode number.
k	the axial wavenumber.
$n_k = kR$	the toroidal mode number.
δ_w	the thickness of the RFP shell.

Symbols Continued

$\boldsymbol{\kappa}_i$	the ion thermal conductivity tensor.
$\kappa_{i\parallel}$	the parallel ion thermal conductivity.
$\kappa_{i\perp}$	the perpendicular ion thermal conductivity.
$\kappa_{i\times}$	the cross ion thermal conductivity.
$\boldsymbol{\kappa}_e$	the electron thermal conductivity tensor.
$\kappa_{e\parallel}$	the parallel electron thermal conductivity.
$\kappa_{e\perp}$	the perpendicular electron thermal conductivity.
$\kappa_{e\times}$	the cross electron thermal conductivity.
$\mathbf{P}_i = p_i\mathbf{1} + \mathbf{\Pi}_i$	the ion stress tensor.
$\mu_{\parallel}$	the parallel ion viscosity.
μ_1, μ_2	the perpendicular ion collisional viscosities.
μ_3, μ_4	the finite ion Larmor radius terms.
$\mathbf{P}_e = p_e\mathbf{1} + \mathbf{\Pi}_e$	the electron stress tensor.
$\eta = \eta_{\perp}$	the resistivity.
$\beta_{\parallel}$	the coefficient of the parallel thermal force.
Γ	the ratio of specific heats.
$\ln\,\Lambda = 24 - 0.5\,\ln n + \ln T_e$	the Coulomb Logarithm.
η_w	the resistivity of the RFP shell.
$\tau_w = \dfrac{a\delta_w}{\eta_w}$	the long time constant of thr RFP shell.
$v_{Ti} = \left(\dfrac{2k_BT_i}{m_i}\right)^{1/2}$	the ion thermal velocity.
$v_{Te} = \left(\dfrac{2k_BT_e}{m_e}\right)^{1/2}$	the electron thermal velocity.
$v_A = \left(\dfrac{B^2}{4\pi\rho}\right)^{1/2}$	the Alfvén velocity.

Symbols Continued

$\omega_{ci} = \dfrac{eB}{m_i c}$	the ion Larmor frequency.
$\omega_{ce} = \dfrac{eB}{m_e c}$	the electron Larmor frequency.
$\omega_{pe} = \left(\dfrac{4\pi e^2 n}{m_e}\right)^{1/2}$	the electron plasma frequency.
$\lambda_D = \dfrac{v_{Te}}{\omega_{pe}}$	the Debye length.
$\lambda_i = v_{Ti}\tau_i$	the ion mean free path.
$\lambda_e = v_{Te}\tau_e$	the electron mean free path.
$a_i = \dfrac{v_{Ti}}{\omega_{ci}}$	the ion Larmor radius.
$\tau_e = 3.44 \times 10^5 \, \dfrac{T_e^{3/2}}{n \ln \Lambda}$	the electron collision time.
$\tau_i = 2.09 \times 10^7 \, \dfrac{T_i^{3/2}}{n \ln \Lambda} \left(\dfrac{m_i}{m_p}\right)^{1/2}$	the ion collision time.
$\tau_A = \dfrac{a}{v_A}$	the Alfvén time.
$\tau_R = \dfrac{4\pi a^2}{c^2 \eta_\perp}$	the resistive diffusion time.
$\tau_v = \dfrac{\rho a^2}{\mu_\parallel}$	the viscous time.
$S = \dfrac{\tau_R}{\tau_A}$	the Lundquist parameter.
$R = \dfrac{\tau_v}{\tau_A}$	the viscous Reynolds number.
$\beta = \dfrac{8\pi p}{B^2}$	the beta value.

Contents

List of Figures

List of Tables

Chapter 1

Background and Motivation

1.1 Introduction

Worldwide energy consumption has been rising at an increasing rate since the middle of the nineteenth century. Since energy demand is correlated with industrialisation, the expected development of the third world suggests that this trend will continue. However, mankind continues to rely largely on the burning of fossil fuels and to a lesser extent, on the nuclear fission of uranium, to meet energy requirements. The limited reserves of both fuels, together with the increasing demand, has been providing a strong motivation to search for alternatives for a number of years.

More recently a concern with the environment has provided further impetus. The problems associated with the disposal of radioactive waste, and the accident at Chernobyl, have led to widespread public opposition to fission reactors. On the otherhand the possibility that the carbon dioxide emitted by fossil fuel burning power stations could lead to an increase in the mean global temperature (the so called "greenhouse effect"), suggests that a return to total reliance on fossil fuels is not the answer. Hence the requirement for a "clean" alternative.

The renewable sources (solar, wind, geothermal and tidal power) are perceived as environmentally clean. However, although they may be useful in special locations (e.g. solar cells in the desert, wind turbines on remote islands), it appears unlikely that they could meet the worlds energy demands alone.

It is for the reasons outlined above that the prospect of controlled nuclear fusion remains as attractive as ever. This process involves the fusing together of light nuclei to form a more tightly bound, heavier nucleus, with the resultant liberation of nuclear binding energy. It is a chain of such fusion reactions that sustain stars, but as far as a terrestrial energy source is concerned the most useful reactions involve isotopes of hydrogen. The easiest of these to realise is the deuterium (^2H) - tritium (^3H) reaction:

$$D + T \rightarrow {}^4He(3.5MeV) + n(14.1MeV)$$

The deuterium required for the reaction is abundant in sea water (1 in 5000 water molecules), but the tritium is radioactive and not found in nature. Instead it must be bred from lithium :

$$^6Li + n \rightarrow T + {^4He} + 4.8MeV$$

$$^7Li + n \rightarrow T + {^4He} + n - 2.5MeV$$

Thus it is envisaged that a blanket of lithium surrounding the fusion reactor would serve the dual purpose of stopping the neutrons produced by the $D - T$ fusions (i.e. converting the kinetic energy into heat) and also of breeding further tritium by the reactions above. The total energy derivable from such a process depends on the worldwide reserves of lithium. Table 1.1 compares the energy equivalent of the estimated resources of lithium with those of fossil fuels and uranium (estimates from reference [1.1]). Although enormous quantities of lithium are contained within the oceans its extraction is at present uneconomic. However, the first two columns of table 1.1 indicate that on the basis of land reserves of lithium alone, the energy that could be derived from $D - T$ fusion is an order of magnitude times that available from fossil fuels. A $D - T$ fusion reactor would also have an environmental advantage over fission reactors, in that it produces comparatively little radioactive waste (although the structure itself would become radioactive). Ultimately it may be possible to achieve the still more difficult conditions necessary for deuterium-deuterium fusion:

$$D + D \rightarrow \begin{cases} T(1.01MeV) & + \quad p(3.02MeV) \quad 50\% \\ \\ {^3He}(0.82MeV) & + \quad n(2.45MeV) \quad 50\% \end{cases}$$

In this case the total energy reserve is not limited by lithium, and so it is practically inexhaustable ($\sim 10^{10}Q$). Additionally the difficulties associated with handling the radioactive tritium gas are removed.

	(i)	(ii)	(iii)
Oil	4	14	
Coal	33	300	
Uranium fission	230	1400	2.5×10^5
D-T fusion (Li)	400	10000	1.5×10^7
D-D fusion (D)			1.5×10^{10}

Table 1.1: Estimated energy equivalent in units of Q (Q=1.055×10^{21} J), for resources of fossil fuels, Uranium, Lithium (for D-T fusion) and Deuterium (for D-D fusion). For comparison, the worldwide rate of consumption of energy is approximately 0.3 Q per year. The estimates come from reference [1.1] and correspond to: (i) reserves with extraction costs less than twice present ones, (ii) reserves with extraction costs 2 to 3 times present ones, (iii) total reserves within the oceans.

For either of these fusion reactions to occur the separation between reacting nuclei must be less than the range of the inter-nuclear force ($\approx 10^{-15}m$). Since the nuclei are positively charged this means that the Coulomb repulsion between them must be overcome. The most extensively studied means of attempting this is "Thermonuclear fusion" in which the fusion material is heated to such high temperatures that a significant fraction of its ions have enough energy to surmount the Coulomb barrier, and become involved in fusion reactions. The alternatives to this method have become known, by comparison, as "cold fusion" approaches. These include the infamous work of Fleischmann and Pons [1.2] in which they claimed to have achieved $D-D$ fusion at room temperatures, using an electrolytic cell with a paladium electrode. Their paper led to great media excitement and worldwide attempts to confirm their results, but many of the initial confirmations have since been withdrawn and the scientific consensus seems to be that Fleicshmann and Pons probably made a calibration error. A less well known cold fusion approach, but one with a firmer scientific basis is "muon catalysed fusion". The muon is an elementary particle which is exactly like an electron in all respects aside from its mass, which is 207 times as large. In muon catalysed fusion the electron in a deuteron atom is replaced by a muon, which, since it has a larger mass, orbits much closer to the nucleus and more effectively screens its positive electric charge. Although the details are very complicated, basically the Coulomb barrier is narrowed by this screening and as a result the probability of quantum-mechanical tunneling through the barrier is increased. Unfortunately, energy is required to create muons and so the practicality of the process rests on the number of fusions that each muon can catalyse. Currently, this number appears to be too small for muon catalysed fusion to be economic [1.3].

Each of the attempts at cold fusion are very much fringe activities in comparison to the considerable effort that has been devoted to thermonuclear fusion research over the past 40 years. The high temperatures required for thermonuclear fusion ensure that the reacting deuterium and tritium gases will be fully ionised. As a result they form an electrically neutral gas of ions and electrons, which is known as a "plasma". For this reason the behaviour of plasmas has great relevance to the problem of controlled fusion.

1.2 The Conditions for Energy Breakeven and Ignition

The power lost by a hot plasma can be written as:

$$P_L = \alpha n^2 T^{1/2} + \frac{3nT}{\tau_E}$$

where the first term represents radiation loss due to bremsstrahlung and the second term represents both convective and conductive losses. The parameter, τ_E is known as the "energy confinement time". If thermonuclear conditions are to be maintained an equal quantity of power must be supplied by external plasma heating. Thus, to be a net producer of energy, a thermonuclear reactor must generate more electrical power than is required to maintain the plasma conditions. The total thermal power which escapes from a thermonuclear plasma consists of the power from fusion reactions, in addition to the radiation, conduction and convection losses:

$$P_T = \frac{1}{4} n^2 \langle \sigma v \rangle Q_f + \alpha n^2 T^{1/2} + \frac{3nT}{\tau_E}$$

where Q_f is the energy released per fusion, and $\langle \sigma v \rangle$ is the rate of fusion reactions. If this is converted into electrical power with efficiency, χ then the condition for energy breakeven is:

$$\chi P_T > P_L$$

Substituting the expressions for P_T and P_L and rearranging yields the "Lawson Criterion" [1.4]:

$$n\tau_E > \frac{3T}{\frac{\chi}{4(\chi-1)}\langle\sigma v\rangle Q_f - \alpha T^{1/2}}$$

For given χ the right-hand side is a function of temperature only. Figure 1.1 (reproduced from reference [1.5]) shows the breakeven condition as a function of temperature for both $D-T$ and $D-D$ plasmas.

Also shown in figure 1.1 are "ignition" curves. Ignition occurs when charged particle products are contained within the reaction region and release sufficient energy through collisions to sustain the thermonuclear conditions without external heating. Now, the power supplied by the charged particle products is:

$$P_C = \frac{1}{4}n^2\langle\sigma v\rangle Q_c$$

where Q_c is the energy released to the charged particles per fusion. The ignition condition is:

$$P_C > P_L$$

and this leads to a more stringent condition on the $n\tau_E$ product:

$$n\tau_E > \frac{3T}{\frac{1}{4}\langle\sigma v\rangle Q_c - \alpha T^{1/2}}$$

The conditions for breakeven and ignition, reduce the problem of controlled thermonuclear fusion to one of obtaining a sufficient $n\tau_E$ product. The techniques employed to do this fall into two classes.

The first, "magnetic confinement", involves the containment of the plasma's particles by a magnetic field. This relies on the fact that charged particles perform Larmor orbits about magnetic field lines, so that in the absence of collisions (or other collective effects) the net motion of a particle in a direction perpendicular to the magnetic field is zero. The loss of particles and energy parallel to the magnetic-field, can be limited by a suitable choice of magnetic geometry.

The second, "inertial confinement", uses laser implosion to increase the particle density to such a degree that the inertia of the nuclei provides sufficient τ_E. This thesis is concerned with devices that fit into the former, magnetic confinement class.

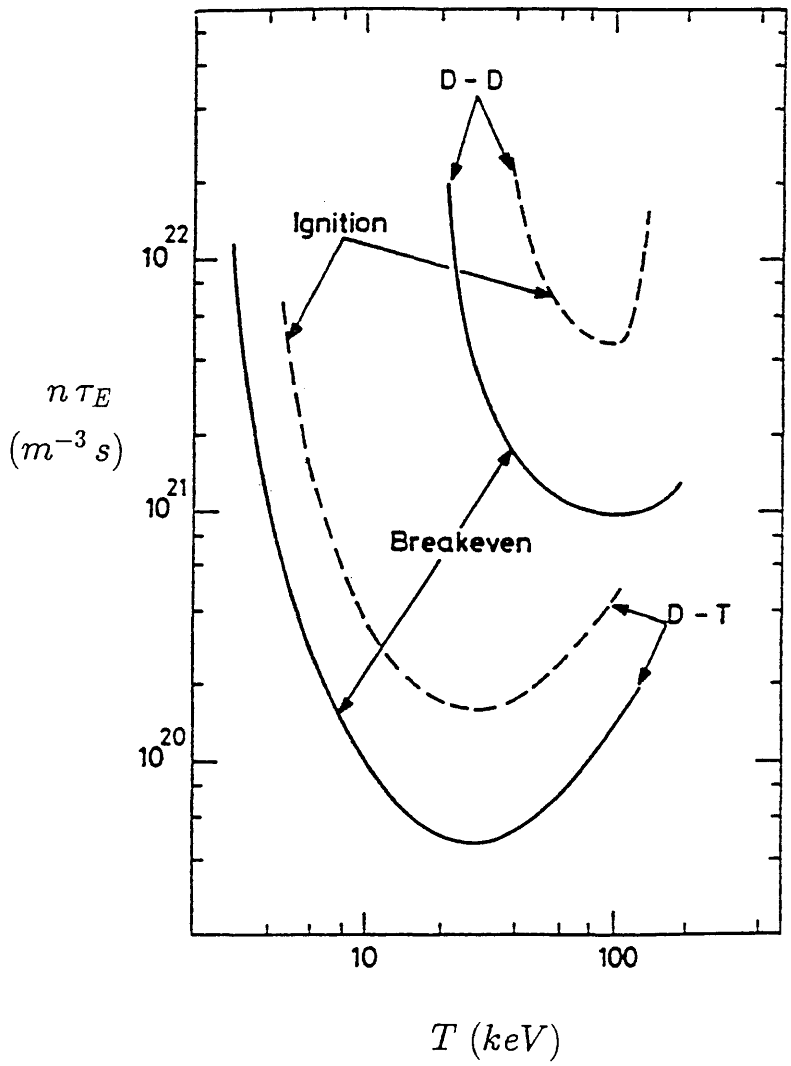

Figure 1.1: $n\,\tau_E$ for breakeven and ignition as a function of temperature, for the D-D and D-T reactions(figure 2 from reference [1.5]).

1.3 Historical Background

In the earliest magnetic confinement experiments, the confining magnetic field was produced solely by an axial current flowing between two electrodes at opposite ends of a cylindrical tube of plasma. Such a current produces an azimuthal magnetic field and this tends to thermally insulate the plasma by pinching it away from the walls of the containing vessel [1.6]. The ohmic dissipation of the current also provides the required plasma heating. Thus these early cylindrical devices, which are known as "Z-pinches", had a pleasing simplicity, with the axial current providing both heating and confinement. Unfortunately, the loss of heat to the electrodes seemed to be a severe limitation on the potential performance of Z-pinches. This led to the emergence of toroidal pinches, in which the plasma forms the single-turn secondary winding of a transformer and the current is driven inductively.

In early linear and toroidal pinch experiments there were signs that the plasma was prone to large-scale instabilities [1.7]. Theoretical work by Kruskal and Schwarzschild [1.8] indicated that pinches were unstable to perturbations that caused the plasma column to either locally constrict ("sausage" instability), or to bend ("kink" instability). Both types of instability were observed in subsequent pinch experiments [1.9], [1.10]. However, by 1957 separate experiments in the UK, the U.S.A and the U.S.S.R. had produced observable numbers of neutrons. Notable amongst these were the results from the toroidal pinch ZETA [1.11], which were released to the press, and misinterpreted as indicating that developing power from fusion was a mere formality. Unfortunately, it transpired that the neutrons produced were not thermonuclear in origin, being instead the result of fusions between ions which had been accelerated to large non-thermal velocities by the plasma instability.

It became obvious from this early research, that further progress depended crucially on finding some means of stabilising pinches against MHD instabilities.

Theoretical analyses by Rosenbluth [1.12], Tayler [1.13] and Shafranov [1.14] suggested that sausage and kink instabilities could be stabilised by an externally applied axial or toroidal field B_ϕ, of the same magnitude as that produced by the current, B_θ. The experimental implementation of this idea, produced an improvement in plasma stability, but residual instabilities persisted. The extension of theoretical work to include both localised pressure-driven instabilities [1.15] and resistive modes [1.16], suggested the cause of the remaining fluctuations.

Two separate means of further improving stability arose. In the U.S.S.R. a large toroidal field ($B_\phi \gg B_\theta$) was introduced to stabilise the gross resistive-kink modes. The resulting "Tokamak" device has since evolved to become the dominant configuration in thermonuclear research. However, up until the late sixties, the West was pursuing a different means of achieving enhanced stability - by introducing high magnetic-shear. This was best achieved by having a toroidal field that reversed at the edge (the so-called "Reversed-Field Pinch" (RFP)). When Ohkawa et al.[1.17] compared the stability of various pinch configurations with $B_\phi \sim B_\theta$, they found that the RFP was indeed the most stable. Meanwhile, the Zeta machine enjoyed a period of improved stability which corresponded to spontaneous generation of a reversed field at the edge. Subsequently, Taylor [1.18] showed that this is consistent with the pinch relaxing to the lowest energy state compatible with magnetic-helicity conservation.

In the eighties many fusion programmes were switched to study the tokamak. As a result, alternatives have been somewhat neglected. This is unfortunate for two reasons. Firstly, many of the alternatives offer the possibility of more economical power than a conventional tokamak could provide. Tokamaks require a large externally applied toroidal field and non-ohmic heating, both of which increase the complexity and overall cost. By comparison, it may be possible to ohmically heat an RFP to ignition, and its smaller toroidal field is less expensive to produce. Still further from the tokamak in terms of complexity is the linear Z-pinch, which has once more become the subject of active fusion research [1.19].

The alternative devices are in all cases less developed than tokamaks but even in the eventuality that tokamaks are proven to be superior, the study of alternatives is viable purely as a facility for the understanding of magnetic-confinement plasma physics. In limiting ourselves to tokamaks we run the danger of missing more general principles that may lead to true advances in understanding.

In all magnetic-confinement systems the MHD stability problem plays a vital part. Aside from gross instabilities which can terminate discharges, smaller-scale instabilities appear to lead to a degradation of the energy confinement time. Theoretical understanding and prediction relies largely on:

(i) identifying the relevant instabilities.

(ii) calculating the consequences of these instabilities.

This work is concerned with the former task. Most of the numerical work and analysis is applied to RFP equilibria although chapter 5 looks at the stability of Z-pinches.

The remaining two sections of this chapter are devoted to a discussion of the MHD model and the concept of linear stability.

1.4 The MHD Model

The state of a plasma is completely specified by the the positions ($\vec{r}$) and velocities ($\vec{u}$) of its constituent electrons and ions. The distribution of velocities and positions is given by the ion and electron distribution functions, $f_e(\vec{r}, \vec{u}, t)$ and $f_i(\vec{r}, \vec{u}, t)$. In principle it is possible to determine these by solving the coupled Boltzmann equations:

$$\frac{\partial f_e}{\partial t} + \vec{u}.\nabla f_e - \frac{e}{m}(\vec{E} + \frac{1}{c}\vec{u} \times \vec{B}).\nabla_u f_e = C_{ee} + C_{ei} \tag{1.1}$$

$$\frac{\partial f_i}{\partial t} + \vec{u}.\nabla f_i + \frac{e}{m}(\vec{E} + \frac{1}{c}\vec{u} \times \vec{B}).\nabla_u f_i = C_{ii} + C_{ie} \tag{1.2}$$

The right-hand side of these equations represent the total effect of collisions on the respective distribution functions. This includes contributions from both like collisions (C_{ee} and C_{ii}) and also unlike collisions (C_{ei} and C_{ie}).

For many practical purposes the kinetic description in terms of distribution functions is unnecessarily detailed, and it is sensible to seek a simplified system of equations by taking velocity moments of equations 1.1 and 1.2. The resulting equations describe the plasma in terms of the macroscopic variables of the number density, temperature and mean velocity of each particle species. The zeroth, first and second moments of equations 1.1 and 1.2 yield:

$$\frac{\partial n_e}{\partial t} + \nabla.(n_e\vec{v}_e) = 0 \tag{1.3}$$

$$\frac{\partial n_i}{\partial t} + \nabla.(n_i\vec{v}_i) = 0 \tag{1.4}$$

$$nm_e(\frac{\partial \vec{v}_e}{\partial t} + \vec{v}_e.\nabla\vec{v}_e) = -\nabla p_e - \nabla.\mathbf{\Pi}_e - en_e(\vec{E} + \frac{1}{c}\vec{v}_e \times \vec{B}) + \vec{R} \tag{1.5}$$

$$nm_i(\frac{\partial \vec{v}_i}{\partial t} + \vec{v}_i.\nabla\vec{v}_i) = -\nabla p_i - \nabla.\mathbf{\Pi}_i + en_i(\vec{E} + \frac{1}{c}\vec{v}_i \times \vec{B}) - \vec{R} \tag{1.6}$$

$$\frac{3}{2}n_e(\frac{\partial T_e}{\partial t} + \vec{v}_e.\nabla T_e) + p_e.\nabla\vec{v}_e = -\nabla.\vec{q}_e - \mathbf{\Pi}_e.\nabla\vec{v}_e + Q + \vec{R}.(\vec{v}_e - \vec{v}_i) \tag{1.7}$$

$$\frac{3}{2}n_i(\frac{\partial T_i}{\partial t} + \vec{v}_i.\nabla T_i) + p_i.\nabla\vec{v}_i = -\nabla.\vec{q}_i - \mathbf{\Pi}_i.\nabla\vec{v}_i - Q \tag{1.8}$$

where the macroscopic variables are defined as:

$$\begin{aligned}
n_\alpha &= \int f_\alpha \, d\vec{u} \\
\vec{v}_\alpha &= \frac{1}{n_\alpha}\int \vec{u}\, f_\alpha \, d\vec{u} \\
T_\alpha &= \frac{1}{3n_\alpha}\int m_\alpha\,(\vec{u}-\vec{v}_\alpha)^2 f_\alpha \, d\vec{u} \\
p_\alpha &= n_\alpha T_\alpha
\end{aligned}$$

and the remaining objects are the following velocity moments of the distribution functions:

$$\begin{aligned}
\mathbf{P}_\alpha &= \int m_\alpha\,(\vec{u}-\vec{v}_\alpha)(\vec{u}-\vec{v}_\alpha)\, f_\alpha\, d\vec{u} = p_\alpha\, \mathbf{1} + \mathbf{\Pi}_\alpha \\
\vec{R} &= \int m_e\,(\vec{u}-\vec{v}_e)\, C_{ei}\, d\vec{u} = -\int m_i\,(\vec{u}-\vec{v}_i)\, C_{ie}\, d\vec{u} \\
\vec{q}_\alpha &= \frac{1}{2}\int m_\alpha\, \vec{u}\,(\vec{u}-\vec{v}_\alpha)^2 f_\alpha\, d\vec{u} \\
Q &= -\frac{1}{2}\int (\vec{u}-\vec{v}_i)\, C_{ie}\, d\vec{u} = \frac{1}{2}\int (\vec{u}-\vec{v}_e)\, C_{ei}\, d\vec{u} + \vec{R}.(\vec{v}_e - \vec{v}_i)
\end{aligned}$$

Equations 1.3 to 1.8 describe the behaviour of the interpenetrating ion and electron fluids. Equation 1.3 expresses conservation of electrons, while 1.5 and 1.7 are the electron momentum and energy equations. Similarly equations 1.4, 1.6 and 1.8 describe the evolution of the ion component. The ion and electron fluids are coupled together by the momentum and energy transfer terms, $\vec{R}$ and Q, and also by the frictional heating of the electrons: $\vec{R}.(\vec{v}_e - \vec{v}_i)$.

Unfortunately, in this form equations 1.3 to 1.8 are not a closed system. Indeed, each order equation contains a higher order moment of the distribution function. Thus, the momentum equations contain the stress tensors, $\mathbf{P}_\alpha$, which are second order moments, and the energy equations contain the heat flux vectors, $\vec{q}_\alpha$, which are third order moments. A further approximation is required to close the system.

Braginskii [1.20] assumed that the distribution functions depart only slightly from a Maxwellian, thus he wrote:

$$f_\alpha = f_\alpha^0 + f_\alpha^1$$

where f_α^0 is a Maxwellian:

$$f_\alpha^0(\vec{r},\vec{u},t) = \left(\frac{m_\alpha}{2\pi T_\alpha}\right)^{3/2} n_\alpha \exp\left\{-\frac{m_\alpha}{2T_\alpha}(\vec{u}-\vec{v}_\alpha)^2\right\}$$

and f_α^1 is a small correction. Maxwellian electron and ion distributions represent the exact solution of the kinetic equations for the case in which spatial and time derivatives vanish identically. Under this condition the "transport terms", $\vec{R}$, Q, $\vec{q}_\alpha$ and $\mathbf{\Pi}_\alpha$ also vanish. Thus all transport is attributable to the deviations of the distributions from exact Maxwellians.

Braginskii solved the kinetic equations for the f_α^1 corrections, and then using these he was able to obtain the transport terms as functions of the macroscopic fluid variables. Thus for example the momentum transfer can be written as the sum of two contributions. One of these is proportional to the electron temperature gradient, while the other is proportional to the relative motion between the ions and electrons:

$$\vec{R} = \vec{R}^J + \vec{R}^T$$

with

$$\begin{aligned}
\vec{R}^J &= en\left\{\eta_{||}\,\vec{b}\,(\vec{b}.\vec{J}) + \eta_\perp\,\vec{b}\times(\vec{J}\times\vec{b}) - \eta_\times\,(\vec{b}\times\vec{J})\right\} \\
\vec{R}^T &= -\beta_{||}\,\vec{b}(\vec{b}.\nabla T_e) - \beta_\perp\,\vec{b}\times(\nabla T_e\times\vec{b}) - \beta_\times(\vec{b}\times\nabla T_e)
\end{aligned}$$

where $\vec{J} = ne(\vec{v}_i - \vec{v}_e)$, and $\vec{b}$ is the unit vector in the direction of the magnetic field. The transport coefficients $\eta_{||}$, $\beta_{||}$, $\eta_\perp$ etc. are functions of temperature, density and magnetic field, which determine the relationship between the thermodynamic forces, $\vec{J}$ and ∇T_e, and the thermodynamic fluxes $\vec{R^J}$ and $\vec{R^T}$. Appendix 1A contains the other transport terms and appendix 1B lists the transport coefficients as calculated by Braginskii [1.20].

The validity of the Braginskii equations is limited by the assumption that the ion and electron distribution functions are very nearly Maxwellian. For this to be a good assumption the following conditions should be satisfied:

(i)

$$\partial/\partial t \ll \nu_{e,i} \tag{1.9}$$

where $\partial/\partial t$ represents the rate of change of any variable within the equations and $\nu_{e,i}$ is the electron (ion) collision frequency.

(ii)

$$L_{\|} \gg \lambda_{e,i} \tag{1.10}$$

where $L_{\|}$ is an equilibrium length-scale in the direction parallel to the field and $\lambda_{e,i}$ is the electron (ion) collisional mean-free path.

(iii)

$$L_{\perp} \gg a_{e,i} \tag{1.11}$$

where $L_{\perp}$ is an equilibrium length-scale in the direction perpendicular to the field and $a_{e,i}$ is the electron (ion) Larmor radius.

The separate conditions for electrons and ions are given by taking the corresponding subscript.

Equation 1.9, can be interpreted as the condition that there are sufficient collisions to drive the distribution function towards a Maxwellian. This in turn means that the Braginskii equations cannot describe processes occurring on time-scales shorter than a collision time. Equations 1.10 and 1.11 are basically the conditions for any fluid theory to be valid. The fluxes in fluid equations are written in terms of first order spatial derivatives, so that a flux at any point is determined only by local gradients. For this to be an accurate picture, plasma particles, (either electrons or ions), must be incapable of sampling changes in the gradients, otherwise second-order or higher derivatives would have to be included. Thus we require that particles typically travel distances much less than the length, L , over which the equilibrium changes, where $L \sim |\nabla\psi|/\psi$ and ψ represents any equilibrium variable. Equations 1.10 and 1.11 express this condition for motions parallel and perpendicular to the magnetic field respectively.

Equation 1.10 is often violated in tokamaks, where the magnetic field curvature in the toroidal direction defines a length-scale much shorter than the typical mean-free path. This has led to the development of "Neoclassical transport theory"[1.21]. However, for the description of many important phenomena in other magnetic confinement devices the Braginskii equations are perfectly valid.

1.4.1 Single Fluid Equations

The small ratio of the electron to ion mass, means that for many purposes the electron inertia may be neglected. To be more specific, this is true for phenomena which:

(i) are much slower than the typical plasma frequencies associated with the electron mass:

$$\partial/\partial t \ll \omega_{pe}, \omega_{ce} \tag{1.12}$$

where ω_{pe} is the electron plasma frequency, and ω_{ce} is the electron Larmor frequency.

(ii) have length-scales much longer than the Debye length, λ_D:

$$\lambda \gg \lambda_D \tag{1.13}$$

If these conditions are satisfied two simplifications can be made to the fluid equations. Firstly, and most obviously, the electron inertial term may be neglected in equation 1.5 . Secondly, the negligible electron mass implies that the electron response will be almost instantaneous. Thus the electrons will move quickly to neutralise any electrostatic fields, with the result that charge neutrality will be maintained to a high degree of approximation throughout the plasma i.e.

$$n_e \approx n_i = n$$

This approximation immediately removes one equation from the two fluid system. Indeed, when the electron mass is neglected the Braginskii equations can be conveniently written in terms of single fluid variables for the mass density, centre of mass velocity and current density:

$$\rho = n m_i \tag{1.14}$$

$$\vec{v} = \vec{v}_i \tag{1.15}$$

$$\vec{J} = ne(\vec{v} - \vec{v}_e) \tag{1.16}$$

The resulting system of single-fluid equations is:

$$\frac{\partial \rho}{\partial t} + \nabla.(\rho \vec{v}) = 0 \tag{1.17}$$

$$\rho \frac{D\vec{v}}{Dt} = \frac{4\pi}{c}\vec{J} \times \vec{B} - \nabla p - \nabla.(\mathbf{\Pi}_i + \mathbf{\Pi}_e) \tag{1.18}$$

$$\vec{E} + \frac{1}{c}\vec{v} \times \vec{B} = \frac{m_i}{\rho e}\left(\frac{1}{c}\vec{J} \times \vec{B} - \nabla p_e - \nabla.\mathbf{\Pi}_e + \vec{R}\right) \tag{1.19}$$

$$\begin{aligned} \frac{D}{Dt}\left\{\frac{p_e}{\rho^{5/3}}\right\} &= \frac{2}{3\rho^{5/3}}\left\{-\nabla.\vec{q}_e - \mathbf{\Pi}_e.\nabla(\vec{v} - \frac{m_i}{\rho e}\vec{J}) + Q - \frac{m_i}{\rho e}\vec{R}.\vec{J}\right\} \\ &\quad + \frac{m_i}{\rho e}\vec{J}.\nabla\left\{\frac{p_e}{\rho^{5/3}}\right\} \end{aligned} \tag{1.20}$$

$$\frac{D}{Dt}\left\{\frac{p_i}{\rho^{5/3}}\right\} = \frac{2}{3\rho^{5/3}}\left\{-\nabla.\vec{q}_i - \mathbf{\Pi}_i.\nabla\vec{v} - Q\right\} \tag{1.21}$$

$$p = p_i + p_e = \frac{\rho}{m_i}(T_i + T_e) \tag{1.22}$$

$$\nabla \times \vec{B} = \frac{4\pi}{c}\vec{J} \tag{1.23}$$

$$\nabla \times \vec{E} = -\frac{1}{c}\frac{\partial \vec{B}}{\partial t} \tag{1.24}$$

$$\nabla.\vec{B} = 0 \tag{1.25}$$

where D/Dt is the "convective derivative":

$$\frac{D}{Dt} = \frac{\partial}{\partial t} + \vec{v}.\nabla$$

Note that the displacement current has been neglected in Ampere's law. This is justified as long as the phase velocities of the waves of interest are much slower than the speed of light, i.e. $\omega/k \ll c$.

1.4.2 Ideal and Resistive MHD

Although simpler than the original kinetic treatment, the single-fluid equations, are still complicated enough to make their analytical solution difficult, and so reduced forms are often sought. Freidberg [1.22], has examined the regimes in which simpler models apply. He assumed $L_{||} \sim L_{\perp} \sim a$ and found that when:

$$\frac{a_i}{a} \rightarrow 0$$

and

$$\left(\frac{m_e}{m_i}\right)^{1/2} \frac{\lambda_i}{a} \rightarrow 0$$

the Braginskii equations plus Maxwell's equations can be reduced to the "resistive MHD" model:

$$\frac{\partial \rho}{\partial t} + \nabla.(\rho\vec{v}) = 0 \tag{1.26}$$

$$\rho\frac{D\vec{v}}{Dt} = \frac{1}{c}\vec{J} \times \vec{B} - \nabla p \tag{1.27}$$

$$\vec{E} + \frac{1}{c}\vec{v} \times \vec{B} = \eta\vec{J} \tag{1.28}$$

$$\frac{D}{Dt}\frac{p}{\rho^{5/3}} = 0 \tag{1.29}$$

$$\nabla \times \vec{B} = \frac{4\pi}{c}\vec{J} \tag{1.30}$$

$$\nabla \times \vec{E} = -\frac{1}{c}\frac{\partial \vec{B}}{\partial t} \tag{1.31}$$

$$\nabla . \vec{B} = 0 \tag{1.32}$$

A still more restrictive model neglects resistivity in Ohm's law, so that equation 16 is replaced by:

$$\vec{E} + \frac{1}{c}\vec{v} \times \vec{B} = 0 \tag{1.33}$$

The resulting "Ideal MHD Model" has been extensively applied in the study of the linear stability of magnetically confined plasmas.

1.5 The Linear Stability Concept

Central to the theoretical analysis of magnetic confinement systems is the concept of stability. As an introduction consider the stability of a mechanical system. The governing equation is Newton's second law:

$$m\frac{d^2x}{dt^2} = -\frac{dV(x)}{dx}$$

Imagine that x is the position of a point mass , m, on some undulating terrain defined by the gravitational potential $V(x)$. Initially the mass is in equilibrium and at rest at $x = x_0$ so that:

$$\left.\frac{d^2x}{dt^2}\right|_{x_0} = \left.\frac{dV(x)}{dx}\right|_{x_0} = 0$$

Expand Newton's law about this point:

$$m\frac{d^2(x - x_0)}{dt^2} = -(x - x_0)\left.\frac{d^2V}{dx^2}\right|_{x_0} + \cdots$$

Let $\xi = x - x_0$, therefore

$$m\frac{d^2\xi}{dt^2} = -\xi\left.\frac{d^2V}{dx^2}\right|_{x_0} + \cdots \tag{1.34}$$

Now we "linearise" i.e. we assume that the displacement from equilibrium, ξ, is so small that quadratic and higher order terms in equation 1.34 are negligible. Thus the equation for the displacement reduces to:

$$\frac{d^2\xi}{dt^2} + \xi\frac{V''}{m} = 0 \tag{1.35}$$

where $V'' = d^2V/dx^2|_{x_0}$ This has a solution:

$$\xi \propto exp\left(i\sqrt{\frac{V''}{m}}t\right)$$

Thus if:

(i) $V'' > 0$, the displacement oscillates but does not grow. This corresponds to the mass being in a well.

(ii) $V'' < 0$, the displacement grows exponentially with growth-rate, $\gamma = \sqrt{V''/m}$. This correponds to the mass being on a peak.

The "linear" analysis presented above is only valid for small displacement, ξ, such that:

$$\xi \ll \frac{V''}{V'''}$$

Eventually a linear instability will violate this condition. Calculation of the subsequent time-evolution of the perturbation requires the inclusion of higher-order terms in the displacement and correpondingly higher-order derivatives of the potential. This means that the long-time behaviour of a linear instability is determined by the global nature of the potential, while linear stability is dependent solely on its local nature (i.e. V'' only).

We conclude that linear theory is useful in determining whether instabilities exist and thus whether a more complicated non-linear treatment is required. Additionally, linear theory is perfectly adequate for determining the conditions necessary to totally avoid an instability. Such "stability conditions" are of particular importance for magnetic confinement. In this thesis the often complicated systems of equations studied, prohibit a non-linear treatment. So we content ourselves with a linear theory and offer the reasons above as justification.

Returning now to the discussion of linear theory, note that in general the analogue to equation 1.35 is not soluble. Extracting the relevant information requires more subtle techniques. Multiply equation 1.35 by ξ:

$$\frac{d}{dt}\left(\frac{m\dot{\xi}^2}{2}+\frac{\xi^2}{2}V''\right)=0$$

where $\dot{\xi}=d\xi/dt$. Thus the term in brackets must be a constant in time. This constant is merely the change in total energy of the mass, (kinetic+potential), due to the displacement. Assuming that $\xi(x,t)=\xi(x)\exp(-i\omega t)$, then we have:

$$-\omega^2\frac{m}{2}\xi^2+\frac{V''}{2}\xi^2=\text{constant}$$

This must be true for all displacements, so the constant is zero. Finally we arrive at the result previously obtained by straightforward solution of equation 1.35:

$$\omega^2=\frac{V''}{m}$$

For a more general system we have:

$$\omega^2=\frac{\delta W(\xi)}{\delta K(\xi)}$$

where $\delta W(\xi)$ is the change in potential energy due to ξ
and $\omega^2\delta K(\xi)$ is the change in kinetic energy due to ξ.
If $\omega^2<0$ then the system is unstable, and since δK is positive definite, the sign of δW alone determines stability:

$$\left.\begin{array}{rcr}\delta W<0 & \Longrightarrow & \text{instability}\\ \\ \delta W>0 & \Longrightarrow & \text{stability}\end{array}\right\}\qquad(1.36)$$

Equation 1.36 is known as "The Energy Principle". Stability to a particular ξ is determined by finding the change in potential corresponding to that ξ. However,

ξ may take on many forms and this method requires a calculation of $\delta W(\xi)$, for all possible displacements, in order to guarantee stability. Clearly, the crucial displacement is the one that minimises δW. Fortunately, using Variational calculus it is possible to derive an (Euler-Lagrange) equation, for this most unstable displacement. The solution of this equation can then be substituted into the energy principle to determine stability. For the special case of the ideal MHD stability of a cylindrical pinch, this last step is not necessary. Newcomb [1.23], has derived theorems that allow stability to be determined purely from the behaviour of the solution to the Euler-Lagrange equation.

Energy principles, such as equation 1.36, have been extensively used to study ideal MHD stability. Energy principles provide insight into the free-energy sources responsible for instability, and in some cases it is possible to determine stability conditions purely by inspection of the δW expression. However for more complicated models that include dissipation (e.g. resistivity, viscosity), the total energy of the displacement is not constant, and energy principles are not usable. In this case, the full system of equations must be solved either by a numerical technique, or analytically, by some form of asymptotic matching. In this thesis an "Initial Value Code" has been used to study the linear stability of a cylindrical plasma described by Braginskii's equations. The code is known as "ODRIC" and was provided to Culham Laboratory by A.A.Mirin and co-workers [1.24] of Lawrence Livermore Laboratory. The next chapter contains a description of ODRIC along with amendments made to the code.

References

[1.1] Knoepfel, H., "Energy 2000" (Gordon and Breach Science Publishers, 1986).

[1.2] Fleischmann, M., Pons, S., J. Electroanal. Chem. **286**, 301 (1989).

[1.3] Froelich, P., Europhysics News **20**, 61 (1989).

[1.4] Lawson, J.D., Proc. Phys. Soc. (London) **B70**, 6 (1957).

[1.5] Laing, E.W., in "Plasma Physics and Nuclear Fusion Research", (Academic Press, 1981), 155.

[1.6] Bennett, W.H., Phys. Rev. **45**, 890 (1934).

[1.7] Cousins, S.W., Ware, A.A., Proc. Phys. Soc. (London) **B64**, 159 (1951).

[1.8] Kruskal, M., Scharwschild, M., Proc. R. Soc. (London) **A223**, 348 (1954).

[1.9] Carruthers, R., Davenport, P.A., Proc. Phys. Soc. (London) **B70**, 49 (1957).

[1.10] Curzon, F.L., Folkierski, A., Lathem, R., Nation, J.A., Proc. R. Soc. (London) **A257**, 386 (1960).

[1.11] Thoneman, P.C., Butt, E.P., Carruthers, R., et al., Nature **181**, 217 (1958).

[1.12] Rosenbluth, M., Los Alamos Scientific Report LA-1850 (1956).

[1.13] Tayler, R.J., Proc. Phys. Soc. (London) **B70**, 1049 (1957).

[1.14] Shafranov, V.D., in "Plasma Physics and the Problem of Controlled Thermonuclear Reactions" (Pergammon Press, 1959) Vol.2, 197.

[1.15] Suydam, B.R., in "Peaceful Uses of Atomic Energy (Proc. 2^{nd} United Nations Int. Conf. Geneva, 1958)", (United Nations, 1958), Vol.31, 157.

[1.16] Furth, H.P., Killeen, J., Rosenbluth, M.N., Phys. Fl. **6**, 459 (1963).

[1.17] Ohkawa, T., Forsen, H.K., Schupp, A.A., Kerst, D.W., Phys. Fl. **6**, 846 (1963).

[1.18] Taylor, J.B., Phys. Rev. Lett. **33**, 1139 (1974).

[1.19] Haines, M.G., Physica Scripta **T2/2**, 380 (1982).

[1.20] Braginskii, S.I., Sov. Phys. J.E.T.P. **6**, 358 (1958).

[1.21] Hinton, F.L., Hazeltine, R.D., Rev. Mod. Phys. **48**, 239 (1976).

[1.22] Freidberg, J.P., Rev. Mod. Phys. **54**, 801 (1982).

[1.23] Newcomb, W.A., Ann. Phys. **10**, 232 (1960).

[1.24] Mirin, A.A., O'Neill, N.J., Killeen, J., Bonugli, R.J., Ellis, M.J., Phys. Fl. **29**, 512 (1986).

[1.25] Epperlein, E.M.., Haines, M.G., Phys. Fl. **29**, 1029 (1986).

Appendix 1A : Transport Terms

(i) Momentum transfer, $\vec{R}$.

$$\vec{R} = \vec{R}^J + \vec{R}^T \tag{1A.1}$$

with

$$\vec{R}^J = en\left\{\eta_{\|}\,\vec{b}\,(\vec{b}.\vec{J}) + \eta_{\perp}\,\vec{b}\times(\vec{J}\times\vec{b}) - \eta_{\times}\,(\vec{b}\times\vec{J})\right\} \tag{1A.2}$$

$$\vec{R}^T = -\beta_{\|}\,\vec{b}(\vec{b}.\nabla T_e) - \beta_{\perp}\,\vec{b}\times(\nabla T_e\times\vec{b}) - \beta_{\times}(\vec{b}\times\nabla T_e) \tag{1A.3}$$

(ii) Energy Transfer, Q.

$$Q = \frac{3}{2}\frac{m_e}{m_i}(T_i - Te) \tag{1A.4}$$

(iii) Electron Heat Flux, $\vec{q}_e$.

$$\vec{q}_e = \vec{q}_e^{\,J} + \vec{q}_e^{\,T} \tag{1A.5}$$

with

$$\vec{q}_e^{\,J} = -\frac{1}{ne}\left\{\beta_{\|}\,T_e\,\vec{b}(\vec{b}.\vec{J}) + \beta_{\perp}\,T_e\,\vec{b}\times(\vec{J}\times\vec{b}) + \beta_{\times}\,T_e\,(\vec{b}\times\vec{J})\right\} \tag{1A.6}$$

$$\vec{q}_e^{\,T} = -\kappa_{e\|}\,\vec{b}\,(\vec{b}.\nabla T_e) - \kappa_{e\perp}\,\vec{b}\times(\nabla T_e\times\vec{b}) - \kappa_{e\times}\,(\vec{b}\times\nabla T_e) \tag{1A.7}$$

(iv) Ion Heat Flux, $\vec{q}_i$.

$$\vec{q}_i = -\kappa_{i\|}\,\vec{b}\,(\vec{b}.\nabla T_i) - \kappa_{i\perp}\,\vec{b}\times(\nabla T_i\times\vec{b}) - \kappa_{i\times}\,(\vec{b}\times\nabla T_i) \tag{1A.8}$$

(v) Stress Tensor, $\mathbf{\Pi}$.

$$\Pi_{zz} = -\mu_0 W_{zz} \tag{1A.9}$$

$$\Pi_{xx} = \frac{\mu_0}{2}W_{zz} - \frac{\mu_1}{2}(W_{xx} - W_{yy}) - \mu_3 W_{xy} \tag{1A.10}$$

$$\Pi_{yy} = \frac{\mu_0}{2}W_{zz} + \frac{\mu_1}{2}(W_{xx} - W_{yy}) + \mu_3 W_{xy} \tag{1A.11}$$

$$\Pi_{xy} = \Pi_{yx} = -\mu_1 W_{xy} + \frac{\mu_3}{2}(W_{xx} - W_{yy}) \tag{1A.12}$$

$$\Pi_{xz} = \Pi_{zx} = -\mu_2 W_{xz} - \mu_4 W_{yz} \tag{1A.13}$$

$$\Pi_{yz} = \Pi_{zy} = -\mu_2 W_{yz} + \mu_4 W_{xz} \tag{1A.14}$$

where the magnetic-field is parallel to z and:

$$W_{jk} = \frac{\partial v_j}{\partial x_k} + \frac{\partial v_k}{\partial x_j} - \frac{2}{3}\delta_{jk}\nabla.\underline{v} \tag{1A.15}$$

Appendix 1B : Braginskii Coefficients

(i) Electron Transport Coefficients.

$$\eta_{\parallel} = \frac{m_e}{ne^2\tau_e}\alpha_0 \tag{1B.1}$$

$$\eta_{\perp} = \frac{m_e}{ne^2\tau_e}\left(1 - \frac{\alpha_1' X_e^2 + \alpha_0'}{\Delta_e}\right) \tag{1B.2}$$

$$\eta_{\times} = \frac{m_e}{ne^2\tau_e} X_e \frac{(\alpha_1'' X_e^2 + \alpha_0'')}{\Delta_e} \tag{1B.3}$$

$$\beta_{\parallel} = n_e \beta_0 \tag{1B.4}$$

$$\beta_{\perp} = n_e \frac{\beta_1' X_e^2 + \beta_0'}{\Delta_e} \tag{1B.5}$$

$$\beta_{\times} = n_e X_e \frac{(\beta_1'' X_e^2 + \beta_0'')}{\Delta_e} \tag{1B.6}$$

$$\kappa_{e\parallel} = \frac{n_e T_e \tau_e}{m_e}\gamma_0 \tag{1B.7}$$

$$\kappa_{e\perp} = \frac{n_e T_e \tau_e}{m_e}\frac{\gamma_1' X_e^2 + \gamma_0'}{\Delta_e} \tag{1B.8}$$

$$\kappa_{e\times} = \frac{n_e T_e \tau_e}{m_e}\frac{(\gamma_1'' X_e^2 + \gamma_0'')}{\Delta_e} \tag{1B.9}$$

where:

$$X_e = \omega_{ce}\tau_e$$

$$\Delta_e = X_e^4 + \delta_1 X_e^2 + \delta_0$$

and for singly charged ions ($Z = 1$):

$$\begin{array}{llll}
\alpha_0 = 0.5129 , & \beta_0 = 0.7110 , & \gamma_0 = 3.1616 , \\
\alpha_0' = 1.837 , & \beta_0' = 2.681 , & \gamma_0' = 11.92 , \\
\alpha_0'' = 0.7796 , & \beta_0'' = 3.053 , & \gamma_0'' = 21.67 , \\
\alpha_1' = 6.416 , & \beta_1' = 5.101 , & \gamma_1' = 21.67 , \\
\alpha_1'' = 1.704 , & \beta_1'' = 1.5 , & \gamma_1'' = 2.5 , \\
\end{array}$$

$$\delta_0 = 3.770 , \quad \delta_1 = 14.79$$

The electron transport coefficients have recently been recalculated by Epperlein and Haines [1.25], via a direct numerical solution of the electron kinetic equation. Their most significant correction occurs for the $\eta_\times$ and $\beta_\perp$ coefficients, for which they derive quite different functional forms from Braginskii in the relevant $\omega_{ce}\tau_e \rightarrow \infty$ limit. The other coefficients are in close agreement with Braginskii. Since, $\eta_\times$ and $\beta_\perp$ are not included in the calculations to be presented in chapters 4 and 5, the Braginskii coefficients are sufficiently accurate for the purposes of this work.

(ii) Ion Transport Coefficients.

$$\kappa_{i\parallel} = 3.906\,\frac{n_i T_i \tau_i}{m_i} \tag{1B.10}$$

$$\kappa_{i\perp} = \frac{n_i T_i \tau_i}{m_i}\frac{(2.0\,X_i^2 + 2.645)}{\Delta_i} \tag{1B.11}$$

$$\kappa_{i\times} = \frac{n_i T_i \tau_i}{m_i}\frac{(2.5\,X_i^2 + 4.65)}{\Delta_i} \tag{1B.12}$$

$$\mu_\parallel = 0.96 n T_i \tau_i \tag{1B.13}$$

$$\mu_1 = n T_i \tau_i \frac{(4.80\,X_i^2 + 2.23)}{\Delta_i''} \tag{1B.14}$$

$$\mu_2 = n T_i \tau_i \frac{(1.20\,X_i^2 + 2.23)}{\Delta_i'} \tag{1B.15}$$

$$\mu_3 = 2 n T_i \tau_i X_i \frac{(4X_i^2 + 2.38)}{\Delta_i''} \tag{1B.16}$$

$$\mu_4 = n T_i \tau_i X_i \frac{(X_i^2 + 2.38)}{\Delta_i'} \tag{1B.17}$$

where:

$$X_i = \omega_{ci}\tau_i$$

$$\Delta_i = X_i^4 + 2.70\,X_i^2 + 0.677$$

$$\Delta_i' = X_i^4 + 4.03\,X_i^2 + 2.33$$

$$\Delta_i'' = 16.0\,X_i^4 + 16.12\,X_i^2 + 2.33$$

Chapter 2

A Description of the ODRIC Linear Stability Code

2.1 Introduction

ODRIC stands for "One-Dimensional Resistive Initial Value Code". It solves a set of fluid equations of the Braginskii-type in cylindrical geometry. The authors of the code are A.A.Mirin and co-workers at the Lawrence Livermore Laboratory, U.S.A. They have already published a complete description of ODRIC [2.1], and so in this chapter we only give a brief description of the code, along with the improvements that have been made.

2.2 Simplifying Assumptions

The use of ODRIC to the study the stability of pinches entails the following assumptions:

(i) The pinch is well descibed by cylindrical geometry $(r,\ \theta,\ z)$.

This means that all perturbed variables can be written as:

$$U(\vec{r}, t) = U(r, t)\exp(im\theta + ikz)$$

where m and k label poloidal and axial fourier harmonics respectively. For an equilibrium with cylindrical symmetry, the different harmonics are not coupled and the calculation is reduced to a one-dimensional problem for each mode, i.e. each (m, k) pairing. In a tokamak where toroidal effects are strong this cylindrical approximation is poor, and fourier harmonics can be strongly coupled (as, for example, in ballooning modes). However, the low q and large aspect ratio conditions of RFP's, means that they may be treated with reasonable accuracy in cylindrical geometry.

(ii) Equilibrium quantities are time-independent.

Consider the following, symbolic system of equations:

$$\hat{\mathbf{L}}\frac{\partial \vec{U}}{\partial t} = \hat{\mathbf{R}}\,\vec{U} \tag{2.1}$$

where $\hat{\mathbf{L}}$ and $\hat{\mathbf{R}}$ are matrix operators, operating on the perturbed variables in the matrix, $\vec{U}$. In a linearised system of equations, $\hat{\mathbf{L}}$ and $\hat{\mathbf{R}}$ contain only zeroth-order, equilibrium quantities. If in addition they are time-independent then the elements of $\vec{U}$ can be separated into the product of a function of space only and a function of time only. For equations with first-order time derivatives, the time variation reduces to:

$$\vec{U}(\vec{r},t) = \vec{U}(\vec{r})\exp(i\omega t)$$

In general ω can be real or imaginary.

This is equivalent to the decoupling of fourier harmonics for cylindrical symmetry, as considered above. In each case the independence of $\hat{\mathbf{L}}$ and $\hat{\mathbf{R}}$ from a variable, (z, θ or t), has meant that the fourier harmonics of that variable are independent of one another. It is therefore possible to reduce the system of equations to a problem in the radial variable only, by replacing poloidal, axial and time derivatives, by im, ik and $i\omega$ respectively. This results in an eigenvalue problem for each (m,k) pairing. However for complicated systems of equations this formalism becomes progressively more difficult. In initial-value codes, such as ODRIC, the time derivatives are not replaced by $i\omega$. Instead, the equations are perturbed and the perturbation is integrated forward in time until the solution has an exponential time dependence.

The assumption of a static equilibrium, requires that the characteristic timescales of the modes we study, are much shorter than those on which the equilibrium changes i.e.

$$\left.\frac{\partial}{\partial t}\right|_{equil} \ll |\omega|$$

(iii) The equilibrium flow velocity, v_0, is negligible.

This reduces the convective time-derivatives to partial derivatives:

$$\frac{\partial}{\partial t} + \vec{v_0}.\nabla \rightarrow \frac{\partial}{\partial t}$$

The equilibrium velocity is negligible for:

$$|\omega| \gg \frac{v_0}{l}$$

where l represents the characteristic length-scale of the solution to the linearised equations, and $1/|\omega|$ is its characteristic time-scale.

(iv) The plasma is directly in contact with a perfectly-conducting wall.
This assumption leads to the simplest possible boundary conditions, but since the wall prevents boundary deforming perturbations, it gives an optimistic picture of stability. Fortunately, for the cases of interest in this thesis the effect of this assumption is either easy to quantify (e.g. the stabilisation of long wavelength $m = 1$ modes in the Z-pinch), or negligible (e.g. for resonant modes in the RFP).

2.3 Boundary Conditions

(i) at $r = 0$ symmetry conditions [2.2] yield different boundary conditions for different poloidal mode numbers, m:

$$b_r = b_\theta = v_r = v_\theta = \frac{dv_z}{dr} = \frac{dT_{i1}}{dr} = \frac{dT_{e1}}{dr} = \frac{d\rho_1}{dr} = 0 \qquad \text{for} \quad m = 0$$

$$v_z = T_{i1} = T_{e1} = \rho_1 = \frac{db_r}{dr} = \frac{db_\theta}{dr} = \frac{dv_r}{dr} = \frac{dv_\theta}{dr} = 0 \qquad \text{for} \quad m = 1$$

$$b_r = b_\theta = v_r = v_\theta = v_z = T_{i1} = T_{e1} = \rho_1 = 0 \qquad \text{for} \quad m \geq 2$$

(ii) at $r = a$ conducting wall and free-flow boundary conditions [2.1]:

$$b_r = v_r = \frac{d(rb_\theta)}{dr} = \frac{d(rv_\theta)}{dr} = \frac{dv_z}{dr} = \frac{db_z}{dr} = \frac{dT_{i1}}{dr} = \frac{dT_{e1}}{dr} = \frac{d\rho_1}{dr} = 0$$

2.4 The Numerics

ODRIC solves a system of equations of the form of equation 2.1. The radial derivatives contained in $\hat{\mathbf{L}}$ and $\hat{\mathbf{R}}$, are centred:

$$\left.\frac{\partial \vec{U}}{\partial r}\right|_j = \frac{\vec{U}_{j+1} - \vec{U}_{j-1}}{r_{j+1} - r_{j-1}}$$

where j labels the variable at the j^{th} radial location. The time differencing is fully implicit, so that the discretised form of equation 2.1 is:

$$\hat{\mathbf{L}}\frac{\vec{U}^{n+1} - \vec{U}^n}{\Delta t} = \hat{\mathbf{R}}\,\vec{U}^{n+1} \tag{2.2}$$

where n labels the n^{th} timestep, and $\Delta t = t^{n+1} - t^n$. Notice that only the variable at the $(n+1)^{th}$ timestep, appears on the right-hand side of this equation, (this is the definition of a fully implicit scheme). Equation 2.2 can be written as:

$$(\hat{\mathbf{L}} - \hat{\mathbf{R}}\Delta t)\vec{U}^{n+1} = \hat{\mathbf{L}}\,\vec{U}^n \tag{2.3}$$

This matrix equation is to be solved at each radial location. Discretising the radial derivatives in the operators, leads to the following general form for the problem:

$$-\hat{\mathbf{A}}_j\vec{U}^{n+1}_{j+1} + \hat{\mathbf{B}}_j\vec{U}^{n+1}_j - \hat{\mathbf{C}}_j\vec{U}^{n+1}_{j-1} = \hat{\mathbf{D}}_j \tag{2.4}$$

Systems such as these are known as "triadiagonal", i.e. the matrix involved has non-zero elements only along the main diagonal and the two nearest adjacent diagonals. Triadiagonal matrix equations may be efficiently solved by an algorithm due to Richtmyer and Morton [2.3], which is explained below.

We begin by casting equation 2.4 in the form:

$$\vec{U}_j + \mathbf{E}_j\vec{U}_{j+1} = \mathbf{F}_j \tag{2.5}$$

where the time subscripts and operator hats, have been dropped. Substituting this equation for $j \to j-1$, into equation 2.4 yields:

$$\vec{U}_j + \mathbf{A}_j(\mathbf{B}_j - \mathbf{C}_j\mathbf{E}_{j-1})^{-1}\vec{U}_{j+1} = (\mathbf{D}_j + \mathbf{C}_j\mathbf{F}_{j-1})(\mathbf{B}_j - \mathbf{C}_j\mathbf{E}_{j-1})^{-1} \tag{2.6}$$

Thus comparing equation 2.5 with equation 2.6, we conclude that:

$$\mathbf{E}_j = \mathbf{A}_j(\mathbf{B}_j - \mathbf{C}_j\mathbf{E}_{j-1})^{-1} \tag{2.7}$$

and

$$\mathbf{F}_j = (\mathbf{D}_j + \mathbf{C}_j\mathbf{F}_{j-1})(\mathbf{B}_j - \mathbf{C}_j\mathbf{E}_{j-1})^{-1} \tag{2.8}$$

Equations 2.5, 2.7 and 2.8 form the algorithm for the solution of the triadiagonal system. Given right-hand ($j = jmax$), and left-hand ($j = 0$) boundary conditions on $\vec{U}$, the calculation proceeds in two sweeps:

(i) The left-hand boundary condition is used to determine $\mathbf{E}_0$ and $\mathbf{F}_0$, and then the $\mathbf{E}_j$ and $\mathbf{F}_j$ are calculated by repeated application of equations 2.7 and 2.8 for increasing j ($j = 1, 2 \ldots jmax - 1$).

(ii) The right-hand boundary condition is used to determine $\vec{U}_{jmax}$ and then using $\mathbf{E}_j$ and $\mathbf{F}_j$ from the first sweep, the $\vec{U}_{jmax}$ are calculated by repeated application of equation 2.5 for decreasing j ($j = jmax - 1, jmax - 2 \ldots 1$).

For initial-value problems this procedure must be carried out at each timestep. Thus, for a system of p equations, the major numerical tasks to be performed, per meshpoint, per timestep, are:

(i) The inversion of a $p \times p$ matrix.

(ii) Four separate multiplications of a $p \times p$ matrix by a $p \times p$ matrix.

(iii) The multiplication of a p-dimensional vector by a $p \times p$ matrix.

In ODRIC, the vector $\vec{U}$ is eight-dimensional in complex variables:

$$\vec{U} = \begin{pmatrix} b_r \\ b_\theta \\ T_{e1} \\ v_r \\ v_\theta \\ v_z \\ \rho_1 \\ T_{i1} \end{pmatrix}$$

Thus even the straightforward numerical tasks outlined above, require considerable computing resources. There is a need to minimise the number of times which these tasks must be carried out, i.e. to minimise the number of timesteps required for convergence. Fortunately, savings in c.p.u. time are possible using a method outlined by Charlton [2.4].

2.5 Charlton's Method

Consider, once more, equation 2.1:

$$\mathbf{L}\frac{\partial \vec{U}}{\partial t} = \mathbf{R}\,\vec{U}$$

We established in section 2.1, that for time independent $\hat{\mathbf{L}}$ and $\hat{\mathbf{R}}$, the solution to this equation takes the form:

$$\vec{U}(\vec{r}, t) = \vec{U}(\vec{r})\exp(i\lambda t)$$

where, in general, λ is a complex frequency. Thus in eigenvalue form:

$$i\lambda\mathbf{L}\,\vec{U} = \mathbf{R}\,\vec{U} \tag{2.9}$$

We wish to find the eigenvalue, λ, which is the exact solution to equation 2.1. However, we are using an initial value technique and so the time derivative on the left-hand side of equation 2.1 is not treated exactly, instead it is discretised to give:

$$(\mathbf{L} - \mathbf{R}\Delta t)\vec{U}^{n+1} = \mathbf{L}\,\vec{U}^{n} \tag{2.10}$$

This equation is solved as outlined in the last section. A frequency, ω, is calculated from the ratio of a perturbed quantity at one timestep, to the same quantity at the preceeding timestep:

$$\exp(i\omega t) = \frac{U^{n+1}}{U^{n}} \tag{2.11}$$

where U is a component of $\vec{U}$. In general the calculated frequency, ω, will differ from the exact frequency, λ. Now we seek a relationship between them. Equation 2.9 may be used to eliminate $\mathbf{R}$ in equation 2.10:

$$\mathbf{L}(1 - i\lambda\Delta t)\vec{U}^{n+1} = \mathbf{L}\,\vec{U}^{n}$$

Thus

$$(1 - i\lambda\Delta t)\vec{U}^{n+1} = \vec{U}^{n}$$

and so from equation 2.11 we arrive at a relationship between the calculated frequency and the exact frequency:

$$\exp(i\omega t) = \frac{1}{(1 - i\lambda\Delta t)}$$

Now writing, $\omega = \omega_R + i\omega_I$ and $\lambda = \lambda_I - i\lambda_R$, this equation may be separated in to its real and imaginary parts.

$$\lambda_I\Delta t = \exp(\omega_I\Delta t)\sin(\omega_R\Delta t) \tag{2.12}$$

and

$$\lambda_R\Delta t = 1 - \exp(\omega_I\Delta t)\cos(\omega_R\Delta t) \tag{2.13}$$

Note that as $\Delta t \rightarrow 0$ then $\omega_R \rightarrow \lambda_I$ and $\omega_I \rightarrow -\lambda_R$. Equations 2.12 and 2.13 may be used to correct inaccuracies due to the use of a finite timestep. They are very useful for codes such as ODRIC, which have equations that can yield many solutions (or modes). The initial value technique relies on convergence to the dominant mode, i.e. the one with the fastest growth-rate. Consider, for example, two modes growing with growth rates γ_1 and γ_2, where $\gamma_1 > \gamma_2$. (In the notation used above $\gamma = -\omega_I$). The ratio of the magnitude of the faster growing mode to that of the slower growing mode is proportional to $\exp([\gamma_1 - \gamma_2]t)$. Convergence requires that $[\gamma_1 - \gamma_2]t$ is large. Thus for given γ_1 and γ_2, the numerical integration must be carried out over many growth-times. However, in the interests of economising on c.p.u. time, we wish to limit the number of timesteps required. Therefore we need to be able to use large timesteps. Equations 2.12 and 2.13 allow this without loss of accuracy. Additionally, if we have some idea of the exact frequency (λ), we can calculate the optimum timestep for convergence. This is the timestep that maximises the growth of the numerical solution during one timestep, i.e. maximises $-\omega_I \Delta t$. Using equation 2.12 to eliminate ω_R from equation 2.13 yields:

$$(1 - \lambda_R \Delta t)\exp(-\omega_I \Delta t) = \cos[\arcsin\{\lambda_I \Delta t \exp(-\omega_I \Delta t)\}]$$

In order to simplify notation, let: $\delta = \lambda_R \Delta t$, $\alpha = -\omega_I \Delta t$, and $\chi = \lambda_I / \lambda_R$. Then this equation is:

$$(1 - \delta)\exp(\alpha) = \cos[\arcsin\{\chi\delta\exp(\alpha)\}] \tag{2.14}$$

Now squaring equation 2.14 and using $\sin^2 x = 1 - \cos^2 x$, yields a relationship for the convergence parameter, α, in terms of the exact frequency and the timestep only:

$$\alpha = \frac{1}{2}\ln\left\{\frac{1}{(1-\delta)^2 + \chi^2\delta^2}\right\} \tag{2.15}$$

Using this equation, α versus δ has been plotted out in figure 2.1, for various values of χ. A simple analysis of equation 2.15 shows that α has a maximum at:

$$\delta = \delta_c = \frac{1}{1 + \chi^2} \tag{2.16}$$

with a corresponding value:

$$\alpha = \alpha_{max} = \frac{1}{2}\ln\left\{1 + \frac{1}{\chi^2}\right\} \tag{2.17}$$

Thus the optimum timestep for convergence is:

$$\Delta t_c = \frac{\delta_c}{\lambda_R}$$

Notice, from equation 2.15, that if the exact frequency is purely imaginary ($\chi = 0$), then there is a resonance condition at $\delta = 1.0$. At this point the calculated growth-rate becomes infinite and convergence is achieved immediately. In studies such as this one, in which numerical work is used to extend analytical results, the frequencies are often known to some degree. In this case Δt may be chosen to:

(i) optimise convergence as explained above.

(ii) converge to a mode other than the fastest growing mode. This can be achieved either by "tuning" Δt to make $\delta \sim 1$ for the required mode, or by making $\delta > 2$ for all faster growing modes. In this latter case equation 2.17 shows that a purely growing mode is "numerically stabilised" if $\lambda_R \Delta t = \delta > 2$.

Charlton et al. [2.4] have used the tuning technique in an initial value code to study tokamak stability. Their Crank-Nicholson time-differencing scheme does not however lead to numerically stabilised solutions, in the manner that the fully-implicit scheme considered here does. Thus in ODRIC we have an additional means of converging to the slower growing solutions. However, it should also be noted, that whereas Charlton's code leads to purely growing (or damped) modes, ODRIC in general yields complex frequencies. It is apparent from equations 2.16 and 2.17, and figure 2.1, that as the exact solutions become more oscillatory (and χ increases), the numerical resonance is progressively more strongly damped. Thus for larger χ the convergence parameter becomes much less sensitive to the choice of timestep, and Charlton's method becomes much less useful. Fortunately, there is a simple method for reducing the oscillatory nature of the numerical solution and thus once again aiding convergence.

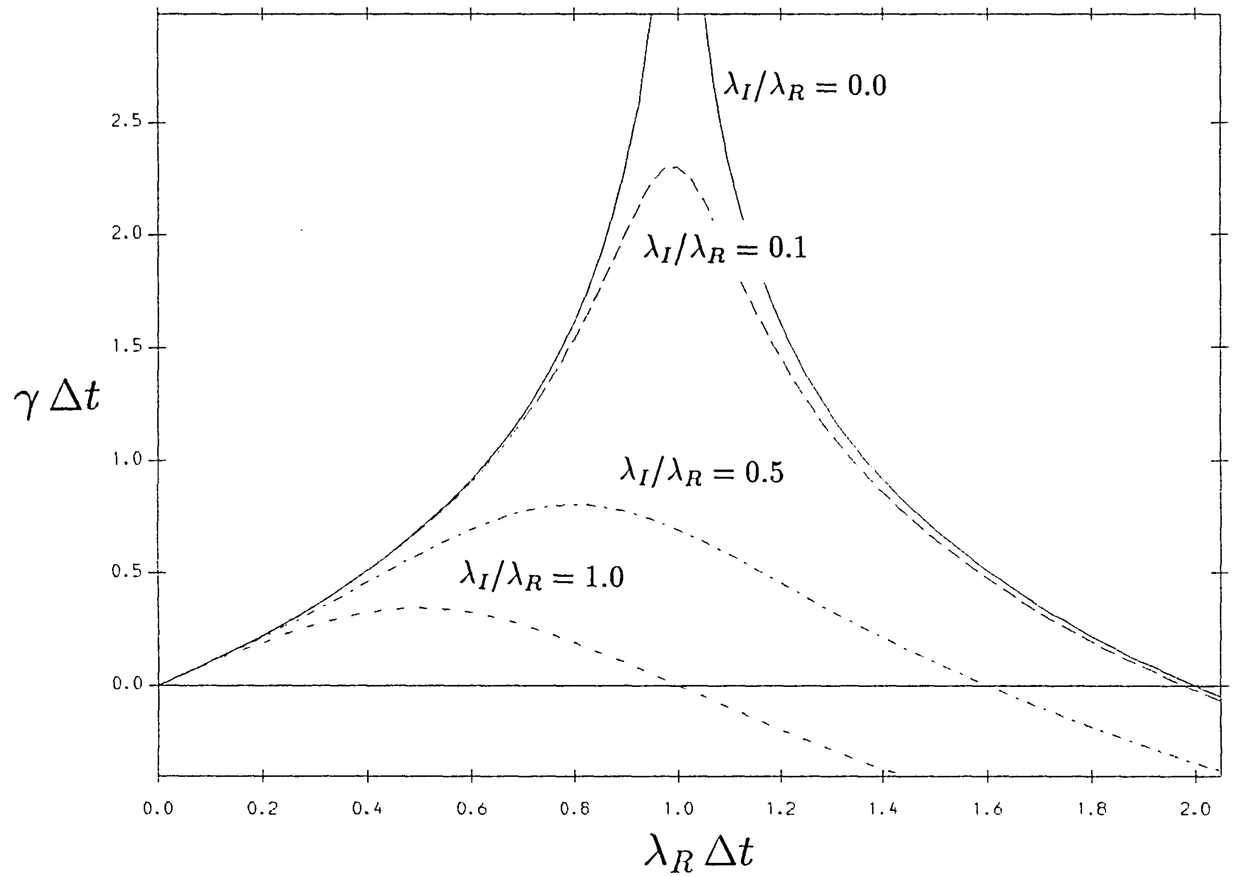

Figure 2.1: Numerically computed growth-rate, γ, versus "true" growth-rate, λ_R, for solutions with various "true" frequencies, λ_I.

2.6 Reducing the Oscillating Nature of the Solution

For the reasons explained above, linear initial-value codes converge slowly to frequencies which have real parts comparable or larger than their growth-rates. This is very unsatisfactory for the study of MHD instabilities in fusion devices, because as we shall see in proceeding chapters, diamagnetic effects often introduce large real frequencies to comparatively slowly growing instabilities. We can alleviate the problem by solving for $\vec{U}' = \vec{U}\exp\{-i\lambda' t\}$ instead of $\vec{U}$ explicitly. Thus equation 2.1 can be written as an equation for $\vec{U}'$:

$$\mathbf{L}(\frac{\partial}{\partial t} + i\lambda')\vec{U}' = \mathbf{R}\,\vec{U}'$$

or in finite difference form:

$$\left(\mathbf{L}\frac{(1+i\lambda'\Delta t)}{\Delta t} - \mathbf{R}\right)\vec{U}'^{n+1} = \frac{\mathbf{L}}{\Delta t}\vec{U}'^{n} \tag{2.18}$$

Thus it is possible to solve for $\vec{U}'$ instead of $\vec{U}$, by replacing Δt by $\Delta t/(1+i\lambda'\Delta t)$, wherever it occurs on the left hand-side of equation 2.4. Now, if $\vec{U}$ has an exact frequency λ, then $\vec{U}'$ has an exact frequency $\lambda - \lambda'$. Thus if λ' is chosen to be of a similar order as the real part of λ, the code has only to converge to a mode with a small real frequency. We know from the previous section that this can be achieved with reasonable efficiency. At the end of the calculation $\vec{U}$ is recovered from $\vec{U} = \vec{U}'\exp(i\lambda'\Delta t)$.

2.7 Summary of Amendments and Additions to ODRIC

In conclusion, the following amendments/improvements have been made to the code:

(i) Equations 2.12 and 2.13 have been implemented to correct frequencies for the effect of using finite timestep.

(ii) Equation 2.3 has been generalised to equation 2.18, to allow the oscillatory part of the frequency to be reduced, and so aid convergence.

(iii) Equilibrium density gradients, which did not appear in the original code, have now been included.

References

[2.1] Mirin, A.A., Bonugli, R.J., O'Neill, N.J., Killeen, J., Comp. Phys. Comm. **41**, 85 (1986).

[2.2] Dibiase, J.A., Killeen, J., J. Comp. Phys. **24**, 158 (1977).

[2.3] Richtmyer, R.D., Morton, K.W., "Difference Methods for Initial Value Problems" (Wiley, New York, 1967), 198.

[2.4] Charlton, L.A., Holmes, J.A., Hicks, H.R., Lynch, V.E., Carreras, B.A., J. Comp. Phys. **63**, 107 (1986).

Chapter 3

Review of Analytical Work on RFP Stability

3.1 Introduction

The reversed field pinch is a toroidal magnetic confinement device in which poloidal and toroidal components of the magnetic field are of a similar magnitude. Its most fundamental phenomena are the spontaneous reversal of the toroidal field at the plasma edge, and the subsequent sustainment of this configuration against resistive diffusion. The self-organisation of the plasma into a reversed field state has been described by a theory due to Taylor [3.1], which is summarised below.

The starting point is the work of Woltjer [3.2], who had shown that in an ideal (dissipationless) plasma, the magnetic helicity, K, associated with each field line is conserved:

$$K = \int_v \vec{A}.\vec{B} d\tau = \text{constant}$$

where the integral is over, v, the volume enclosing a given field line, and $\vec{A}$ is the magnetic vector potential. Taylor recognised that K would no longer be conserved in the more realistic case of a resistive plasma. In fact, resistivity allows field lines to break and reconnect, so that the identity of each field line is not defined for all time. Instead, Taylor postulated that the magnetic helicity of the entire plasma volume, v_0, would be conserved:

$$K_0 = \int_{v_0} \vec{A}.\vec{B} d\tau = \text{constant} \tag{3.1}$$

Equation 3.1 acts as a constraint on the states that are accessible to the plasma. One would expect the minimum energy state to be favoured, so Taylor minimised the magnetic energy of the plasma subject to equation 3.1. The resulting field is given by:

$$\nabla \times \vec{B} = \mu \vec{B} \tag{3.2}$$

where μ is constant over the entire plasma volume. It is determined solely by the helicity, K_0, and the toroidal flux, ψ. The general solution of equation 3.2 (reference [3.3]) is:

$$\vec{B} = \sum a_{m,k}\vec{B}^{m,k}(\vec{r})$$

where the $a_{m,k}$ are arbitrary constants. The $\vec{B}^{m,k}$ are given by:

$$\left.\begin{array}{rcl} B_r^{m,k} &=& -B_0\dfrac{r}{y}[kJ_m'(y) + \mu\dfrac{m}{y}J_m(y)]\sin(m\theta + kz) \\[2ex] B_\theta^{m,k} &=& -B_0\dfrac{r}{y}[\mu J_m'(y) + k\dfrac{m}{y}J_m(y)]\cos(m\theta + kz) \\[2ex] B_z^{m,k} &=& B_0 J_m\cos(m\theta + kz) \end{array}\right\} \tag{3.3}$$

where $y = r\,(\mu^2 - k^2)^{1/2}$, J_m is the m^{th} order Bessel function, and B_0 is a constant. Notice, that the general solution can contain any number of components. However, we must now apply the boundary condition, which for a perfectly conducting wall at $r = a$ is: $B_r(a) = 0$. This condition is satisfied by the axisymmetric $m = 0, k = 0$ component for all μ, but only satisfied by the other components at certain discrete values of μ. The first of these discrete values corresponds to the $m = 1, k \sim 1.25$ component and occurs at $\mu a = 3.11$. Thus the Taylor theory of "relaxed states" predicts:

(i) For $\mu a < 3.11$ the magnetic field will take up the axisymmetric ($m = 0, k = 0$) form:

$$\left.\begin{array}{rcl} B_r &=& 0.0 \\[1ex] B_\theta &=& B_0 J_1(\mu r) \\[1ex] B_z &=& B_0 J_0(\mu r) \end{array}\right\} \tag{3.4}$$

This equilibrium is known as the "Bessel Function Model (BFM)". B_z and B_θ are plotted out in figure 3.1. Notice that for $\mu a > 2.4$ the axial field, B_z, reverses. Thus the theory predicts a reversed field to occur in the pinch for $\Theta > 1.2$, where $\Theta = B_\theta(a)/\langle B_z\rangle = \mu a/2$. This is impressively close to the point at which reversal was observed to occur in Zeta, at $\Theta \sim 1.4$.

(ii) If the volt-seconds are increased such that Θ reaches 1.55, a helical perturbation will appear in the equilibrium. Any further volt-seconds do not increase Θ or the current ($I = \mu\psi$), instead the plasma takes up a more helical form [3.4]. Thus the theory predicts current saturation at $\Theta \sim 1.55$. This was first observed in HBTX1A [3.4].

It is evident that relaxed state theory is a significant contribution to the understanding of RFP behaviour. However, the experimentally observed plasmas differ from the BFM in two significant ways. Firstly, the kinetic pressure is not negligibly small in RFP plasmas. Typically $\beta \sim 5 - 10\%$, yet the BFM confines no pressure. This shortcoming is not surprising since the relaxed state has been derived from the minimisation of the magnetic energy alone, i.e. the thermal energy has been neglected throughout. Secondly, the "μ-profiles" are observed to depart from the constancy that defines the BFM. In fact, the parallel current, ($J_{||} = \vec{J}.\vec{B}/B = \mu B$), appears to decay to zero at the plasma edge. There have been various attempts to extend the theory to account for these discrepancies with experiment. Unfortunately, none have added significantly to its predictive power.

The failure of the plasma to reach a fully relaxed state would appear to be associated with the "sustainment" phenomenon. This is the process by which the pinch maintains a reversed field despite resistive diffusion. All resistive plasmas suffer from magnetic field diffusion according to the curl of Ohm's law:

$$\frac{\partial \vec{B}}{\partial t} = \eta \nabla^2 \vec{B} - \nabla \times (\vec{v} \times \vec{B})$$

Thus to maintain a static state the diffusive term must be balanced by the second term on the right-hand side of this equation. In general this is possible if a non-equilibrium flow velocity, $\vec{v}_0$, is assumed. The resulting induced $\vec{v}_0 \times \vec{B}$ electric field maintains the configuration. However, if an axisymmetric equilibrium has a field zero (or reversal point), it cannot be maintained by such a steady state flow. Consider, once again, Ohm's Law:

$$\vec{E} + \vec{v} \times \vec{B} = \eta \vec{J}$$

Now writing:

$$\vec{E} = -\nabla\phi - \frac{\partial \vec{A}}{\partial t}$$

we have:

$$-\frac{\partial \vec{A}}{\partial t} = \eta \vec{J} - \vec{v} \times \vec{B} + \nabla\phi \tag{3.5}$$

For a steady state we require $\partial/\partial t = 0$. Thus the poloidal component of equation 3.5 yields:

$$v_\theta B_r - v_r B_z - \frac{1}{r}\frac{\partial\phi}{\partial\theta} = \eta J_\theta$$

Now, for an axisymmetric equilibrium $B_r = \partial/\partial\theta = 0$, and so for a steady state:

$$-v_r B_z = \eta J_\theta \tag{3.6}$$

At the reversal point $B_z = 0$ and this equation is violated, i.e. the equilibrium cannot be sustained by a steady state flow. The experimental observation that RFP equilibria can exist for many resistive diffusion times, therefore leads to the conclusion that there must be some time dependent activity that sustains the configuration. In this case equation 3.6 is replaced by:

$$\langle \tilde{\vec{v}} \times \tilde{\vec{B}} \rangle_\theta = \eta J_\theta \tag{3.7}$$

where $\tilde{\vec{v}}$ and $\tilde{\vec{B}}$ are the fluctuating parts of the velocity and magnetic field respectively, and the angled brackets represent a time average. It is widely believed that the required fluctuations are provided by the non-linear evolution, and interaction, of MHD instabilities. Successful numerical simulations of RFP's using 3-dimensional MHD models [3.5, 3.6, 3.7], would seem to support this belief.

In view of the necessity for fluctuations/instabilities in the RFP, it is perhaps not surprising that the Taylor relaxed state is not experimentally observed. By definition, this configuration has the minimum free energy available to drive instabilities. Thus, even if the pinch was at some instant in the fully relaxed state, it would diffuse away from this state until there were sufficient fluctuations for equation 3.7 to be satisfied. In this way the quasi-steady state is a result of the competition between resistive diffusion and relaxation.

The complexity involved in the 3-D numerical simulation of RFP's requires the plasma model chosen to be as simple as possible. Typically a zero-beta, incompressible ($\nabla.\vec{v} = 0$), resistive MHD model is assumed. Although this is sufficient to yield both spontaneous reversal and sustainment, the resulting magnetic fluctuation level is normally larger than that detected in experiments. Additionally, the exclusion of thermal pressure means that the simulations can yield no information on the crucial subject of energy confinement. Apparently, more realistic models need to be studied to compliment the simulations. In particular, calculation of the transport properties of the RFP requires the identification of the relevant confinement degrading instabilities. This latter task is the subject of this and the next chapter, in which the linear stability of RFP equilibria is examined.

In the remainder of this chapter we review some of the most significant pieces of theoretical research on MHD stability of the RFP. This is useful as a grounding for the interpretation of the numerical results to be presented in the next chapter. Beginning with the comparatively simple ideal MHD model, the remaining subsections cover progressively more complicated models.

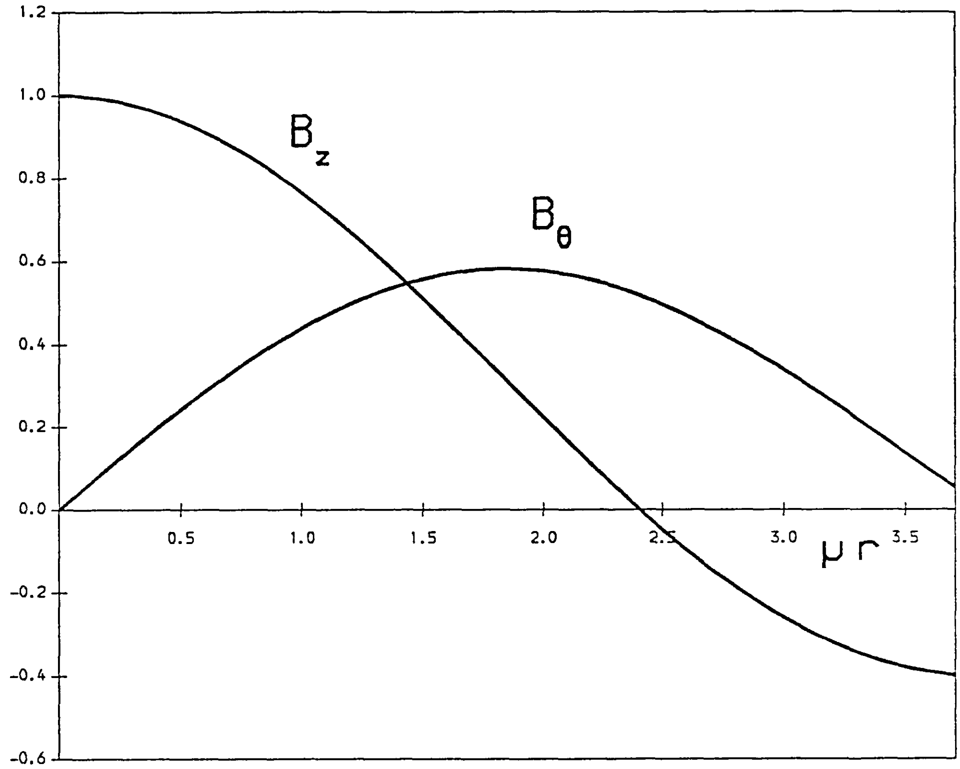

Figure 3.1: Magnetic field profiles for the BFM: $B_z = J_0(\mu r)$, $B_\theta = J_1(\mu r)$.

3.2 Ideal MHD Stability

The equations of ideal MHD are:

$$\begin{aligned}
\frac{\partial \rho}{\partial t} + \nabla.(\rho \vec{v}) &= 0 \\
\rho \frac{D\vec{v}}{Dt} &= \vec{J} \times \vec{B} - \nabla p \\
\vec{E} + \vec{v} \times \vec{B} &= 0 \\
\frac{D}{Dt}\left(\frac{p}{\rho^{\Gamma}}\right) &= 0 \\
\nabla \times \vec{E} &= -\frac{\partial \vec{B}}{\partial t} \\
\nabla \times \vec{B} &= \vec{J} \\
\nabla.\vec{B} &= 0
\end{aligned}$$

where Γ is the ratio of specific heats, and the equations are written in rationalised Gaussian units, with the velocity of light set equal to unity. This is the system to be followed in the remainder of this thesis.

In order to linearise these equations, we write all variables as a time independent equilibrium quantity plus a small time dependent perturbation, e.g. $\vec{B} = \vec{B}_0 + \vec{b}(t)$, $\vec{v} = \vec{v}_0 + \vec{v}_1(t)$. We neglect any equilibrium flow, i.e. set $\vec{v}_0 = 0$ (for a discussion of this assumption see chapter 2), and to simplify notation, drop the subscripts on $\vec{B}_0$ and $\vec{v}_1$. Now, neglecting terms that are second or higher order in perturbed quantities, we arrive at the linear equations:

$$\frac{\partial \rho_1}{\partial t} + \nabla.(\rho_0 \vec{v}) = 0 \tag{3.8}$$

$$\rho_0 \frac{\partial \vec{v}}{\partial t} = \vec{J}_0 \times \vec{b} + \vec{J}_1 \times \vec{B} - \nabla p_1 \tag{3.9}$$

$$\vec{E}_1 + \vec{v} \times \vec{B} = 0 \tag{3.10}$$

$$\frac{1}{\rho_0^\Gamma}\left\{\frac{\partial p_1}{\partial t}+\vec{v}.\nabla p_0\right\}+\frac{p_0}{\rho_0^{\Gamma+1}}\left\{\frac{\partial \rho_1}{\partial t}+\vec{v}.\nabla \rho_0\right\} = 0 \tag{3.11}$$

$$\nabla \times \vec{E}_1 = -\frac{\partial \vec{b}}{\partial t} \tag{3.12}$$

Equations 3.8 and 3.11 yield:

$$\frac{\partial p_1}{\partial t}+\vec{v}\nabla p_0+\Gamma p_0 \nabla \vec{v}=0 \tag{3.13}$$

The time-independent nature of the coefficients of perturbed quantities, implies that the evolution of the perturbation has an exponential form (see chapter 2). Thus the perturbed quantities may be written as:

$$\vec{X}(\vec{r},t)=\vec{X}(\vec{r})\exp(i\omega t)$$

where ω is a frequency to be determined. It is also useful to introduce the "displacement vector", $\vec{\xi}$, which is defined by:

$$\vec{v}=\frac{\partial \vec{\xi}}{\partial t}=i\omega\vec{\xi}$$

Then the curl of Ohm's law (equation 3.10) along with Faraday's Law (equation 3.12) yields:

$$\vec{b}=\nabla \times (\vec{\xi}\times\vec{B}) \tag{3.14}$$

while from equation 3.13 the perturbed pressure is:

$$p_1=\vec{\xi}.\nabla p_0+\Gamma p_0 \nabla.\vec{\xi} \tag{3.15}$$

Now substituting equations 3.14 and 3.15 into equation 3.9:

$$-\omega^2\rho_0\vec{\xi}=(\nabla\times\nabla\times(\vec{\xi}\times\vec{B}))\times\vec{B}+(\nabla\times\vec{B})\times\nabla\times(\vec{\xi}\times\vec{B})+\nabla\left\{\vec{\xi}.\nabla p_0+\Gamma p_0\nabla.\vec{\xi}\right\} \tag{3.16}$$

This is a vector equation for the displacement. It is analogous to equation 1.35, and may be used, (as shown in section 1.3), to derive an energy principle. Thus when we multiply by $\partial\vec{\xi}/\partial t$ and integrate over time, the right-hand side of equation 3.16 yields the change in potential energy per unit volume, due to $\vec{\xi}$. Then, integrating over the volume of the plasma gives the total change in potential energy of the plasma, δW_p. The sign of δW_p determines stability via equation 1.36.

The energy integral has been given in various forms, but perhaps the most revealing is due to Greene and Johnson [3.9]:

$$\delta W_p = \frac{1}{2}\int d\tau \left\{ \left[\vec{b} - \vec{B}\left(\frac{\vec{\xi}.\nabla p_0}{B^2}\right)\right]^2 + \Gamma p_0(\nabla.\vec{\xi})^2 - \left(\frac{\vec{J}_0.\vec{B}}{B^2}\right)(\vec{\xi}\times\vec{B}).\vec{b} - 2(\vec{\xi}.\nabla p_0)(\vec{\xi}.\vec{\kappa}) \right\} \tag{3.17}$$

where $d\tau$ is an element of volume and

$$\vec{\kappa} = (\frac{\vec{B}}{B}\nabla).\frac{\vec{B}}{B}$$

is the magnetic field line curvature. (This equation has been derived assuming that the radial components of the displacement and perturbed magnetic field vanish at the plasma surface, i.e. $\xi_r(a) = b_r(a) = 0$). The first two terms of equation 3.17 are positive definite and thus they have a stabilising influence. However, the remaining two terms may be negative and so they are the driving terms for instability.

(i) $-(\vec{J}_0.\vec{B}/B^2)(\vec{\xi}\times\vec{B}).\vec{b}$ represents the change in free energy associated with the current. It can lead to instability for $\vec{J}_0.\vec{B} \neq 0$, i.e. parallel currents may drive instability.

(ii) $-2(\vec{\xi}.\nabla p_0)(\vec{\xi}.\vec{\kappa})$ represents the change in free energy associated with pressure gradients. It is destabilising for $\vec{\kappa}.\nabla p_0 > 0$, i.e. when the curvature of the field and the pressure gradient are in the same direction.

Instabilities that are driven by parallel currents are known as "kinks" and instabilities driven by pressure gradients are known as "interchanges". However, this terminology can be misleading since generally instabilities arise from a combination of both driving terms.

Equation 3.17 is the change in potential energy of the plasma alone. If the plasma is surrounded by vacuum then $\xi(a) \neq 0$, and the total potential energy change is:

$$\delta W = \delta W_p + \delta W_s + \delta W_v$$

where δW_s is the work done in distorting the plasma surface and δW_v is the change in potential energy of the vacuum. If the plasma is directly in contact with a perfectly conducting wall, $\xi(a) = 0$ so that $\delta W_s = \delta W_v = 0$, and any resulting instabilities are known as "internal modes". On the otherhand, if an instability distorts the plasma surface it is known as an "external mode".

Equation 3.17 may be reduced to a more convenient form for cylindrical pinches [3.10]:

$$\delta W_p = \frac{\pi}{2} \int_0^a dr \left\{ f \left(\frac{d\xi}{dr} \right)^2 + g\xi^2 \right\} \tag{3.18}$$

where ξ is the radial component of displacement vector, a is the plasma radius and

$$f = \frac{r^3(\vec{k}.\vec{B})^2}{m^2 + k^2r^2} = \frac{r(krB_z + mB_\theta)^2}{m^2 + k^2r^2}$$

$$g = \frac{2k^2r^2}{m^2 + k^2r^2}\frac{dp}{dr} + \frac{(m^2 + k^2r^2 - 1)}{(m^2 + k^2r^2)}\frac{(krB_z + mB_\theta)^2}{r} + \frac{2k^2r^2}{(m^2 + k^2r^2)^2}(k^2r^2B_z^2 - m^2B_\theta^2)$$

In order to determine stability we must determine the sign of the minimum value of δW_p. If δW_p is negative the energy principle tells us that the plasma is unstable (see section 1.3). The displacement that minimises δW_p is provided by variational calculus:

$$\frac{d}{dr}\left(f\frac{d\xi}{dr} \right) - g\xi = 0 \tag{3.19}$$

This is "Newcomb's equation". Its solution may be substituted back into the energy integral to reveal whether the plasma is stable or not. However, theorems due to Newcomb [3.10] may be used to determine stability (or otherwise) directly from the solution of equation 3.19, i.e. without the need to compute equation 3.18. Some of Newcomb's theorems will be used later in this thesis. For the time being though, just consider the structure of equations 3.18 and 3.19. Note that Newcomb's equation has regular singular points wherever $f = 0$, i.e. wherever $\vec{k}.\vec{B} = 0$. These radial locations are known as "resonant points", since they correspond to positions where the pitch of the perturbation matches that of the equilibrium magnetic field. Also, we observe from equation 3.18, that the $f(d\xi/dr)^2$ term is positive definite and thus that it is a stabilising contribution. However at a resonant point, $r = r_s$, this contribution vanishes, and so we might expect perturbations localised here to be the most unstable. The stability analysis for displacements that are localised around resonant points was carried out by Suydam [3.11] and is summarised below.

3.2.1 A Local Stability Condition

We begin by expanding equation 3.19 about the resonant point, $r = r_s$, where $f(r_s) = f'(r_s) = 0$. (As usual primes denote radial derivatives). Let $x = |r - r_s|$ and write:

$$f = \frac{1}{2}f_s''x^2 = \frac{r_s B_\theta^2 B_z^2}{B^2}\left(\frac{P'}{P}\right)^2 x^2$$

and

$$g = \frac{2B_\theta^2}{B^2}\frac{dp}{dr}$$

where $P = rB_z/B_\theta$ is known as the "pitch". Thus equation 3.19 becomes:

$$\frac{d}{dx}\left(x^2\frac{d\xi_s}{dx}\right) + D_s\xi_s = 0 \qquad (3.20)$$

where the "Suydam parameter",

$$D_s = -\frac{2p'}{B_z^2 r_s}\left(\frac{P'}{P}\right)^2$$

Equation 3.20 has a series solution:

$$\xi_s = Ax^{\nu}(1 + a_1x + a_2x^2 + \cdots) + Bx^{-\nu-1}(1 + b_1x + b_2x^2 + \cdots)$$

where $A, B, a_1, b_1, a_2, b_2, \cdots$ are constants and:

$$\nu = -\frac{1}{2} + \frac{1}{2}(1 - 4D_s)^{1/2}$$

At least one of these solutions for ξ_s is singular in the $x \to 0$ limit. Thus it is not possible to use ξ_s directly as a trial function in the energy integral. Instead we must seek to construct a well behaved unstable displacement ($\delta W_p < 0$) by modifying the behaviour of ξ_s as $x \to 0$.

For $D_s > 1/4$, ν is complex and ξ_s takes the following form for small x:

$$\xi_s = C|x|^{-1/2} \cos\{\chi \ln x + \phi\} \tag{3.21}$$

where $C^2 = 4AB$, $\chi = (D_s - 1/4)^{1/2}$, and $\tan\phi = i(B - A)/(B + A)$. As $|x| \to 0$ the amplitude of ξ_s becomes infinitely large, and it oscillates infinitely rapidly in $|x|$. This is obviously unphysical behaviour and we conclude that the solution is not suitable for computing the energy integral. Nevertheless equation 3.21 may be used as the basis for a well-behaved displacement:

$$\xi = \xi_s \quad \text{for} \quad |x| > \epsilon$$

$$\xi = \xi_s(\epsilon) = \xi_c \quad \text{for} \quad |x| < \epsilon$$

It is straightforward to calculate the energy integral (equation 3.18) for this trial function:

$$\delta W_p = \frac{\pi}{2}\left[f\xi_s\frac{d\xi_s}{dr}\right]_0^{r_s-\epsilon} + \frac{\pi}{2}\left[g\xi_c^2 r\right]_{r_s-\epsilon}^{r_s+\epsilon} + \frac{\pi}{2}\left[f\xi_s\frac{d\xi_s}{dr}\right]_{r_s+\epsilon}^{a}$$

Now applying the boundary conditions $\xi(0) = \xi(a) = 0$ we evaluate this expression and find:

$$\delta W_p = -\frac{C^2\pi f_s''}{2}\left[\left(D_s - \frac{1}{2}\right)\cos^2\theta + \chi\cos\theta\sin\theta\right]$$

where $\theta = \chi \ln|x| + \phi$. An alternative form for this expression is:

$$\delta W_p = -\frac{C^2\pi f_s''}{4}\left[\left(D_s - \frac{1}{2}\right) + D_s \cos\left\{\cos^{-1}\left(\frac{2D_s - 1}{2D_s}\right) + 2\theta\right\}\right]$$

We must choose the value of ϵ which minimises δW_p, and since $f_s'' > 0$ this corresponds to making the argument of the cosine equal to $2\pi n$:

$$\delta W_p^{min} = -\frac{C^2\pi f_s''}{2}\left(D_s - \frac{1}{4}\right)$$

Thus we have a negative δW_p and an unstable displacement whenever $D_s > 1/4$.

To determine whether there is an instability for $D_s < 1/4$ the above procedure must be repeated for real ν. However, in this case it is not possible to construct a well behaved displacement that makes the energy integral negative. Thus for perturbations localised around a resonant point we have the necessary stability condition:

$$D_s < 1/4$$

or equivalently

$$-\frac{dp}{dr} < \frac{rB_z^2}{8}\left(\frac{P'}{P}\right)^2 \tag{3.22}$$

This is "Suydam's criterion", which expresses the maximum stable pressure gradient for a given magnetic field configuration. It arises from the competition between the destabilising interchange term, and the stabilising effect of "shear". This can be seen more clearly if equation 3.22 is rewritten as:

$$\vec{\kappa}.\nabla p < \frac{B^2}{8}\frac{(\vec{k}.\vec{B})'^2}{|\vec{k}||\vec{B}|} \tag{3.23}$$

where $\vec{k} = \vec{\hat{\theta}} m/r + \vec{\hat{z}} k$ and in a cylinder the curvature vector is given by:

$$\vec{\kappa} = -\vec{\hat{r}}\frac{B_\theta^2}{r^2 B^2}$$

Previously, examination of the energy integral indicated that any $\vec{\kappa}.\nabla p > 0$ has a destabilising influence (i.e. lowers δW_p). From equation 3.23 we see that finite, positive values of $\vec{\kappa}.\nabla p$ can be made stable by the radial variation of the field (i.e. the shear). This can be understood by recalling that for $\vec{k}.\vec{B} \neq 0$ there is a stabilising term in the energy integral. This term arises from the work required to bend magnetic field lines. At the resonant point the pitch of the perturbation matches that of the field lines and no work is required. However, even a short distance from the resonance, $\vec{k}.\vec{B}$ need not be precisely zero and there can be a resulting stabilising contribution to the energy integral. Thus Suydam's criterion states the rate at which $\vec{k}.\vec{B}$ must change in order to stabilise a given interchange driving term.

Note that equation 3.22 is a only a necessary condition for stability. It cannot be a sufficient condition since the analysis is a local one, i.e. it assumes that the perturbation is localised about a resonant point. The absence of the parallel current driving term from Suydam's condition, implies that it has a negligible effect on this class of displacements. However, now we consider more global modes in which the parallel current will be seen to be of great importance.

3.2.2 Global Stability Requirements

Examination of the energy integral can yield some general stability requirements, that may be used to construct equilibria that are stable to ideal MHD instabilities.

Consider a system that has a perfectly conducting wall at $r = a$. In this case equation 3.18 contains the information about plasma stability. Note, from equation 3.18, that a sufficient condition for stability is: $g(r) > 0$ for $0 < r < a$. However, in general there is a non-negligible stabilising contribution from the $f(d\xi/dr)^2$ term, so that this condition is too stringent to be useful. Nevertheless, the functional form of g must have an important influence on stability. We consider $m = 1$ modes and write g in terms of the pitch, P:

$$g = \frac{2k^2r^2}{1+k^2r^2}\frac{dp}{dr} + \frac{k^2 r B_\theta^2}{(1+k^2r^2)^2}(kP+1)(kP[3+k^2r^2]+k^2r^2-1) \qquad (3.24)$$

(The choice of $m = 1$ is not as arbitrary as it may appear. The first of Newcomb's theorems [3.10] states: " A linear pinch is stable for all values of m and k if and only if it is stable for $m = 1$, $-\infty < k < \infty$ and for $m = 0$, $k \to 0$." Thus in cylindrical geometry the stability of $m = 1$ is of particular significance). The pressure decreases outwards in pinches and so the first term of g is normally destabilising. However, we neglect this term and consider purely current driven modes, i.e.

$$g = g_J = \frac{k^2 r B_\theta^2}{(1 + k^2 r^2)^2}(kP + 1)(kP[3 + k^2 r^2] + k^2 r^2 - 1) \tag{3.25}$$

The sufficient condition (for current driven modes), $g_J > 0$, yields:

$$kP < -1 \quad \text{or} \quad kP > \frac{1 - k^2 r^2}{3 + k^2 r^2} \tag{3.26}$$

Now, if there is some region of the plasma over which g_J is negative, we might expect that a displacement localised here would be unstable. Specifically, a function that is zero in the $g_J > 0$ regions and a finite constant in the $g_J < 0$ region, will avoid both stabilising terms in the energy integral, equation 3.18. Figure 3.2 shows various pitch profiles, and the regions over which g_J is negative. Also shown in figures 3.2(i) and 3.2(ii) are the unstable trial functions. Figure 3.2(i) corresponds to a tokamak type profile, i.e. a monotonically increasing pitch profile which, by symmetry, has a minimum on axis. While figure 3.2(ii) is similar to the recently measured "Ultra-Low q (ULQ)" profiles [3.12], which have a pitch minimum off axis. In both cases, the eigenfunctions shown indicate that a pitch minimum is unstable to current driven modes. Additionally, Suydam's criterion indicates that localised pressure driven modes will also be unstable at a pitch minimum, (for any negative pressure gradient). We conclude that a cylindrical plasma can only be stable if it has a monotonically decreasing pitch profile, since this is the only way that a minimum in the pitch can be avoided.

The above constraint on the equilibrium can be strengthened for the case when a vacuum region exists between the plasma edge, $(r = r_p)$, and the conducting wall, $(r = a)$. The vacuum magnetic field is given by:

$$\nabla \times \vec{B} = \vec{J} = 0$$

with the corresponding pitch, P_v:

$$P_v(r) = \left(\frac{r}{r_p}\right)^2 P(r_p)$$

where $P(r_p)$ is the pitch at the plasma edge. For monotonically decreasing $P(r)$ this equation implies a pitch minimum at $r = r_p$ if $P(r_p) > 0$. Thus for stability with a vacuum region we require $P(r_p) < 0$, i.e. the pitch must reverse somewhere within the plasma. The RFP corresponds to such a configuration.

In conclusion, the attempt to avoid the instabilities associated with pitch minima has lead to an RFP type equilibrium. In contrast, tokamak equilibria would appear to be unstable because they have a pitch minimum. However, this is an incorrect conclusion since we have neglected the toroidal geometry of this device.

The most elementary effect of the toroidal geometry is the quantisation of the axial wavenumber:

$$k = \frac{n_k}{R_0}$$

where R_0 is the major radius of the torus, and n_k is an integer (the toroidal mode number). Thus for toroidal machines, k should be replaced by n_k/R_0. So that $g_J > 0$ gives (for $m = 1$):

$$n_k q < -1 \quad \text{or} \quad nq < -\frac{R_0^2 - n_k^2 r^2}{3R_0^2 + n_k^2 r^2} \tag{3.27}$$

where $q = P/R_0$ is the "safety factor". Note that if $n_k q < -1$, $m = 1$ current driven modes are stable. For a tokamak-profile this sets a limit on the on-axis value of q (for negative n_k):

$$q(0) > -\frac{1}{n_k}$$

Thus for $n_k = -1$ the configuration is stable if $q(0) > 1$. This requirement appears to be very important in tokamaks where its violation is associated with the "sawtooth" phenomenon.

Ensuring that the on-axis q is larger than unity, is also enough to avoid the localised pressure-driven modes. This is because, for a large aspect ratio tokamak, Suydam's criterion should be replaced by Mercier's criterion [3.13]:

$$-\frac{dp}{dr}(1-q^2) < \frac{rB_z^2}{8}\left(\frac{P'}{P}\right)^2 \tag{3.28}$$

The $-p'q^2$ term is due to toroidal curvature, which unlike the poloidal curvature, is favourable for stability. For $q > 1$ the toroidal curvature is sufficient to allow a negative pressure gradient to be supported even at a pitch minimum. (Note however, that toroidicity does not provide stability to all localised pressure driven modes. Regions of unfavourable curvature exist on the outside of a torus and this can lead to poloidally localised "ballooning" instabilities). We also note in passing that Mercier's criterion reduces to Suydam's criterion for small q. Thus in an RFP, where typically $q < 1/3$, there is only a small toroidal correction.

The above offers an interesting insight into the very different natures of tokamak and RFP configurations. It is apparent that the tokamak is very dependent on its toroidal geometry. The $q > 1$ requirement demands a large axial field in a moderate aspect ratio tokamak, or a moderate axial field in a very tight aspect ratio tokamak. On the otherhand the RFP can be stable even in cylindrical geometry. Instead it relies on the shear associated with the reversed field to provide stability. Consequently, there are no constraints on the aspect ratio of an RFP and its geometry may be selected to minimise engineering difficulty and cost. This is one of the reasons that RFP's are still widely studied, despite the more advanced status of tokamak research.

Having established the special nature of RFP equilibria, we now summarise further stability constraints on such configurations.

(i) **Pressure Profile on Axis**

In a cylindrically symmetric equilibrium, continuity at the origin requires that any non-zero variable must have zero first derivative. Thus both $P'(0) = 0$ and $p'(0) = 0$. This means that Suydam's criterion must be re-evaluated, including the next order terms in the expansion about $r = r_s$. The resulting stability condition for small r, is:

$$\left[\frac{1}{2}B_z(0)\frac{\sigma''(0)}{\sigma(0)}\right]^2 r^2 + 8p''(0) > 0$$

where $\sigma = 1/P$. The first term is positive definite but becomes negligibly small as $r \rightarrow 0$. Thus for stability we require:

$$p''(0) \geq 0$$

i.e. the pressure profile must be hollow or flat on-axis.

(ii) **Depth of Field Reversal**

Recall equation 3.26, which gives the conditions for stability to $m = 1$ current driven modes. For $k > 0$ and small k^2r^2 we have:

$$P < -\frac{1}{k} \quad \text{or} \quad P > \frac{1}{3k}$$

Thus for a reversed pitch-profile we must have:

$$P(0) > -\frac{1}{3}P(a)$$

This is a limitation on the depth of reversal of the axial field. If the radius of the current channel, r_c, is defined by $r_c^2 = I/\pi J_z(0)$, then this condition can be written as [3.14]:

$$\frac{r_c^2}{a^2} < -3\frac{B_z(0)}{B_z(a)}$$

This expresses the importance of the conducting wall for RFP stability. If the conducting wall is too far from the current channel, current driven instabilities will occur.

(iii) **Poloidal Beta Limit**

Robinson [3.15] has considered the stability of $m = 0$ modes. Using a trial function in the energy principle, he has derived a limit on the total plasma pressure that can be confined without loss of stability. Specifically, there is a condition on the poloidal beta:

$$\beta_\theta = \frac{4}{a^2 B_\theta^2} \int_0^a rp dr < \frac{1}{2}$$

Conditions (i) to (iii) above may be used as guidelines in the attempt to construct MHD stable equilibria. Robinson [3.15] has carried out this procedure and arrives at an equilibrium that appears stable, for β_θ as large as 31%. Unfortunately values of 5 to 10% are more typical in RFP experiments. We conclude that marginal Ideal MHD stability does not accurately describe the RFP, and proceed to more complete stability models.

3.3 Resistive MHD Stability

The only change in going from ideal to resistive MHD is in Ohm's law, which becomes:

$$\vec{E} + \vec{v} \times \vec{B} = \eta \vec{J}$$

Taking the curl:

$$\frac{\partial \vec{B}}{\partial t} = \nabla \times (\vec{v} \times \vec{B}) - \eta \nabla \times \nabla \times \vec{B} \tag{3.29}$$

The linearised version of this equation yields:

$$\vec{b} = \nabla \times (\vec{\xi} \times \vec{B}) + \frac{\eta}{\gamma} \nabla^2 \vec{b} \tag{3.30}$$

where we have written $\vec{v} = \gamma \vec{\xi}$, i.e. γ is the growth rate. Equation 3.30 is the resistive version of equation 3.14. Note the additional term, which represents diffusion of the magnetic field. At high temperatures the $\eta \propto T^{-3/2}$ dependence of the resistivity, means that this term is small even for slowly growing instabilities. However, the resistivity proves to have a significant effect on plasma stability.

Consider equation 3.30. We expand the first term on the r.h.s.:

$$\nabla \times (\vec{\xi} \times \vec{B}) = -(\vec{\xi}.\nabla)\vec{B} - \vec{B}\nabla.\vec{\xi} + (\vec{B}.\nabla)\vec{\xi} + \vec{\xi}\nabla.\vec{B}$$

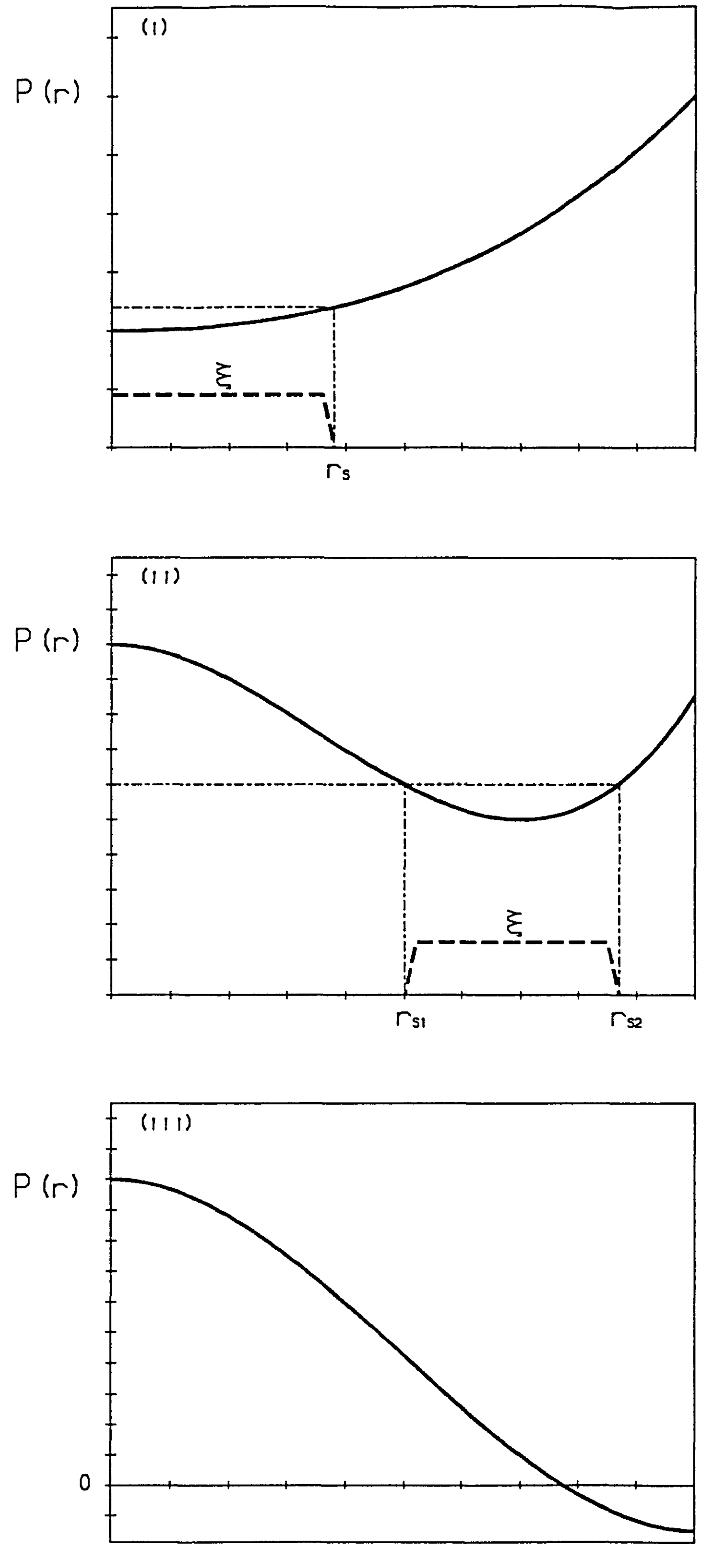

Figure 3.2: (i) a monotonically increasing pitch-profile with a minimum on axis, (ii) a pitch-profile with a minimum off axis, (iii) a monotonically decreasing and reversing pitch profile.
For profiles (i) and (ii) the pitch minimum allows an unstable eigenfunction, ξ, to be constructed.

Now using $\nabla.\vec{B} = 0$ and $B_r = 0$ (for an axisymmetric equilibrium), we conclude:

$$\nabla \times (\vec{\xi} \times \vec{B})|_r = (\vec{B}.\nabla)\xi$$

where once again ξ is the radial component of $\vec{\xi}$. Thus the radial component of equation 3.30 becomes:

$$b_r = (\vec{B}.\nabla)\xi + \frac{\eta}{\gamma}\nabla^2\vec{b}|_r$$

and for $\xi(\vec{r}) = \xi(r)\exp(im\theta + ikz)$:

$$b_r = i(\vec{k}.\vec{B})\xi + \frac{\eta}{\gamma}\nabla^2\vec{b}|_r \tag{3.31}$$

where $\vec{k} = \hat{\vec{\theta}}m/r + \hat{\vec{z}}k$. Equation 3.31 indicates that the resistive term is not negligible at the resonant points, where $\vec{k}.\vec{B} = 0$. At these locations the radial magnetic field obeys a diffusion equation, i.e. close to the resonant points the field can diffuse through the plasma. This is contrary to the case in ideal MHD, in which the magnetic field is "frozen" into the plasma. To demonstrate this we integrate equation 3.29 over a surface, $\vec{S}$:

$$\int \frac{\partial \vec{B}}{\partial t}.d\vec{S} = \int \nabla \times (\vec{v} \times \vec{B}).d\vec{S} + \eta \int \nabla^2 \vec{B}.d\vec{S} \tag{3.32}$$

Now Stoke's theorem allows us to write:

$$\int \nabla \times (\vec{v} \times \vec{B}).d\vec{S} = \oint (\vec{v} \times \vec{B}).d\vec{l} = -\oint \vec{B}.(\vec{v} \times d\vec{l})$$

where $d\vec{l}$ is a line element and $\oint$ represents integration along a contour that encloses $\vec{S}$. Thus equation 3.32 becomes:

$$\int \frac{\partial \vec{B}}{\partial t}.d\vec{S} + \oint \vec{B}.(\vec{v} \times d\vec{l}) = \eta \int \nabla^2 \vec{B}.d\vec{S} \tag{3.33}$$

The l.h.s. of this equation is the total time-derivative of the magnetic flux, ψ, that intersects the surface, where:

$$\psi = \int \vec{B}.d\vec{S}$$

The first term of equation 3.33, represents the change in the flux due to the time variation of the field, whilst the second term is the change due to the time variation of $\vec{S}$. Therefore we have:

$$\frac{d\psi}{dt} = \frac{\partial\psi}{\partial t} + \vec{v}.\nabla\psi = \eta \int \nabla^2 \vec{B}.d\vec{S} \tag{3.34}$$

Note that in the absence of resistivity, the flux threading a given fluid element is constant. For this reason the magnetic field is said to be "frozen" into the plasma. In contrast, resistivity permits the flux intersecting a given element to change. As a result the resistivity allows the magnetic field an additional degree of freedom, with which we might expect new instabilities to be associated.

The equations that govern resistive stability are:

$$\gamma^2 \rho \vec{\xi} = (\nabla \times \vec{B}) \times \vec{b} + (\nabla \times \vec{b}) \times \vec{B} + \nabla(\vec{\xi}.\nabla p_0 + \Gamma p_0 \nabla.\vec{\xi}) \tag{3.35}$$

$$\vec{b} = \nabla \times (\vec{\xi} \times \vec{B}) + \frac{\eta}{\gamma}\nabla^2 \vec{b} \tag{3.36}$$

These equations replace equation 3.16. Notice that resistivity increases the order of the equations from second to fourth order in perturbed variables. This obviously increases the mathematical complexity of the problem. However, we may utilise the fact that the resistivity is only important in a narrow layer about the resonant surface. This means that most of the plasma can be described by the simpler ideal equations. Whilst in the resistive layer, the problem is simplified because its narrowness allows equilibrium variables to be treated as constants (defined at $r = r_s$). Asymptotic matching of the ideal and resistive layer solutions will then define the complete solution, and yield a dispersion relation for the growth-rate. We now consider the layer equations in more detail, following the original work of Coppi, Greene and Johnson [3.16] (hereafter CGJ).

Even allowing for the spatial independence of equilibrium quantities, the layer equations remain too complicated for an analytic solution. Fortunately they may be simplified by an "ordering procedure". This is merely the process of selecting solutions of a certain type. Effectively, constraints are placed on the solution and these are then used to determine the relative magnitudes of quantities in the system of equations. Generally this allows certain higher order terms to be neglected and results in a simplification of the problem. Below we summarise the ordering used by CGJ.

To begin with we define a co-ordinate system such that:

$$\vec{b} = \hat{\vec{r}} b_r + \hat{\vec{i}}_{||} b_{||} + \hat{\vec{i}}_{\perp} b_{\perp}$$

where $\hat{\vec{i}}_{||}$ is the unit vector in the direction of the magnetic field and $\hat{\vec{i}}_{\perp} = \hat{\vec{r}} \times \hat{\vec{i}}_{||}$. Each perturbed variable can be written as an expansion in a small parameter, ϵ. Thus, for example:

$$\begin{aligned}\vec{b} = \hat{\vec{r}}(b_r^{(0)} + \epsilon b_r^{(1)} + \epsilon^2 b_r^{(2)} + \cdots) \quad &+ \quad \hat{\vec{i}}_{||}(b_{||}^{(0)} + \epsilon b_{||}^{(1)} + \epsilon^2 b_{||}^{(2)} + \cdots) \\ &+ \quad \hat{\vec{i}}_{\perp}(b_{\perp}^{(0)} + \epsilon b_{\perp}^{(1)} + \epsilon^2 b_{\perp}^{(2)} + \cdots)\end{aligned}$$

We choose the expansion parameter to be the distance from the singular surface, $\epsilon = r - r_s$, and consider the radial derivative of a perturbed quantity to be a factor $1/\epsilon$ larger than the quantity itself. Now the following assumptions are made:

(i)

$$\vec{b} \sim \epsilon \vec{\xi} \tag{3.37}$$

This ensures that the $(\vec{k}.\vec{B})\vec{\xi}$ term on the r.h.s. of equation 3.36 is of the same order as the first term on the l.h.s.

(ii)

$$\vec{B}.\vec{b} + p_1 \sim 0 \tag{3.38}$$

This is the condition for pressure balance along the field-lines. It's validity is dependent on the relevant motions being much slower than the magneto-acoustic velocity, i.e. $\gamma^2 \ll k_{\perp}^2(B^2 + \Gamma p)/\rho$ where $k_{\perp}$ is the component of the wavevector perpendicular to the field. Thus, equation 3.38 specialises the analysis to instabilities that grow much slower than ideal modes.

Theses two assumptions allow the relative magnitudes of the components of $\vec{b}$ and $\vec{\xi}$ to be determined. To begin with, $\nabla.\vec{b} = 0$ to all orders, implies:

$$b_r \sim \epsilon b_{\|}, \epsilon b_{\perp}$$

So, from equation 3.37 we conclude :

$$b_r \sim \epsilon^2, b_{\|} \sim b_{\perp} \sim \epsilon$$

Now equation 3.38 yields:

$$Bb_{\|}^{(1)} - p\xi_r - \Gamma p(\nabla.\vec{\xi}) = 0 \tag{3.39}$$

Thus to $O(\epsilon^{-1})$:

$$(\nabla.\vec{\xi})^{(-1)} \sim \frac{\xi_r^{(0)}}{\epsilon} = 0 \Longrightarrow \xi_r^{(0)} \sim 0$$

and to $O(\epsilon)$ equation 3.39 gives:

$$(\nabla.\vec{\xi})^{(0)} = 0 \Longrightarrow \xi_r \sim \epsilon\xi_{\|}, \epsilon\xi_{\perp}$$

So the ordering demanded by equations 3.37 and 3.38 is:

$$\vec{b} = \hat{\vec{r}}(\epsilon^2 b_r^{(2)} + \cdots) + \hat{\vec{i}}_{\|}(\epsilon b_{\|}^{(1)} + \cdots) + \hat{\vec{i}}_{\perp}(\epsilon b_{\perp}^{(1)} + \cdots) \tag{3.40}$$

$$\vec{\xi} = \hat{\vec{r}}(\epsilon\xi_r^{(1)} + \cdots) + \hat{\vec{i}}_{\|}(\xi_{\|}^{(0)} + \cdots) + \hat{\vec{i}}_{\perp}(\xi_{\perp}^{(0)} + \cdots) \tag{3.41}$$

Using this ordering we find that the resistive layer is described in lowest-order by:

$$\begin{aligned}
\frac{d\xi_r}{dr} + \frac{ikB}{B_\theta}\xi_{\perp} &= 0 && (3.42)\\
\frac{db_r}{dr} + \frac{ikB}{B_\theta}b_{\perp} &= 0 && (3.43)\\
Bb_{\|} &= p\xi_r + \Gamma p(\nabla.\vec{\xi}) && (3.44)\\
\rho\gamma^2 B\xi_{\|} &= -p'b_r + i(\vec{k}.\vec{B})'xb_{\|} && (3.45)
\end{aligned}$$

$$\rho\gamma^2\xi_r'' = \frac{2k^2B}{r_s}b_{\|} + i(\vec{k}.\vec{B})'xb_r'' \tag{3.46}$$

$$b_r - \frac{\eta}{\gamma}b_r'' = i(\vec{k}.\vec{B})'x\xi_r \tag{3.47}$$

$$b_{\|} - \frac{\eta}{\gamma}b_{\|}'' = i(\vec{k}.\vec{B})'x\xi_{\|} - B(\nabla.\vec{\xi}) - \frac{(p+B^2)'}{B}\xi_r \tag{3.48}$$

where $x = r - r_s$, and each equilibrium quantity is evaluated at $r = r_s$. Equations 3.42 and 3.43 are $\nabla.\vec{\xi} = 0$ and $\nabla.\vec{b} = 0$ respectively, while equation 3.44 is merely the assumed pressure balance along the field. Equations 3.47 and 3.48 are the radial and parallel components of Ohm's law. Equation 3.45 is the parallel component of the momentum equation. Thus, equation 3.46 is the only equation that is neither a component of equation 3.35 or 3.36, nor directly derived from the ordering. This equation is known as the "annihilated momentum equation", and it results from operating on equation 3.35 with the operator $\nabla.(\vec{B}/B)\times$. For further details the reader is referred to CGJ [3.16].

The system of equations 3.42 to 3.48 can be reduced to three second order differential equations:

$$\Psi'' = Q(\Psi + X\xi) \tag{3.49}$$

$$\xi'' = \frac{X^2}{Q}\xi + \frac{X}{Q}\Psi - \frac{1}{Q}\Upsilon \tag{3.50}$$

$$\Upsilon'' = Q\left(1 + \frac{X^2}{Q^2} + \frac{2}{\Gamma\beta}\right)\Upsilon + Q\left(s - D - \frac{2D}{\Gamma\beta}\right)\xi + \frac{D}{Q}X\Psi \tag{3.51}$$

where $\xi = \xi_r$,

$$\Psi = \frac{-ir_s}{kP'B_\theta L_r}b_r,$$

$$\Upsilon = -2Br_sP'^2B_\theta^2 b_{\|}$$

and $Q = \gamma/Q_r$, $X = x/L_r$ with

$$Q_r = \left(\frac{\eta k^2 P'^2 B_\theta^2}{\rho r_s^2}\right)^{1/3}$$

and

$$L_r = \left(\frac{\rho \eta^2 r_s^2}{k^2 P'^2 B_\theta^2} \right)^{1/3}$$

The remaining symbols in the equations are equilibrium parameters:

$$\begin{aligned} D &= -2p' r_s / B_\theta^2 P'^2 \text{ is Suydam's parameter} \\ \beta &= 2p(r_s)/B^2 \text{ is the beta value at the resonant point} \\ s &= 4/P'^2 \end{aligned}$$

The first thing to notice about equations 3.49 to 3.51, is their behaviour under the reflection $X \to -X$. By inspection we can see that the parity of Ψ is always opposite to that of Υ and ξ. Thus there are two solutions, one corresponding to an even parity ξ (odd Ψ) and the other corresponding to an odd parity ξ (even Ψ). The relevant conditions at the origin are:

$$\text{TWISTING} \qquad \xi'(0) = 0 \; ; \; \Upsilon'(0) = 0 \; ; \; \Psi(0) = 0 \tag{3.52}$$

$$\text{TEARING} \qquad \xi(0) = 0 \; ; \; \Upsilon(0) = 0 \; ; \; \Psi(0)' = 0 \tag{3.53}$$

In general the "twisting" and "tearing" parity modes have different growth-rates, and so they can be considered as separate instabilities. We will consider them in turn, following the work of Finn and Mannheimer [3.17]. To begin with, "Tearing ordering" is assumed, i.e. $\gamma \sim \eta^{3/5}$, $r - r_s \sim \beta \sim D \sim \eta^{2/5}$. This ordering has proved to yield dispersion relations which are most complete, in the sense that the matching conditions to the external region appear, in addition to the local layer parameters. The reader is referred to Greene [3.18] for further details. Under tearing ordering, equation 3.49 yields, to lowest order:

$$\Psi'' = 0 \Rightarrow \Psi = AX + B$$

where A and B are constants. This solution for Ψ may be used in the remaining layer equations.

3.3.1 Twisting Parity Modes

The twisting mode boundary condition (equation 3.52), demands that $B = 0$. Thus to lowest order in X, $\Psi = 0$ and equations 3.50 and 3.51 decouple from equation 3.49. The resulting fourth-order system can be solved in terms of Hermite functions, ultimately yielding the dispersion relation [3.17]:

$$Q^{3/2} = \frac{\Gamma\beta(2l+1)}{2}\left(\frac{2D}{\Gamma\beta} - s - (2l+1)^2\right) \tag{3.54}$$

where l labels the l^{th}-order Hermite function. Notice that the $l = 0$ harmonic is the most unstable, so that the stability condition for twisting modes is:

$$\frac{2D}{\Gamma\beta} < s + 1 \tag{3.55}$$

3.3.2 Tearing Parity Modes

The tearing mode boundary condition, implies that Ψ is a constant. (This is the so called "constant-Ψ approximation"). The resulting equations have been solved by CGJ [3.16], to yield a complicated dispersion relation, which gives the growth rate in terms of the layer parameters and the matching conditions. To make the meaning of the dispersion relation more obvious, we consider the incompressible limit:

$$\frac{2D}{\Gamma\beta} \to 0$$

which yields:

$$L_r\Delta' = G\left(Q^{5/4} - \frac{\pi D}{4Q^{1/4}}\right) \tag{3.56}$$

where $G \sim 2.12$ is a constant and Δ' is determined by the solutions in the ideal regions either side of the resistive layer. In the incompressible limit:

$$\Delta' = \left.\frac{b'_{r+}}{b_{r+}}\right|_{r_s} - \left.\frac{b'_{r-}}{b_{r-}}\right|_{r_s} \tag{3.57}$$

where b_{r-} and b_{r+} are the ideal solutions for $r < r_s$ and $r > r_s$ respectively. Equation 3.56 contains two terms that can drive instability. Most obvious is the familiar destabilising effect of pressure-gradient, which is contained within the Suydam parameter, D. Additionally, instabilities may be driven by Δ', i.e. by favourable energy changes that occur outside the layer. Thus Δ' contains the effect of parallel currents etc.

There are two special limits of equation 3.56.

(i) When there is no pressure-gradient, $D = 0$ and:

$$Q \propto (L_r\Delta')^{4/5} \Rightarrow \gamma \propto \eta^{3/5}\Delta'^{4/5}$$

Thus for $\Delta' > 0$ there is an instability. These instabilities are known as "tearing modes".

(ii) When $\Delta' = 0$:

$$Q = \left(\frac{\pi D}{4}\right)^{2/3} \Rightarrow \gamma \propto \eta^{1/3}D^{2/3}$$

In this case $D > 0$ leads to a unstable "resistive-g" mode. Notice that resistivity has strengthened the stability condition for pressure-driven modes, from $D < 1/4$ (Suydam's criterion) to $D < 0$.

If both D and Δ' are non-zero, equation 3.56 indicates that both must be negative for stability.

3.4 Resistive-Drift Stability

Now we extend the resistive MHD model by including the Hall terms in Ohm's Law:

$$\vec{E} + \vec{v} \times \vec{B} = \eta\vec{J} + \frac{1}{ne}(\vec{J} \times \vec{B} - \nabla p_e) \tag{3.58}$$

The Hall terms have two effects on plasma stability. Not surprisingly the existing resistive modes are modified, but additionally there are a new class of modes that are associated with charge separation. These "drift modes" are essentially electrostatic in nature, and exist even in the $\eta \rightarrow 0$ limit. So for illustrative purposes, we consider the simplest case of electrostatic perturbations ($\vec{b} = 0$) in a collisionless plasma, with uniform magnetic field in the z direction [3.19]. We write perturbed quantities as:

$$n(\vec{r}) = n(x)\exp(ik_{\|}z + iky + i\omega t)$$

where the equilibrium density and temperature vary only in the x direction. The system of equations to be solved are:

$$\begin{aligned}
\frac{\partial n}{\partial t} + \nabla.(n\vec{v}) &= 0 \\
nM\frac{D\vec{v}}{Dt} &= \vec{J} \times \vec{B} - \nabla(p_e + p_i) \\
\vec{E} + \vec{v} \times \vec{B} &= \frac{1}{ne}(\vec{J} \times \vec{B} - \nabla p_e) \\
\frac{D}{Dt}\left(\frac{T_i}{n^{2/3}}\right) &= 0
\end{aligned}$$

where n is the number density (of both ions and electrons), and M is the ion mass. The last of these equations is the adiabatic law for the ions. In addition we need an electron equation of state. We assume that electron thermal conduction along the field-lines is sufficiently rapid for the electron temperature perturbation to be negligibly small, i.e. we set $T_{e1} = 0$.

Ohm's law and the momentum equation give the velocity perpendicular to the magnetic field:

$$\vec{v_\perp} = \frac{\vec{E} \times \vec{B}}{B^2} + \frac{\vec{B} \times \nabla p_i}{neB^2} + \frac{\vec{B} \times D\vec{v}/Dt}{\omega_{ci}B}$$

where $\omega_{ci} = eB/M$ is the larmor frequency. For mode frequency, $\omega \ll \omega_{ci}$, the last term of this expression is negligible. Under this assumption it is possible to derive a polynomial for ω [3.19]:

$$\omega^3 - \omega_{*e}\omega^2 - \frac{k_{\|}^2}{M}\left(T_e + \frac{5}{3}T_i\right) - \frac{k_{\|}^2}{M}T_i\left(\eta_i - \frac{2}{3}\right) = 0 \qquad (3.59)$$

$$\omega_{*e} = \frac{-kT_e}{eB}\frac{n'}{n}$$

and

$$\eta_i = \frac{T_i'/T_i}{n'/n}$$

For $k_{\|}v_{ti} \ll \omega_{*e}$ equation 3.59 yields three roots, which are the marginally stable electron drift wave:

$$\omega = \omega_{*e}$$

and the two remaining roots:

$$\omega = \pm\left(\frac{2}{3} - \eta_i\right)$$

Thus there is an instability if $\eta_i > 2/3$. This branch of the dispersion relation is known as the " η_i- mode".

The derivation above is of course very idealised. In a fusion device the magnetic field is not uniform, and $k_{\|}$ is a function of x. When this is taken account of, equation 3.59 is replaced by a second order differential equation.(The derivatives are in fact $O(ka_i)$ terms that have been neglected in equation 3.59, see [3.20]). The eigenvalue condition for the equation then yields a dispersion relation , which has an η_i mode solution [3.20, 3.21]. Thus it is safe to conclude that this instability is not a result of the simplifying assumptions used in deriving equation 3.59. However, more careful analyses do conclude that the critical value of η_i, should in fact be derived from kinetic theory. (The fluid theory is only applicable for $\eta_i \gg 1$ [3.21]).

Having established the existence of a new type of instability that is driven by ion temperature gradients, we proceed to consider modifications to the resistive instabilities considered in the previous subsection. When the Hall term is included [3.22], equations 3.49 to 3.51 are replaced by:

$$\Psi'' = Q(\Psi + X\xi) + iQ_*\Psi + i\frac{Q_*}{D}\Upsilon X \tag{3.60}$$

$$\xi'' = \frac{X^2}{Q}\xi + \frac{X}{Q}\Psi - \frac{1}{Q}\Upsilon \tag{3.61}$$

$$\begin{aligned}\Upsilon'' &= Q\left(1 + \frac{X^2}{Q^2} + \frac{2}{\Gamma\beta}\right)\Upsilon + Q\left(s - D - \frac{2D}{\Gamma\beta}\right)\xi \\ &+ \frac{D}{Q}X\Psi + iQ_*\frac{2}{\Gamma\beta}\kappa_T(\Upsilon - D\xi) - iQ_*Q^2\frac{s}{D}\xi''\end{aligned} \tag{3.62}$$

where $Q_* = \omega_{*e}/Q_r$ and

$$\kappa_T = \frac{\eta_i - \Gamma + 1}{1 + \eta_i + T_e/T_i}(1 + \eta_e)$$

Finn, Mannheimer and Antonsen [3.22] solved this system of equations numerically, without using the constant-Ψ approximation. They found a strong stabilising effect on both twisting and tearing parity modes. In particular, modes with both $D > 0$ and $\Delta' > 0$ were completely stable at moderate values of $g = sQ_*/2D$. However, it should be noted that in most cases they assumed $\kappa_T = 0$, which has the effect of excluding η_i-modes from their analysis.

Hahm and Chen [3.23] reconsidered equations 3.60 to 3.62 for modes in the "semicollisional regime", which is defined by:

$$\frac{C_s}{\omega_{ci}} > L_r$$

where $C_s = (T_e/M)^{1/2}$ is the ion sound speed. They conclude that for semicollisional modes, the ion sound terms are negligible and so the Fourier-transformed layer equations can be reduced from fourth to second order. This allows the following dispersion relation to be derived:

$$\omega(\omega - \epsilon\omega_{*e})(\omega - [1-\epsilon]\omega_{*e}) = -i\lambda\left(\frac{\pi}{2}D(1-\epsilon) + \Delta' b_\theta^{1/2}\frac{\omega^{1/2}[\omega - (1-\epsilon)\omega_{*e}]^{1/2}}{\pi(\omega - \omega_{*e})}\right)^2 \tag{3.63}$$

where $b_\theta = \epsilon\omega^2/D$, $\epsilon = s\Gamma\beta/2D$, and λ is proportional to the parallel resistivity. This dispersion relation is valid for both tearing parity and twisting parity modes (set $\Delta' = 0$). It has been derived neglecting the effect of perpendicular resistivity (i.e. perpendicular particle transport). Equation 3.63 has an unstable root for all values of ω_{*e}, and thus the resistive modes are never completely stabilised. However, when Hahm and Chen included the effect of perpendicular resistivity as a perturbation on the solution of equation 3.63, they found that modes with $\Delta' \leq 0$ could be stable. In fact for $\Delta' = 0$ there is the following critical Suydam parameter below which a mode is stable:

$$D < \frac{1}{\sqrt{2}\pi^2}\left(\frac{\tau}{1+\tau}\right)^2 \frac{S}{(\omega_{ci}\tau_A)^3}\left(\frac{\eta_\perp}{\eta_\|}\right)^{1/2} ka\frac{a}{r_s}\frac{B_\theta}{B}\frac{\Gamma\beta^2}{\sqrt{s}} \tag{3.64}$$

where $\tau_A = a\sqrt{\rho/B^2}$, $S = \tau_R/\tau_A = a^2/(\eta_\| \tau_A)$ and $\tau = T_e/T_i$. Equation 3.64 has been derived from equation 36 of reference [3.23], assuming that the electron and ion pressure profiles have the same shape.

3.5 Full Braginskii Stability for $T_i = 0$

Finn and Drake [3.24] have extended equations 3.60 to 3.62 to include the effect of finite electron thermal conduction. This means that the free energy of the electron temperature gradient is available to drive instabilities. In the semicollisional regime, Finn and Drake find that a tearing parity mode, can be driven by either perpendicular transport (of particles or heat), or curvature. Figure 3.3 is a reproduction of figure 2(a) from reference [3.24]. It shows the stability diagram for the mode driven solely by curvature, where:

$$\omega_c = -\frac{\beta k B_\theta}{ner_s}$$

and

$$f = \frac{\eta_e}{1+\eta_e}$$

Notice that there is an unstable range of ω_c/ω_{*e}, that shrinks as the electron temperature gradient is reduced (i.e. f is reduced). The major effect of cross-field transport, is to destabilise the mode even when it is below the lower threshold in the curvature frequency. This is demonstrated by the dotted-line in figure 3.3.

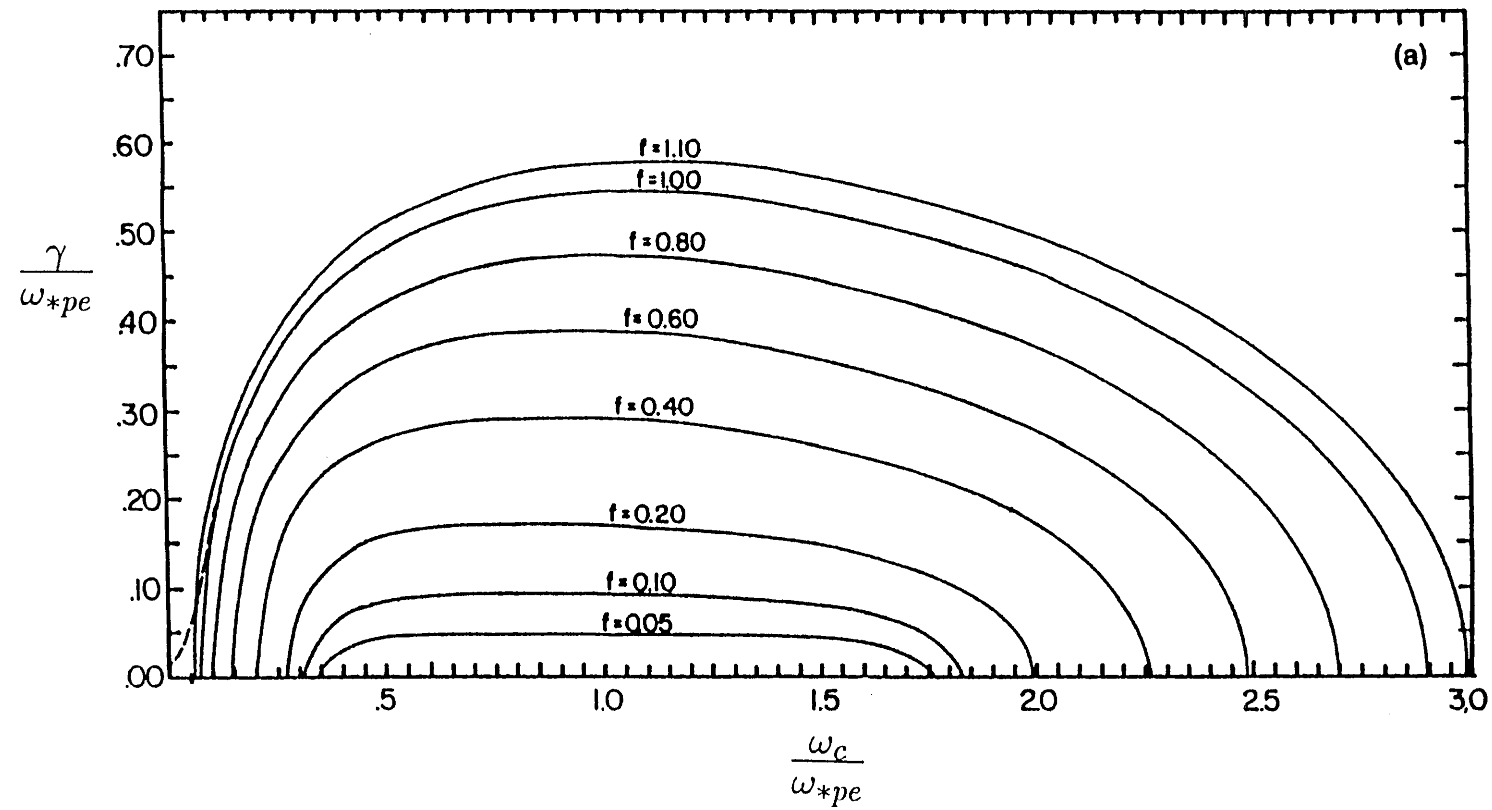

Figure 3.3: Stability diagram for the M.C.D. mode (figure 2 of ref. [3.24]). The parameter f determines the effect of the temperature gradient: $f = \eta_e/(1+\eta_e)$. The solid lines show the mode driven by curvature only, i.e. without cross-field transport. The dashed line demonstrates the destabilising influence of cross-field transport below the lower curvature threshold.

3.6 Conclusions

We can draw the following conclusions from the review of linear stability presented in this section:

(i) RFP profiles can be constructed that are completely stable to ideal modes, even when inflated to large β values.

(ii) Stability according to resistive MHD, requires $D < 0$ and $\Delta' < 0$ for every mode. This means that any (negative) pressure gradient is linearly unstable.

(iii) If the Hall terms are included in Ohm's Law, both twisting and tearing parity resistive modes can be stabilised by coupling to drift waves. In the semicollisional regime this stabilisation is largely due to perpendicular particle transport, and leads to a critical D value for each mode.

Additionally the drift terms permit an electrostatic instability that is driven by ion temperature gradients (the η_i mode).

(iv) If the electrons do not obey an adiabatic equation of state (and generally they do not), electron temperature gradients can drive a tearing parity instability ("Magnetic Curvature Drift Instability"). In this case the mode is unstable over a range of the parameter:

$$\frac{\omega_c}{\omega_{*e}} = \frac{2p}{p_e' r_s} \frac{B_\theta}{B}$$

References

[3.1] Taylor, J.B., Phys. Rev. Lett. **33**, 1139 (1974).

[3.2] Woltjer, L., Proc. Nat. Acad. Sci. **44**, 489 (1958).

[3.3] Chandrasekhar, S., Kendall, P.C., Astrophys. J. **126**, 457 (1957).

[3.4] Bodin, H.A.B., Newton, A.A., Nucl. Fus. **20**, 1255 (1980).

[3.5] Kirby, P., Culham Report CLM-P803 (1987).

[3.6] Nebel, R.A., Caramana, E.J., Schnack, D.D, Phys. Fl. **B1**, 1671 (1989).

[3.7] Strauss, H.R., Phys. Fl. **29**, 3008 (1986).

[3.8] Mirin, A.A., O'Neill, N.J., Killeen, J., Bonugli, R.J., Ellis, M.J., Phys. Fl. **29**, 512 (1986).

[3.9] Greene, J.M., Johnson, J.L., Plasma Phys. **10**, 729 (1968).

[3.10] Newcomb, W.A., Ann. Phys. **10**, 232 (1960).

[3.11] Suydam, B.R., in Peaceful Uses of Atomic Energy (Proc. 2^{nd} United Nations Int. Conf. Geneva, 1958) (United Nations,1958), Vol.31, 157.

[3.12] Asakura, N., Fujisawa, A., Fujita, T., et al., in Plasma Physics and Controlled Fusion (Proc. 13^{th} Int. Conf. Kyoto, 1986) (IAEA, Vienna, 1987), Vol.2, 433.

[3.13] Mercier, C., Nucl. Fus. **1**, 47 (1960).

[3.14] Freidberg, J.P., Rev. Mod. Phys. **54**, 801 (1982).

[3.15] Robinson, D.C., Plasma Phys. **13**, 439 (1971).

[3.16] Coppi, B., Greene, J.M.,Johnson, J.L., Nucl. Fus. **6**, 101 (1966).

[3.17] Finn, J.M., Mannheimer, W.M., Phys. Fl. **25**, 697 (1982).

[3.18] Greene, J.M., Introduction to Resistive Instabilities, Ecole Polytechnique Federale de Lausanne Report LRP 114/76 (1976).

[3.19] Horton, C.W., Varma, R.K., Phys. Fl. **15**, 620 (1972).

[3.20] Coppi, B., Rosenbluth, M.N., Sagdeev, R.Z., Phys. Fl. **10**, 582 (1967).

[3.21] Guzdar, P.N., Chen, L., Tang, W.M., Rutherford, P.H., Phys. Fl. **26**, 673 (1983).

[3.22] Finn, J.M., Mannheimer, W.M., Antonsen, T.M., Phys. Fl. **26**, 962 (1983).

[3.23] Hahm, T.S., Liu Chen, Phys. Fl. **28**, 2432 (1985).

[3.24] Finn, J.M., Drake, J.K., Phys. Fl. **29**, 3672 (1986).

Chapter 4

The Effect of Transport Terms on RFP Stability

4.1 Introduction

The major practical and conceptual problem in magnetic confinement devices is that of the anomalous transport of particles and heat. In Reversed Field Pinch (RFP) experiments this manifests itself as a much lower beta value than would be achievable on the basis of classical collisional transport.

The current favoured explanation for anomalous transport is as the outcome of turbulence generated by plasma instability. Thus theoretical prediction relies on:

(i) Identifying the confinement degrading instability (or instabilities).

(ii) Developing a non-linear model of the relevant instability.

(iii) Estimating the transport that results from its non-linear evolution.

In tokamak physics there has been a considerable quantity of work dealing with each of these steps. However, in the RFP community the theoretical emphasis has been on understanding the dynamo mechanism that maintains the configuration, and less on an understanding of anomalous transport (although these are almost certainly connected). Consequently, even the models used to study the linear stability of RFP's, have rarely been more complex than resistive MHD, which although a useful model, is not an accurate description for many current experiments. Thus even (i) cannot be said to have been properly tackled. The purpose of this work is to partially rectify this by considering the stability of an RFP equilibrium according to more complete plasma models.

The low q and large aspect ratio of typical RFP's, means that one may reasonably simplify the problem by assuming cylindrical geometry. Then Fourier analysing in poloidal and axial directions reduces the equations for the perturbation to a separate problem for each Fourier harmonic. Effectively this means that the perturbed variables (represented by the vector $\vec{U}$) are written as:

$$\vec{U}(\vec{r}) = \vec{U}(r)\exp(im\theta + ikz)$$

and the cylindrical symmetry implies that each Fourier "mode", which is defined by given values of m and k, is uncoupled from all other Fourier modes. The effects of additional physics are expected to be especially important for resonant modes, i.e. ones for which:

$$\vec{k}.\vec{B} = \frac{m}{r}B_\theta + kB_z = 0$$

at some point within the plasma. At the resonant point the ideal equations become singular and even small terms can become important. The classic example of this is resistivity, which although a negligibly small correction throughout most of the plasma becomes important within a "resistive layer" of the resonance. Indeed, the inclusion of resistivity introduces additional instabilities that are not possible in an ideal MHD model (see section 3.2).

The narrowness of the resistive layer facilitates an asymptotic matching procedure in which the full resistive equations are solved within the layer (with equilibrium variables treated as constants), and the ideal MHD equations are solved elsewhere [4.1]. The asymptotic matching of the resistive solution with the ideal solutions on both sides of the layer, then yields a dispersion relation for the linear modes of the plasma. Other terms can be treated by including them in the equations which describe the resonant layer. Such "layer theories" were reviewed in chapter 3.

The asymptotic matching procedure is attractive for two reasons. Firstly, the dispersion relation that results is general in the sense that it separates the global stability properties of the equilibrium (which are determined by the solution outside the layer), from the details of the layer physics. This means that a change in the layer physics does not invalidate the calculation of the relevant global stability parameter (usually Δ'), which needs only be calculated once for each plasma equilibrium. Secondly, the inclusion of non-ideal terms in only a narrow layer often allows an analytical solution that would not otherwise be possible. Unfortunately, this is less likely to be true for the more complex plasma models that interest us here, which would yield layer equations requiring a numerical treatment. With this in mind one is led to consider whether a numerical solution of the complete equations across the entire plasma radius is just as worthwhile. Such a method loses some of the generality of the layer treatment but includes the effects of additional terms throughout the plasma (i.e. not just close to the resonance). As such it is applicable even when layer theories begin to breakdown (layer theories are only strictly applicable in the limit that the layer thickness is infinitesimally small).

In this chapter a purely numerical method has been used to study the stability of resonant modes within a RFP equilibrium. However, a careful comparison with the existing layer theories has been carried out in the attempt to achieve both a more general understanding of the effects of additional physics, and also an appreciation of the limitations of the layer theories. Results have been obtained using the linear stability code, ODRIC [4.2], which was described in chapter 2. This code solves the Braginskii fluid equations [4.3] in cylindrical geometry using an initial value method [4.4]. ODRIC was supplied to Culham laboratory by Mirin and co-workers (hereafter MOKBE) of Lawrence Livermore laboratory. The previous published results by this group [4.5] are the prime motivation for this chapter. They studied the stability of a tearing mode stable (TMS) RFP equilibrium [4.6] to resistive-g modes (section 3.3). According to simple resistive MHD, g-modes will be unstable in RFP equilibria with any finite (negative) pressure gradient ([4.7] and section 3.3), so that these modes are a favourite explanation for anomalous transport in RFP's. However, reference [4.5] reports that including all the terms available in ODRIC causes "all modes tested to stabilise". Clearly, the possibility of an RFP equilibrium that is completely stable is intriguing and worthy of further study.

Prior to reference [4.5] there were a number of numerical studies of RFP stability. Most of these have been based around results from initial value codes much like ODRIC. Extensive stability studies have been carried out by Robinson and co-workers [4.8], using progressively more complex plasma models. This culminated in the code GNSTAB which included:

- compressibility
- isotropic resistivity
- Hall terms in Ohm's law
- anisotropic thermal conductivity
- the full ion stress-tensor.

Both Hosking and Robinson [4.9], and Hender and Robinson [4.10] have used GNSTAB to study resistive-g mode stability. Hosking and Robinson highlighted the effect of parallel ion viscosity and found that g-modes could be completely stabilised at low but non-zero values of beta. Hender and Robinson included both Hall terms and the full ion stress tensor. They found interesting behaviour with increasing Larmor radius : first the damping of the g-mode and then the re-emergence of an instability at higher Larmor radii (see figure 4 of reference [4.10]). However, this behaviour was not discussed and they also reported that : " the inclusion of Hall effect alone makes the interchanges more unstable", in apparent contradiction with the more recent analytical work of Finn, Mannheimer and Antonsen [4.11] (hereafter FMA).

Thus when MOKBE [4.5] decided to use ODRIC to study RFP stability, there remained some anomalies to be resolved. The code itself extended the equations of GNSTAB to include :

- separate ion and electron temperature equations
- the thermoelectric effect in Ohm's law (parallel only)
- Hall terms and Ohmic heating in the electron temperature equation.

In order to emphasize pressure-driven modes MOKBE used an equilibrium which is stable to both ideal modes and tearing modes at zero beta [4.6]. Specifically they chose an equilibrium with pitch profile , $P = rB_z/B_\theta$:

$$P(r) = \frac{1}{3}\left(2 - \frac{9}{4}\left(\frac{r}{a}\right)^2 - \frac{81}{200}\left(\frac{r}{a}\right)^4\right)$$

where a is the plasma radius. The pressure profile was chosen to give a Suydam parameter of $D = 0.2$ at each radial location, ($D < 0.25$ corresponds to Suydam's condition [4.12]), where:

$$D = \frac{-2p'}{B_z^2 r}\left(\frac{P'}{P}\right)^2$$

Here, p is the pressure and the primes denote radial derivatives. It is important to note at this point that all of the pressure gradient was assumed to be due to the temperature gradient, i.e. the equilibrium density was taken to be uniform across the plasma radius. MOKBE studied the stability of this equilibrium for parameters appropriate to ZT-40M [4.13], first using a simple resistive model but then gradually introducing more of the terms available in ODRIC.

Initially they included just the Hall terms in Ohm's Law, and found that the "tearing parity" or resistive-g mode (odd parity v_r and even parity b_r across the resistive layer), was stabilised with increasing Hall parameter ($1/\omega_{ci}\tau_A$). This appears to agree with the findings of FMA [4.11]. However, MOKBE also found a "twisting parity" mode (even parity v_r and odd parity b_r across the layer), which had a growth rate increasing with Hall parameter. They seem to have assumed that this is the twisting parity resistive mode, but do not show any Lundquist parameter scalings to confirm this. If this mode is merely a resistive mode that is being amended by the Hall effect, then the numerical result is in fact in conflict with FMA [4.11], who predict that drift effects stabilise both tearing and twisting parity modes. MOKBE presumably feel that the discrepency is due to FMA's assumption that the electrons are isothermal along field lines (i.e. $\kappa_{e\|} = \infty$). They proceed to show that including the ZT-40 values of thermal conductivity can completely stabilise the twisting mode, and that it is the parallel thermal conductivity coefficients that are most important in this respect. However, they do not include the effect of the electron parallel thermal conductivity alone, and so it is not possible to confirm agreement with FMA (who assume $\kappa_{e\|} = \infty$, $\kappa_{i\|} = 0$). Thus there remains some uncertainty about the effect of Hall terms on pressure driven resistive modes and in particular about the exact nature of the twisting parity mode described by MOKBE.

MOKBE also considered the effect of the ion-stress tensor alone (i.e. neglecting Hall terms and thermal conductivities), and found a stabilising influence on both $m = 0$ and $m = 1$ modes. They show that the $m = 1$ mode is more strongly damped at lower values of Lundquist parameter (i.e. in a more resistive plasma).

Finally, MOKBE report the effect of including all the available terms : " for all resonant combinations of ($m = 0, 1, 2, 3; |n| = 1, 9, 17, 25, 33$), the resulting mode is stable". This is the result that was mentioned earlier as the stimulus for this chapter. When considered alongside the analytical work which was reviewed in chapter 3, it suggests the following questions :

(i) where is the η_i-mode [4.14]?
This mode is unstable when $\eta_i > 2/3$, and the flat density profile assumed in reference [4.5] corresponds to $\eta_i = \infty$. Thus the inclusion of the Hall terms (drift effects), might be expected to yield unstable η_i-modes that are supposedly robust to ion viscosity and thermal conductivity [4.15].

(ii) where is the "Magnetic Curvature Drift mode" of Finn and Drake [4.16] ?
This is a semicollisional tearing parity mode which is driven by coupling to the electron temperature gradient via either magnetic curvature, or cross-field transport of particles or heat. Although it is derived from the cold ion Braginskii equations (i.e. neglecting ion viscosity and ion thermal conductivity), Finn and Drake claim : " Ion temperature effects, specifically ∇p_i and ion gyroviscous terms, are unimportant for this mode".

Thus both of these instabilities might have been expected to persist even when all the available terms were included.

In the remainder of this chapter we aim to investigate these outstanding questions, and in particular emphasize the agreements and disagreements with the existing analytical work.

4.2 The Model

Below we list the full system of normalised equations available in ODRIC. The corresponding normalisations are shown in table 4.1.

$$\begin{aligned}
\frac{\partial \rho}{\partial t} + \nabla.(\rho \vec{v}) &= 0 && (4.1)\\
\rho \frac{\partial \vec{v}}{\partial t} &= \vec{J} \times \vec{B} - \frac{1}{2}\nabla(p_e + p_i) + \frac{1}{2}\nabla.\mathbf{\Pi}_i && (4.2)\\
\vec{E} + \vec{v} \times \vec{B} &= \eta \vec{J} + \frac{\nu}{\rho}\left(\vec{J} \times \vec{B} - \frac{1}{2}\nabla p_e\right) - 0.71\nabla_{\|}T_e && (4.3)\\
\frac{\rho}{\Gamma - 1}\frac{\partial T_i}{\partial t} &= -p_i \nabla.\vec{v} + \nabla.(\kappa_i.\nabla T_i) + 3\frac{m_e}{m_i}\frac{\rho}{\tau_e}(T_e - T_i) && (4.4)\\
\frac{\rho}{\Gamma - 1}\frac{\partial T_e}{\partial t} &= -p_e \nabla.\vec{v} + \nabla.(\kappa_e.\nabla T_e)\\
&+ 2\vec{J}.(\vec{E} + \vec{v} \times \vec{B}) + 3\frac{m_e}{m_i}\frac{\rho}{\tau_e}(T_i - T_e) && (4.5)\\
\nabla \times \vec{E} &= -\frac{\partial \vec{B}}{\partial t} && (4.6)\\
p_e &= \rho T_e && (4.7)\\
p_i &= \rho T_i && (4.8)
\end{aligned}$$

Here Γ is the ratio of specific heats and τ_e is the electron-ion collision time. The parameter ν expresses the magnitude of the Hall effect:

$$\nu = \frac{1}{\omega_{ci}\tau_A}$$

The remaining symbols have their usual meanings.

Variable	Normalisation
r	a
B	$\bar{B} = B_z(0)$
ρ	$\bar{\rho} = \rho(r_s)$
p	$\bar{p} = \frac{\bar{B}^2}{8\pi}$
v	$v_A = \frac{\bar{B}}{(4\pi\bar{\rho})^{1/2}}$

Table 4.1: The normalisation used in ODRIC .

The transport coefficients contained in the ion stress-tensor, $\mathbf{\Pi}_i$, the ion and electron thermal conductivity tensors, $\boldsymbol{\kappa}_i$ and $\boldsymbol{\kappa}_e$, and the resistivity tensor, $\boldsymbol{\eta}$, have been calculated by Braginskii [4.3], and are listed in appendix 1B. In all but the former case the transport tensors can be written in terms of just three coefficients representing transport parallel to the magnetic-field, and in two orthogonal directions perpendicular to the magnetic-field , e.g.

$$\boldsymbol{\kappa}_e.\nabla T_e = \kappa_{e\|}\vec{b}(\vec{b}.\nabla T_e) + \kappa_{e\perp}\vec{b} \times (\nabla T_e \times \vec{b}) + \kappa_{e\times}(\vec{b} \times \nabla T_e)$$

where $\vec{b}$ is the unit vector in the direction of the equilibrium magnetic-field. The ion stress-tensor is defined in terms of five coefficients. Three of these are identifiable as the components of collisional viscosities, while the remaining two are entirely attributable to the effects of finite larmor radius.

Equations 4.1 to 4.8 constitute the normalised Braginskii equations [4.3] with the following simplifications:

- The resistivity is treated as a scalar: $\eta_{\parallel} = \eta_{\perp} = \eta$, $\eta_{\times} = 0$.
- Electron inertia is neglected in Ohm's law (equation 4.3).
- Electron viscosity is neglected in equations 4.1 and 4.3.
- Only the parallel component of the thermoelectric effect is included in Ohm's law.
- The component of the heat flux due to friction has been neglected in the electron temperature equation.
- Equilibrium flow velocities have been neglected so that in the linearised equations convective derivatives are replaced by partial derivatives:

$$\frac{\partial}{\partial t} + \vec{v}.\nabla \rightarrow \frac{\partial}{\partial t}$$

The reader is referred to reference [4.5] for further details of these approximations.

Equations 4.1 to 4.8 are linearised about the chosen equilibrium and then solved in cylindrical geometry for the perturbation, $\vec{U}$, where:

$$\vec{U} = \begin{pmatrix} b_r \\ b_\theta \\ T_{e1} \\ v_r \\ v_\theta \\ v_z \\ \rho_1 \\ T_{i1} \end{pmatrix}$$

The problem is reduced from 3 spatial dimensions to 1 spatial dimension, by Fourier transforming in in both poloidal and axial directions. Effectively one writes:

$$\vec{U}(\vec{r}, t) = \vec{U}(r, t)\exp(im\theta + ikz)$$

The assumed cylindrical symmetry of the equilibrium, implies that different (m, k) pairings (i.e. "modes") are uncoupled, so that each may be treated in isolation. The reader is referred to chapter 2 for details of the initial-value technique that is used to solve the resulting system of equations.

The transport coefficients and their normalisations are given in table 4.3. These coefficients correspond to the $\omega_{ci}\tau_i \rightarrow \infty$ limit of the expressions derived by Braginskii [4.3]. Note that the normalised resistivity corresponds to S^{-1} where S is the Lundquist parameter:

$$S = \frac{\tau_R}{\tau_A} = \frac{4\pi a^2}{c^2 \tau_A} \frac{1}{\eta_\perp}$$

Like MOKBE we calculate transport coefficients using ZT-40M [4.13] parameters as our reference point:

$$\begin{aligned} a &= 20\ cm \\ \bar{n} &= 3 \times 10^{13}\ cm^{-3} \\ \bar{T}_e &= \bar{T}_i = 300\ eV \\ \bar{B} &= 4000\ G \end{aligned}$$

For a fully ionised pure deuterium plasma, these parameters yield:

$$\begin{aligned} S &= 7.266 \times 10^5 \\ \nu &= 0.294 \\ \bar{\tau}_e &= 17.128 \end{aligned}$$

The remaining normalised transport coefficients are shown in the third column of table 4.3. Each of the transport coefficients are taken to be uniform across the plasma radius. (Note that this excludes rippling modes from the analysis). In the remainder of this chapter the transport coefficients will often be expressed as a fraction of the ZT-40M value e.g. $\nu = 0.294\, C_\nu$, $\kappa_{e\|} = 2281.0\, C_{\kappa_{e1}}$, $\kappa_{e\perp} = 7.32 \times 10^{-8}\, C_{\kappa_{e2}}$, $\kappa_{e\times} = 8.32 \times 10^{-3}\, C_{\kappa_{e3}}$.

Transport Coefficient	Normalisation	ZT-40M value
$\eta = \dfrac{m_e}{ne^2\tau_e}$	$\dfrac{4\pi a^2}{c^2\tau_A}$	1.38×10^{-6}
$\kappa_{e\parallel} = 3.1616\,\dfrac{m_i}{m_e} nT_e\tau_e$	$\dfrac{\rho a^2}{\tau_A}$	2281.00
$\kappa_{e\perp} = 4.664\,\dfrac{m_i}{m_e}\dfrac{nT_e}{\omega_{ce}^2\tau_e}$	"	7.32×10^{-8}
$\kappa_{e\times} = \dfrac{5}{2}\dfrac{m_i}{m_e}\dfrac{nT_e}{\omega_{ce}}$	"	8.32×10^{-3}
$\kappa_{i\parallel} = 3.900\, nT_i\tau_i$	"	64.69
$\kappa_{i\perp} = \dfrac{2nT_i}{\omega_{ci}^2\tau_i}$	"	1.33×10^{-6}
$\kappa_{i\times} = \dfrac{5}{2}\dfrac{nT_i}{\omega_{ci}}$	"	8.32×10^{-3}
$\mu_\parallel = 0.96\, nT_i\tau_i$	$\dfrac{\rho a^2}{2\tau_A}$	31.85
$\mu_1 = \dfrac{3}{10}\dfrac{nT_i}{\omega_{ci}^2\tau_i}$	"	4.00×10^{-7}
$\mu_2 = \dfrac{6}{5}\dfrac{nT_i}{\omega_{ci}^2\tau_i}$	"	1.60×10^{-6}
$\mu_3 = \dfrac{nT_i}{2\omega_{ci}}$	"	3.33×10^{-3}
$\mu_4 = \dfrac{nT_i}{\omega_{ci}}$	"	6.66×10^{-3}

Table 4.2: Normalised transport coefficients for ZT-40M parameters.

The equilibrium we use is the same T.M.S. equilibrium that was used by MOKBE. However, we do not restrict ourselves to flat density profiles, instead considering equilibria that have a uniform η_T, where

$$\eta_T = \left(\frac{dT}{dr}\frac{1}{T}\right)\left(\frac{d\rho}{dr}\frac{1}{\rho}\right)^{-1}$$

For all the cases we consider, the ion and electron temperatures are equal everywhere, so that $\eta_T = \eta_i$. The pressure gradient remains the same as for MOKBE (i.e. $D = 0.2$ everywhere), but it is now decomposed into temperature and density gradients according to:

$$\frac{dp}{dr} = T\frac{d\rho}{dr}(1+\eta_T) = \rho\frac{dT}{dr}\left(\frac{\eta_T}{1+\eta_T}\right)$$

Integrating these equations leads to:

$$T = Cp^{\frac{\eta_T}{1+\eta_T}}$$

$$\rho = \frac{1}{C}p^{\frac{1}{1+\eta_T}}$$

where C is a constant to be determined by the boundary conditions. We choose C such that the density is unity at the resonant surface. This means that the inertial term within the layer is always of a similar magnitude, and guarantees that modes that are insensitive to temperature gradients have the same normalised growth-rate for all η_T.

The beta value of the equilibrium is dependent on both the pressure profile (i.e. D), and the pressure at the edge. Table 4.2 lists values of central beta, β_0, and the poloidal beta, β_θ, for $D = 0.2$ and various normalised edge pressures, where:

$$\beta_0 = \frac{2p(0)}{B(0)^2}$$

$$\beta_\theta = \frac{4\int r\,p(r)\,dr}{a^2 B_\theta^2(a)}$$

$\hat{p}(a)$	β_0	β_θ
0.00	0.087	0.121
0.02	0.107	0.156
0.05	0.137	0.225
0.10	0.187	0.339

Table 4.3: Central and poloidal beta values for the $D = 0.2$ T.M.S. equilibrium at various normalised edge pressures.

The results below refer to the stability of $m = 0$, $ka = 1.0$ for this equilibrium. The specialisation to this particular mode is made in order to highlight the effects of the various terms in the full system of equations. Beginning with resistive MHD in section 4.3, progressively more physics is introduced through sections 4.4 to 4.6. Particular emphasis is placed on the identification of the various branches of instability, and on comparison with previous analytical work .

In section 4.7 the radial profiles of various local stability parameters are plotted out for the TMS equilibrium. These embody the stability of this equilibrium according to the work of Finn and Mannheimer [4.17], Hahm and Chen [4.18], and Finn and Drake [4.16]. Comparison is made with the complete stability that was reported by MOKBE.

4.3 Resistivity

We begin by including resistivity only, and attempt to compare the results with the analytical work described in section 3.3. For this case equations 4.1 to 4.8 are reduced to the far simpler model below:

$$\frac{\partial \rho}{\partial t} + \nabla.(\rho \vec{v}) = 0 \tag{4.9}$$

$$\rho \frac{\partial \vec{v}}{\partial t} = \vec{J} \times \vec{B} - \frac{1}{2}\nabla(p_e + p_i) \tag{4.10}$$

$$\vec{E} + \vec{v} \times \vec{B} = \eta \vec{J} \tag{4.11}$$

$$\frac{\rho}{\Gamma - 1}\frac{\partial T_i}{\partial t} + p_i \nabla.\vec{v} = 3\frac{m_e}{m_i}\frac{\rho}{\tau_e}(T_e - T_i) \tag{4.12}$$

$$\frac{\rho}{\Gamma - 1}\frac{\partial T_e}{\partial t} + p_e \nabla.\vec{v} = 3\frac{m_e}{m_i}\frac{\rho}{\tau_e}(T_i - T_e) \tag{4.13}$$

$$\nabla \times \vec{E} = -\frac{\partial \vec{B}}{\partial t} \tag{4.14}$$

$$p = p_i + p_e = \rho(T_e + T_i) \tag{4.15}$$

Recall, from section 3.3, that the resistive layer equations have two distinct solutions with differing behaviour at the resonant point, $r = r_s$. The twisting parity mode has a zero in the radial magnetic field perturbation at $r = r_s$, while the tearing parity mode has a zero in the radial velocity perturbation. Remember that the latter can be driven by both Δ' and the pressure gradient at the resonance (resistive-g mode), while the former is driven only by the local pressure gradient. In general Δ' is non-zero, so that the twisting and tearing modes have non-degenerate growth-rates and should be observable as separate solutions to the linearised equations.

The analytical work of Finn and Mannheimer [4.17], indicates that the twisting mode is stabilised by compressibility leading to the stability condition (also equation 3.55):

$$\frac{2D}{\Gamma\beta} < s + 1 \tag{4.16}$$

where $s = 4/P'^2$, Γ is the ratio of specific heats and β is defined at $r = r_s$. Thus for larger $\Gamma\beta$ a larger value of Suydam parameter, D, can be supported without loss of stability. For the $m = 0$ mode in the TMS equilibrium ($D = 0.2$), stability is predicted for :

$$\Gamma\beta > 0.17$$

or with $\Gamma = 5/3$:

$$T(1) > 0.007$$

Note that in MOKBE, $T(1) = 0.1$, so the twisting parity $m = 0$ mode should have been stable according to Finn and Mannheimer.

Below we attempt to verify the stabilisation of the twisting mode by artificially reducing $\Gamma\beta$ and using Charlton's technique to observe both twisting and tearing parity modes under identical conditions. The two separate parity resistive modes have of course been identified using shooting methods (e.g. [4.11]), but previous initial value approaches have relied on convergence to the fastest growing mode and have therefore been incapable of resolving the slower growing instabilities. Thus an orthodox initial value code could only yield conclusions on the fastest growing mode, i.e. tell us that for $\Gamma\beta$ greater than some value the tearing parity mode is dominant. Once the growth-rate of the twisting mode is reduced below that of the tearing parity mode it would effectively be invisible to the code, and further stabilisation could not be followed. Thus this is a situation where Charlton's method enables additional results to be extracted. The reader is referred to section 2.5 for details of the technique.

Figure 4.1 shows the normalised growth-rates of both twisting and tearing parity $m = 0$, $k = 1.0$ modes versus $\Gamma\beta$. For convenience, the variation in $\Gamma\beta$ has been achieved by varying the ratio of specific heats while keeping $T(1) = 0.1$ (i.e. keeping β constant). A more physically meaningful situation would involve setting $\Gamma = 5/3$ and varying the value of the edge temperature. However, some experimentation shows that the growth-rates depend only on the product of Γ and β and are insensitive to their individual values (in agreement with [4.17]). Thus we are at liberty to choose the means of varying this parameter. Notice that for very small values of $\Gamma\beta$ the twisting mode is dominant. This is presumably due to the suppression of the tearing parity mode by $\Delta' < 0$. As $\Gamma\beta$ is increased the growth-rate of the twisting mode is quickly reduced while the tearing mode asymptotes to a growth rate $\gamma\tau_A \approx 2.1 \times 10^{-3}$. It becomes extremely difficult to observe the twisting mode for $\Gamma\beta > 0.17$ and figure 4.1 suggests that the mode is stable at $\Gamma\beta \approx 0.18$. This compares well with the Finn and Mannheimer prediction of 0.17.

Figures 4.3 and 4.4 show the profiles of perturbed variables for twisting and tearing parity modes respectively. In both cases there are large gradients at the resonant point of $r_s = 0.883$. However, comparing the profiles of specific variables demonstrates the very different nature of these two instabilities. For example, the opposite parities of the v_r perturbations immediately identifies each mode. Perhaps of greater significance are the b_r perturbations, which indicate that the tearing parity mode leads to the formation of magnetic islands (b_r at $r = r_s$ non-zero), while the twisting mode merely bends field lines.

Finally, we should check that we are observing resistive modes by checking the scaling with resistivity. This has been carried out and yields the analytical $\gamma\tau_A \propto S^{-1/3}$ scaling at large S. At small values of S the behaviour diverges significantly from the layer theory predictions, for reasons associated with approximations of the theory. This is discussed further in Appendix 4A, in which ODRIC growth-rates have been compared with the exact analytical growth-rates for tearing modes in a Bessel function equilibrium.

To summarise this section we have:

(i) identified twisting and tearing parity modes as independent branches of instability

(ii) observed the compressional stabilisation of the twisting mode with increasing $\Gamma\beta$.

4.4 Resistivity and Hall terms

The equations are those of the previous section but with Ohm's law (equation 4.11) replaced by:

$$\vec{E} + \vec{v} \times \vec{B} = \eta \vec{J} + \frac{\nu}{\rho}\left(\vec{J} \times \vec{B} - \frac{1}{2}\nabla p_e\right) \tag{4.17}$$

Figure 4.2 demonstrates the effect of gradually introducing the Hall terms through the parameter ν. $C_\nu = 0.0$ corresponds to the resistive MHD model considered above, while $C_\nu = 1.0$ corresponds to the ZT-40M value. The branch labelled (1) is the the tearing parity, pressure-driven, resistive mode, which will hereafter be termed the "resistive-g mode". Notice that this branch is stabilised by the Hall terms, in agreement with the work of Finn, Mannheimer and Antonsen [4.11], and also Hahm and Chen [4.18]. For a negligible Δ' and equal electron and ion temperatures, the stability condition is given by equation 3.64:

$$\nu^3 S > \sqrt{2}\pi^2 \left(\frac{r_s}{a}\right) \frac{1}{(ka)} \left(\frac{B}{B_\theta}\right) \frac{\sqrt{s}D}{\Gamma\beta^2} \tag{4.18}$$

The parameters appropriate to figure 4.2 are: $r_s/a = 0.883$, $B/B_\theta = 0.52$, $\beta = 0.445$, $ka = 1.00$, $s = 1.392$, $\Gamma = 5/3$, $S = 7.266 \times 10^5$. Thus equation 4.19 yields:

$$\nu > 0.046$$

or as a fraction of the ZT-40M value:

$$C_\nu > 0.155$$

Again, this is in reasonable agreement with the numerical results which indicate stability for $C_\nu \gtrsim 0.17$.

Figure 4.5 shows the profiles for the resistive-g mode at $C_\nu = 0.16$. Here the mode is strongly coupled to the electron drift wave, leading to a more complicated mode structure and a large real frequency.

Branch (2) shown in figure 4.2 is the twisting parity mode observed by MOKBE. Its profiles are shown in figure 4.6. Although it is of a similar structure to the twisting resistive mode shown in figure 4.3, it has much less localised velocity perturbations. Also observable "underneath" branch (2) is an instability with an odd parity v_r perturbation. Its behaviour with C_ν, and its mode structure (figure 4.7) suggest that it is the first harmonic of branch (2). Presumably there are also slower growing higher harmonics.

It is important to identify the mechanism responsible for the emergence of branch (2) (and its higher harmonics). MOKBE suggest that this instability is in fact the twisting parity resistive mode driven unstable by the Hall terms. However, this appears to be in disagreement with FMA [4.11], who conclude that both twisting and tearing parity, pressure-driven, resistive modes can be stabilised by coupling to drift waves. Fortunately the discrepancy can be traced to an assumption used in this reference. Referring back to equation 3.62, note that the parameter κ_T was set to zero by FMA, so that effectively they assumed $\eta_i = 2/3$. This is in contrast to the results of figure 4.2 or those of MOKBE which have been obtained using a uniform density equilibrium (i.e. $\eta_i = \infty$). In order to determine whether a genuine discrepancy exists we must examine the effect of finite density gradient on branches (2) and (3). This is achieved using the straightforward extension of the TMS equilibrium described in the introduction to this chapter.

Figure 4.8 shows the growth-rates of branches (2) and (3) versus $1/(1+\eta_i)$. As the equilibrium density gradient is introduced branches (2) and (3) are both suppressed and become marginally stable at $\eta_i \approx 2/3$. Thus there is no instability for $\eta_i \leq 2/3$ and the numerical results do not contradict FMA. More importantly, this stability condition coincides with that for η_i modes (section 3.4). Additional experimentation, reveals that branches (2) and (3) are driven specifically by the ion temperature gradient (rather than the electron temperature gradient), and that their growth-rates scale little with resistivity. The latter point would seem to rule them out as a variant of a resistive mode and strongly suggests that they are the zeroth and first harmonic η_i modes. Likewise we are led to a similar conclusion about the identity of the 'even mode' observed by MOKBE.

In summary introducing the Hall terms has two discernable effects:

(i) the stabilisation of resistive-g modes by coupling to the electron drift wave

(ii) the introduction of a new instability (the η_i mode) that is driven unstable by ion temperature gradients if $\eta_i \geq 2/3$.

4.5 Resistivity, Hall terms and Electron Thermal Conductivity

Now we extend the model of the previous section by including the electron thermal conductivity. Thus equation 4.15 is replaced by:

$$\frac{\rho}{\Gamma - 1}\frac{\partial T_e}{\partial t} + p_e \nabla.\vec{v} = \nabla.(\kappa_e.\nabla T_e) + 3\frac{m_e}{m_i}\frac{\rho}{\tau_e}(T_i - T_e) \tag{4.19}$$

The relevant layer theory is that of Finn and Drake [4.16], which was summarised in section 3.5. Here the reader should recall the major conclusion of Finn and Drake: 'finite electron thermal conductivity allows access to the free energy source associated with the electron temperature gradient, and this can drive a tearing parity instability (the MCD mode), provided that the curvature frequency lies within a given range, or that there is some cross-field transport of particles or heat'. In this section we set out to identify the MCD mode and confirm the behaviour reported by Finn and Drake.

Figure 4.9 is basically a repeat of figure 4.2 but now with electron thermal conductivity included. Additionally the edge temperature has been reduced to

$T(1) = 0.01$ (from 0.1) so that the ω_c/ω_{*e} ratio is comfortably within the range for unstable MCD modes (see figure 3.3). The branch marked (1) is the resistive-g mode branch that has been considered in the previous sections. At small values of C_ν the g-mode is suppressed much as it is in figure 4.2. However, increasing C_ν does not totally stabilise this branch, instead the growth-rate reaches a minimum (approximately where it was previously stable) and then increases with C_ν. In figure 4.9 the mode is now marked (4) although it is actually the continuation of the g-mode branch. Also shown in figure 4.9 is the zeroth-order η_i mode, which is little affected by the electron thermal conductivity.

Figure 4.12 shows the mode structure of branch (4) at the ZT-40M value of the Hall parameter. The b_r profile indicates that this is an island forming, tearing parity instability. However, the velocity profiles are significantly different from those of the simple resistive-g mode (fig 4.4). This is not inconsistent with the MCD mode in which the velocity perturbation plays a less central role than it does in normal tearing or g-modes (see ref [4.16]). There are additional reasons to identify branch (4) with the MCD mode:

- the behaviour of branch (2)/(4) with increasing drift frequency is very similar to that reported by Finn and Drake (see figure 3.3)
- the frequency of branch (4) at $C_\nu = 1.0$ is $\omega\tau_A = 0.0438$, which is comparable to the electron drift frequency for this equilibrium: $\omega_{*e}\tau_A = 0.0478$, and also consistent with the MCD mode.

Thus we can tentatively identify branch (4) with the MCD mode. However, before we can confirm this we must check that the mode is dependent on both the electron temperature gradient and the ω_c/ω_{*e} ratio.

Figure 4.11 shows the growth-rate and frequency versus the edge temperature. Varying the edge temperature is equivalent to varying ω_c/ω_{*e} since:

$$\frac{\omega_c}{\omega_{*e}} = \frac{4\beta}{DP'^2}$$

or in this specific case:

$$\frac{\omega_c}{\omega_{*e}} \approx 25.6(0.02 + T(1))$$

Thus the range $0.0 \leq T(1) \leq 0.1$ corresponds to $0.51 \leq \omega_c/\omega_{*e} \leq 3.07$. Figure 3.3 indicates that the MCD mode should be unstable in the range $0.05 \leq \omega_c/\omega_{*e} \leq 2.9$. However, although figure 4.11 indicates a reduction in growth-rate as T(1) increases the mode remains unstable even at T(1)=0.1 ($\omega_c/\omega_{*e} = 3.07$). This discrepancy is perhaps attributable to the neglect of cross-field transport and Δ' in figure 3.3.

Figure 4.12 shows the growth-rate and frequency of branch (4) versus $1/(1+\eta_e)$. It is clear that the mode is driven by the electron temperature gradient. As η_e is reduced (i.e. ∇T_e reduced) the instability is suppressed, and its growth rate is negligibly small below $\eta_e \approx 0.25$.

Finally, figure 4.10 shows the growth-rates of the resistive-g mode , the η_i mode, and branch (4) versus Lundquist parameter. Here, the g-mode branch is shown in the absence of Hall terms ($C_\nu = 0$). It demonstrates the characteristic $S^{-1/3}$ scaling at large S and resistive damping at low S (see Appendix 4A). Of the two branches observable at $C_\nu = 1.0$, the η_i mode shows very little dependence on resistivity, while branch (4) tends to the g-mode scaling at large S. Interestingly, branch (4) is also strongly suppressed at low S, which is perhaps associated with the breakdown of the semicollisional ordering.

Thus to summarise this section, we conclude that in the presence of finite electron thermal conductivity there exist two quite distinct instabilities:

(i) a mode that is driven by the ion temperature gradient, that has previously been identified as the η_i mode.

(ii) a drift-resistive g-mode that is driven by the electron temperature gradient and is identifiable as the MCD mode of Finn and Drake [4.16].

These conclusions remain valid for the full cold-ion Braginskii equations ,i.e. both instabilities are insensitive to the additional inclusion of Ohmic heating and the Thermoelectric effect.

4.6 The Effect of Ion Transport on MCD and η_i Modes

Having established the important instabilities in the cold-ion limit we proceed now to examine the effect of ion transport (i.e. finite ion temperature) on these modes.

To begin with we remind the reader of a result obtained in reference [4.5]. In that paper, the mode that we have identified as the η_i-mode was reported to be stabilised by the introduction of thermal conductivity, although the separate effects of the electron and ion thermal conductivities was not investigated. However, the results of the previous section show that the η_i mode is little affected by electron thermal conductivity and so we must conclude that the ion thermal conductivity is responsible for the suppression observed by MOKBE [4.5].

Figure 4.14 shows the effect of ion parallel transport (i.e. $\mu_{\|}$ and $\kappa_{i\|}$), on the growth-rate and frequency of the η_i mode. The dependent variable, α, is the ratio of the ion parallel transport coefficients to their reference ZT-40M values. Thus $\alpha = 0.0$ corresponds to the (cold-ion) model of the previous section, while $\alpha = 1.0$ corresponds to the ZT-40M values. An increase in α may be considered as due to an increase in ion temperature, since $\mu_{\|} \propto \kappa_{i\|} \propto \alpha \propto T_i^{5/2}$. Thus one visualises increasing the ion temperature from zero up to the ZT-40M value. Associated with the increasing ion temperature is a decrease in the ion-ion collision frequency, ν_{ii}, since $\nu_{ii} \propto T_i^{-3/2} \propto \alpha^{-3/5}$. The variation of ν_{ii} as a function of α is also shown in figure 4.14.

It is immediately obvious from figure 4.14 that ion parallel transport can have a strong stabilising influence on η_i modes. In fact, the $m = 0$, $ka = 1.0$

mode is stable for α greater than about 0.28 and is therefore stable for ZT-40M parameters. This is presumably a similar stabilisation to that observed by MOKBE. However, we must be cautious here.

Notice that the ion-ion collision frequency has a similar magnitude to the mode frequency, suggesting that we are at the limit of validity of the fluid model. The Braginskii fluid equations are derived by assuming that both electron and ion distribution functions can be approximated by a Maxwellian plus a small correction (reference [4.3] and section 1.4). Thus the model may only be applied to processes occurring on much longer timescales than those required for the respective distribution functions to approach local thermal equilibrium (i.e. a local Maxwellian distribution). For electrons this demands:

$$\nu_{ee} \gg \omega$$

and for ions:

$$\nu_{ii} \gg \omega$$

where ω represents the frequency of the process (or mode) to be described. From figure 4.14 we see that ν_{ii} is less than ω for values of α greater than about 0.02. Consequently, one can have no confidence in the stabilisation of the η_i mode that is predicted using the fluid theory. Further progress requires the use of kinetic theory for the ions. A similar conclusion applies also to the MCD mode, since this mode has an even larger frequency.

Although the parallel ion transport cannot be described using fluid theory, the perpendicular ion transport remains valid provided:

$$L_\perp \gg a_i$$

where $L_\perp$ is a typical equilibrium length-scale in the direction perpendicular to the magnetic field. For the reference case of ZT-40M parameters $a_i/a = 0.044$, and this condition is easily fulfilled. Thus if parallel ion transport is neglected the Braginskii equations still provide an adequate description.

Figure 4.15 shows the growth-rates of both η_i and MCD modes versus ion Larmor radius. The ion parallel transport has been neglected but $\mu_1, \mu_2, \mu_3, \mu_4, \kappa_{i\perp}$ and $\kappa_{i\times}$ are all included. At $C_{a_i} = 0$ the model corresponds to that of the previous section. As C_{a_i} is increased the η_i mode (branch(2)) is little affected, but the MCD mode (branch(4)) is noticeably suppressed. This latter point seems to be in contradiction with Finn and Drake [4.16] who claim that the MCD mode is insensitive to the ion dynamics. However, the disagreement is quantitative rather than qualitative, since the mode remains unstable even at the twice the reference Larmor radius.

Thus we can draw the following conclusions from this section:

(i) it is often inappropriate to use Braginskii ion parallel transport when describing instabilities in RFP's and tokamaks. Many of the relevant instabilities have large frequencies ($\omega \approx \omega_{*e}$), and this coupled to the high temperatures and low densities, means that the ions are effectively collisionless ($\omega \gg \nu_{ii}$).

(ii) the inclusion of the finite ion Larmor radius terms, has a mildly destabilising effect on the η_i mode but a more obvious stabilising influence on the MCD mode. However, both ($m = 0, ka = 1.0$) modes remain unstable at the reference ZT-40M value of the ion Larmor radius.

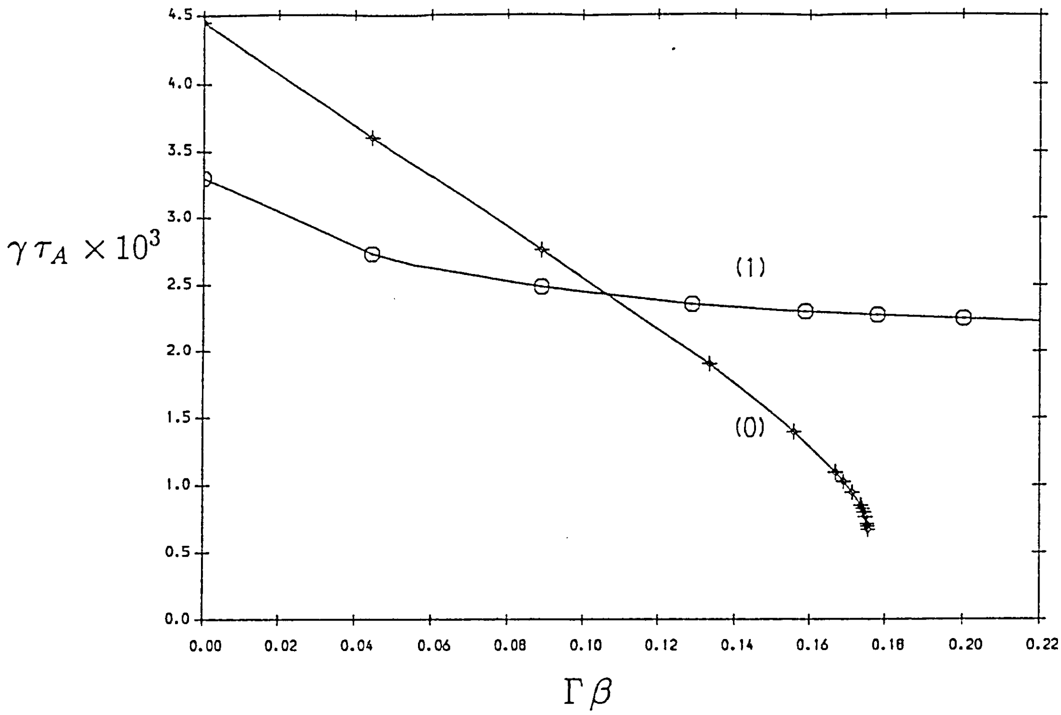

Figure 4.1: Growth-rate versus the value of $\Gamma\,\beta$ at the resonant point for even parity (0) and odd parity (1) modes. $S = 7.266 \times 10^5$, $T(1) = 0.1$.

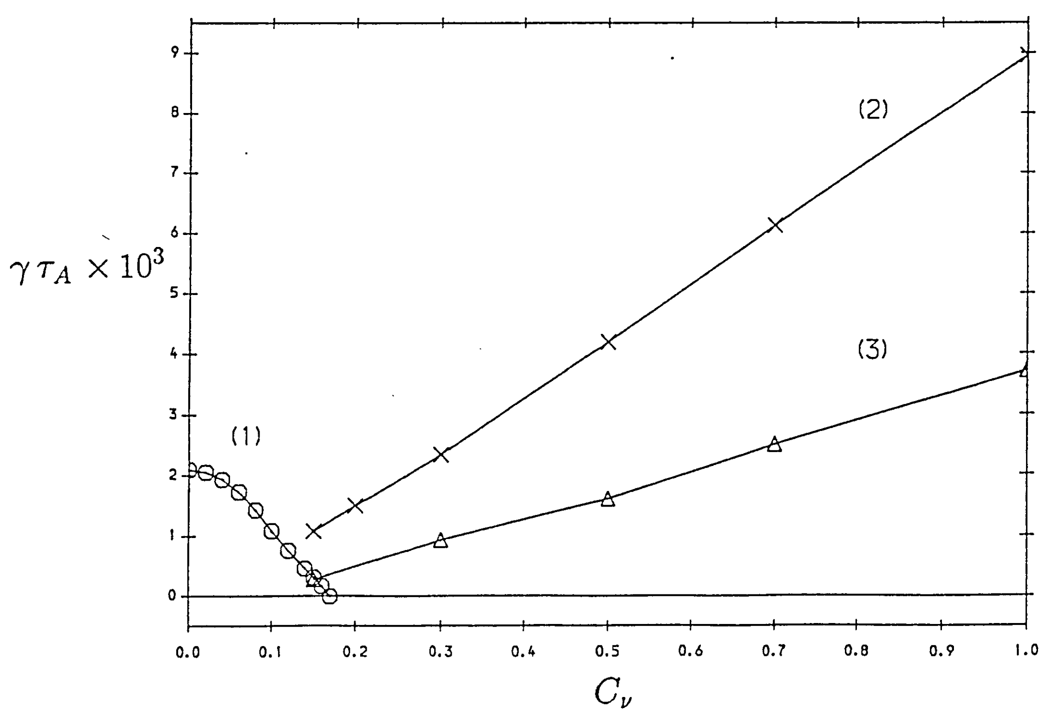

Figure 4.2: Growth-rate versus Hall parameter ($\nu = 0.294 \times C_\nu$). $S = 7.266 \times 10^5$, $T(1) = 0.1$.

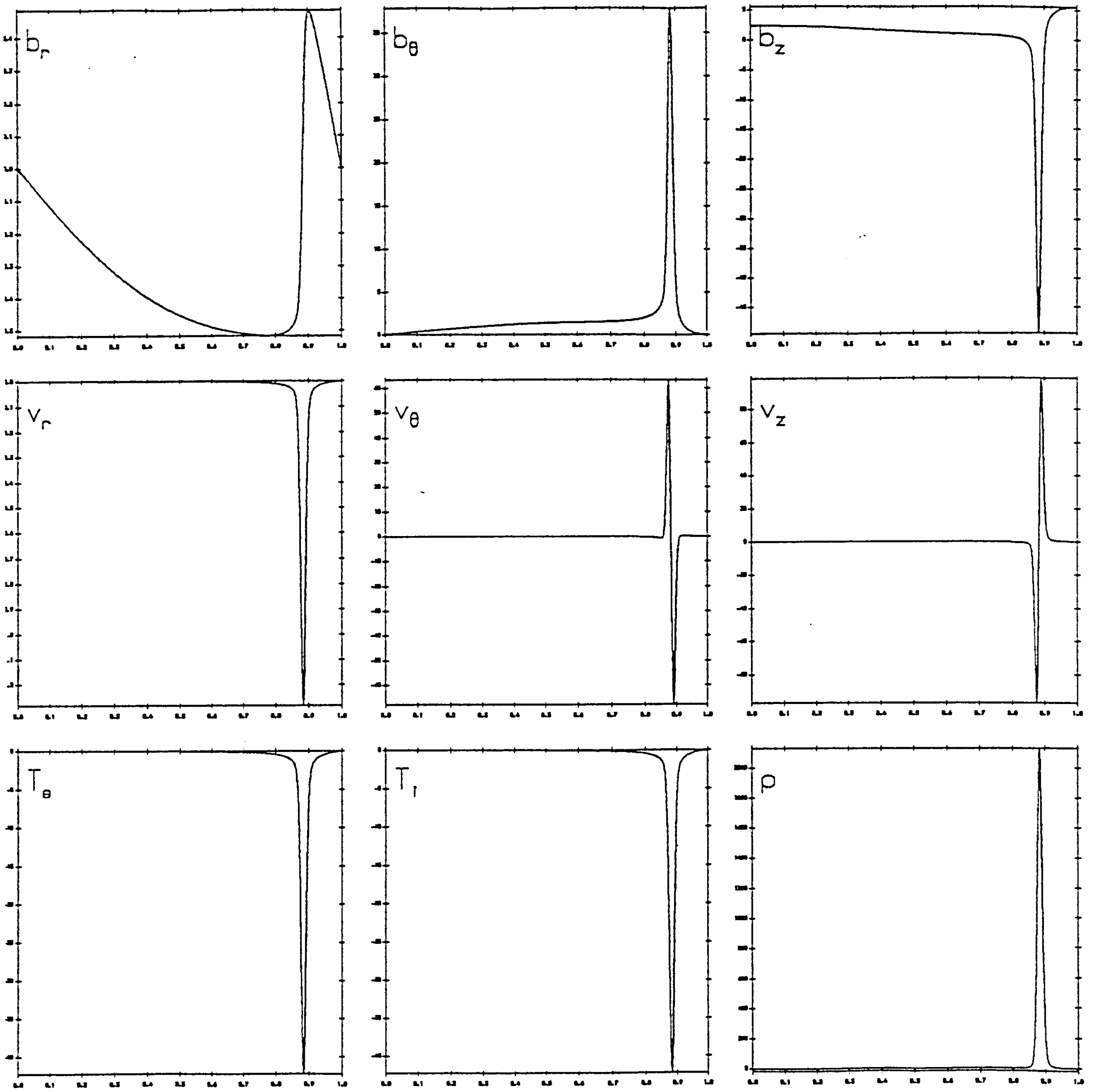

Figure 4.3: Profiles of perturbed variables for branch (0). $S = 7.266 \times 10^5$, $T(1) = 0.0$; $\gamma\,\tau_A = 1.999 \times 10^{-3}$.

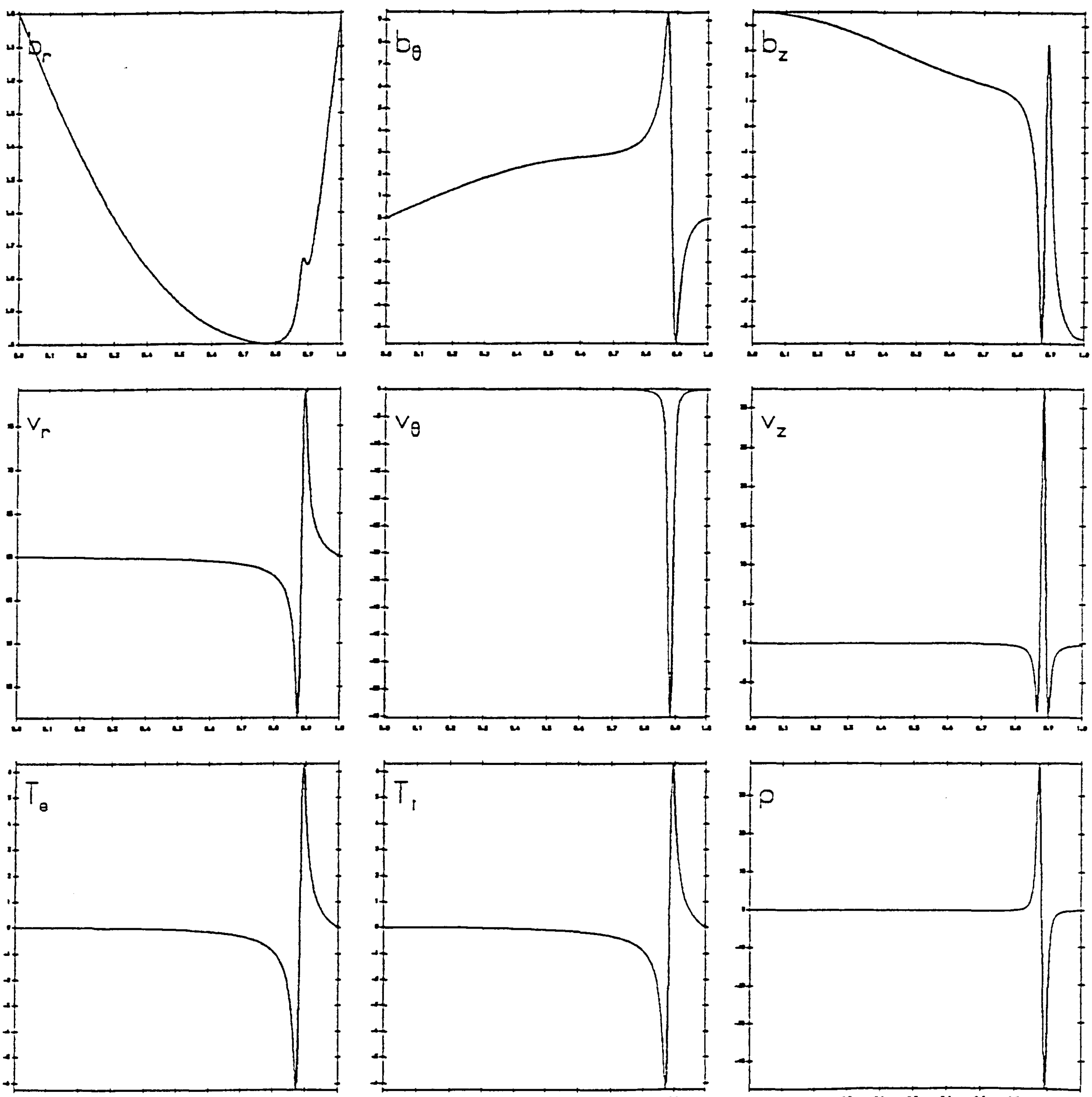

Figure 4.4: Profiles of perturbed variables for branch (1). $S = 7.266 \times 10^5$, $T(1) = 0.1$; $\gamma\,\tau_A = 2.096 \times 10^{-3}$.

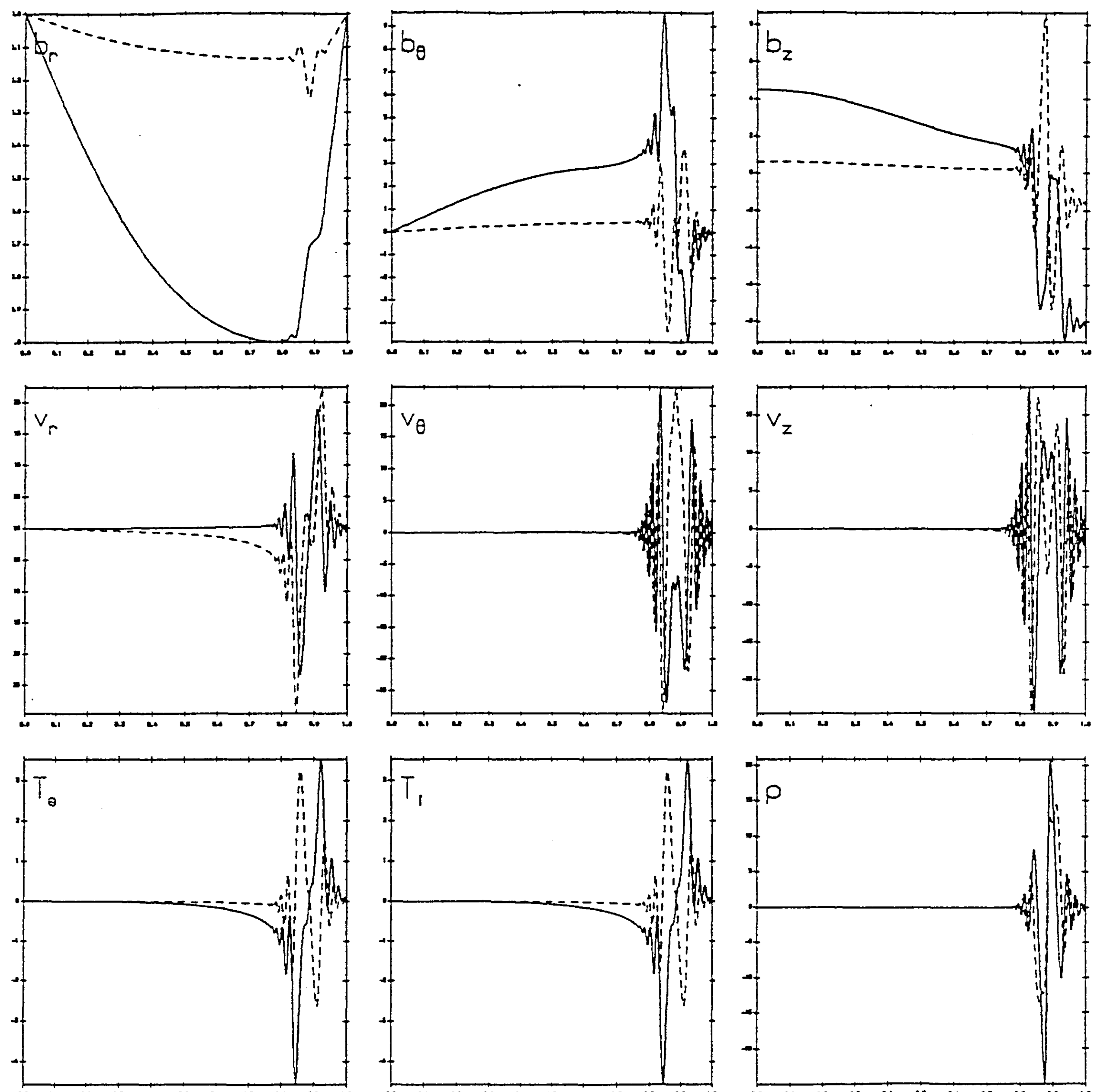

Figure 4.5: Profiles of perturbed variables for branch (1). The real part of the perturbation is represented by the continuous line and the imaginary part by the dotted line. $S = 7.266 \times 10^5$, $T(1) = 0.1$, $C_\nu = 0.16.$; $\gamma \tau_A = (0.1654 + i\,5.237) \times 10^{-3}$.

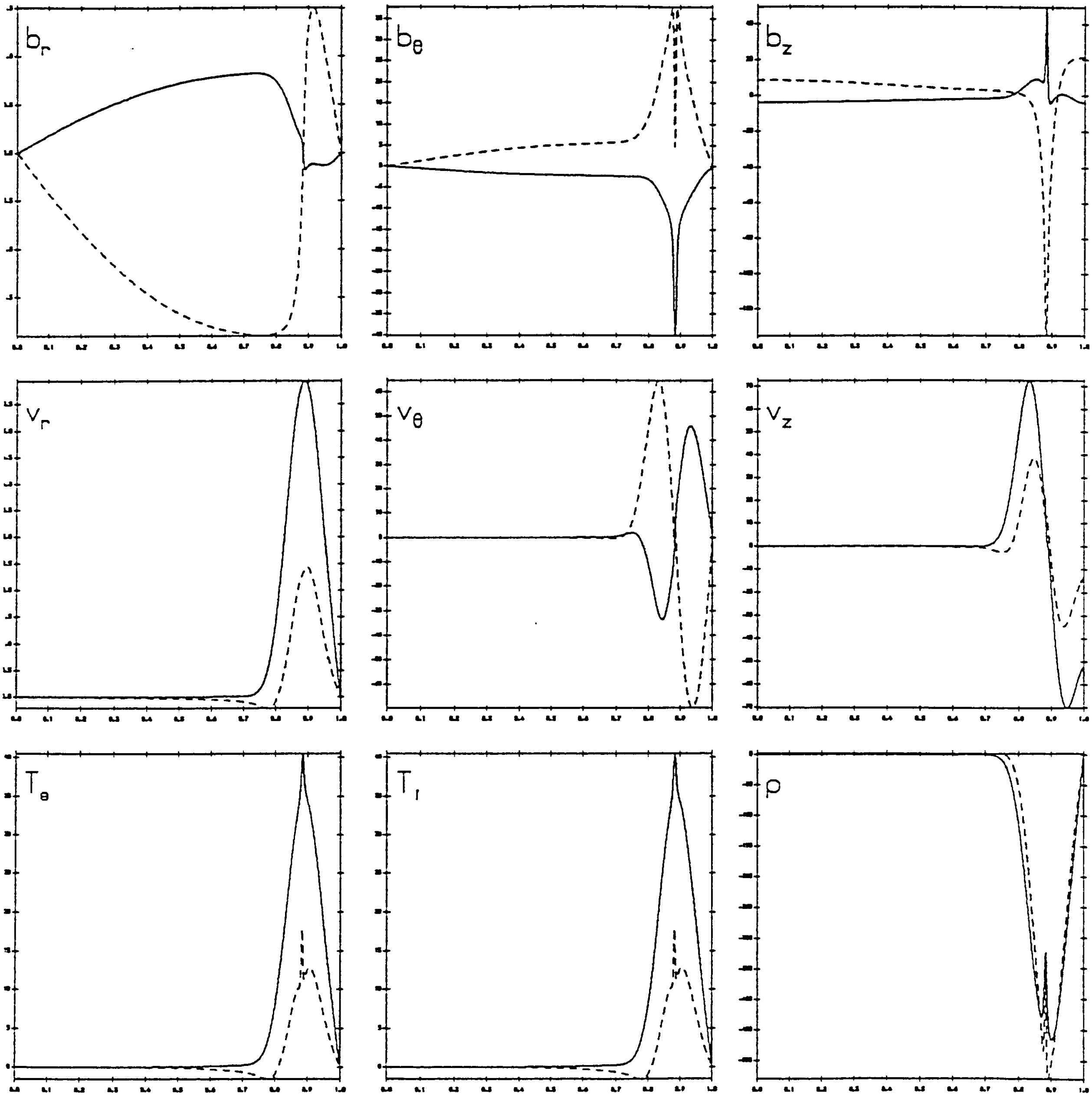

Figure 4.6: Profiles of perturbed variables for branch (2). $S = 7.266 \times 10^5$, $T(1) = 0.1$, $C_\nu = 1.0$, $\eta_i = \eta_e = \infty$; $\gamma\,\tau_A = (8.960 + i\,1.440) \times 10^{-3}$.

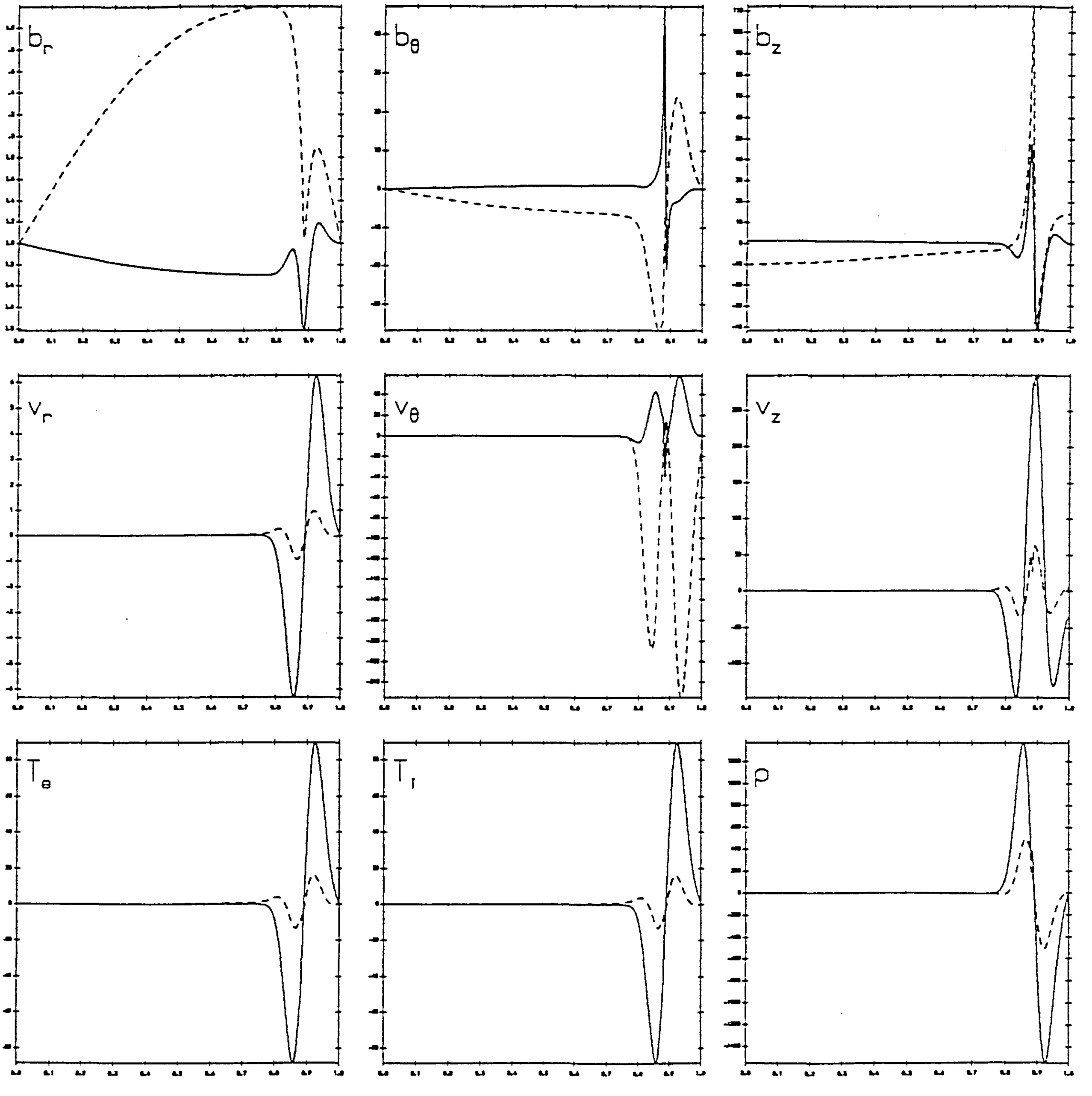

Figure 4.7: Profiles of perturbed variables for branch (3). $S = 7.266 \times 10^5$, $T(1) = 0.1$, $C_\nu = 1.0$, $\eta_i = \eta_e = \infty$; $\gamma\,\tau_A = (3.718 + i\,0.315) \times 10^{-3}$.

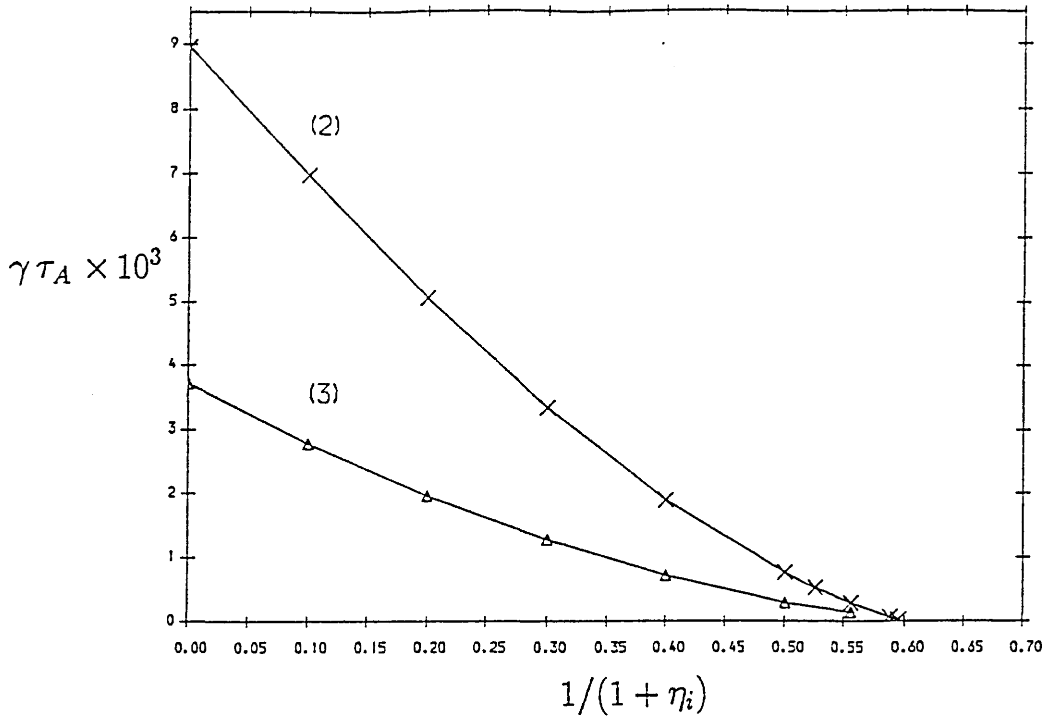

Figure 4.8: Growth-rate versus $1/(1+\eta_i)$ for branches (2) and (3). $S = 7.266 \times 10^5$, $T(1) = 0.1$, $C_\nu = 1.0$, $\eta_i = \eta_e$.

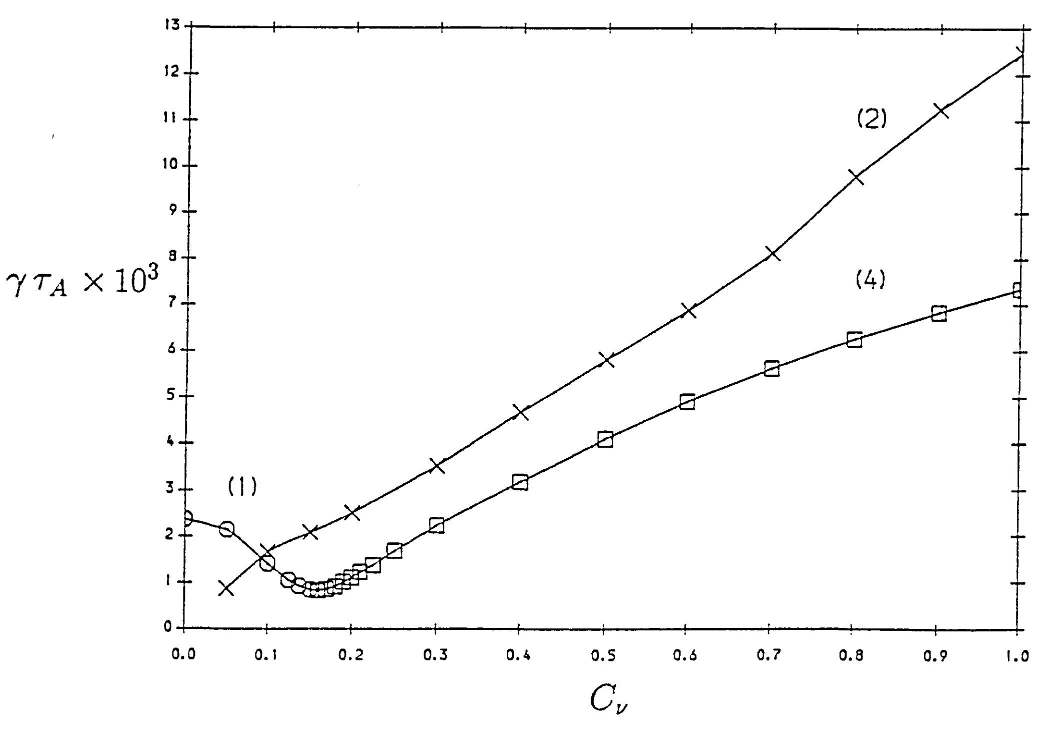

Figure 4.9: Growth-rate versus Hall parameter including electron thermal conductivity. $S = 7.266 \times 10^5$, $T(1) = 0.01$, $C_{\kappa_e} = (1,1,1)$, $\eta_i = \eta_e = \infty$.

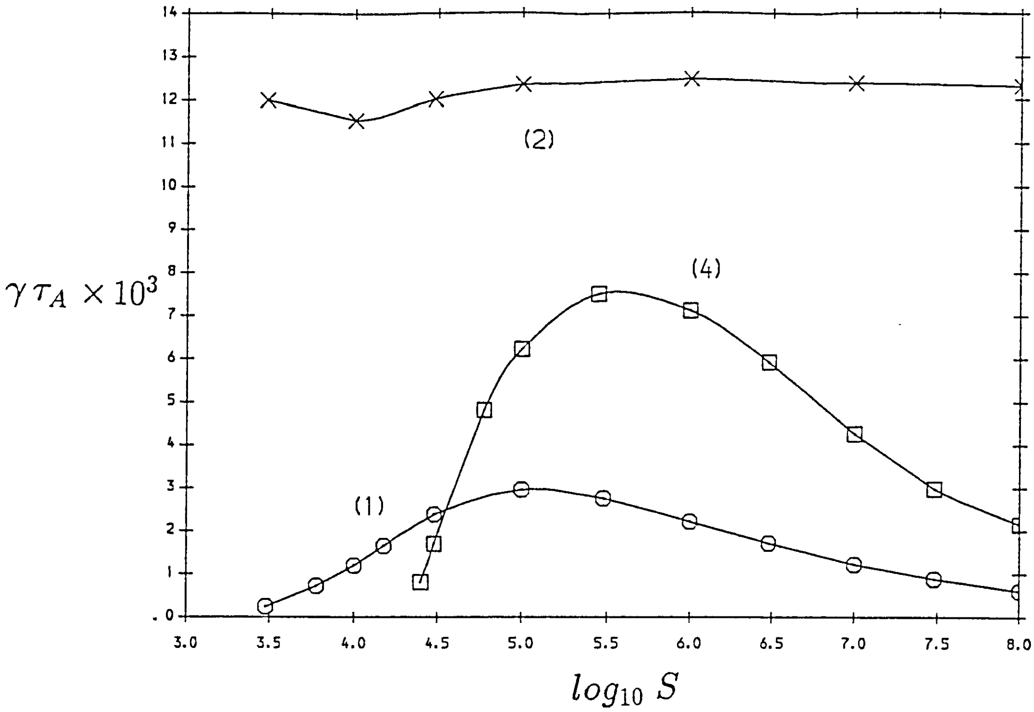

Figure 4.10: Growth-rate versus the logarithm of the Lundquist parameter for branches (1),(2) and (4). For branch (1) : $C_\nu = 0.0$, for branches (2) and (4) : $C_\nu = 1.0$. $T(1) = 0.01$, $C_{\kappa_e} = (1,1,1)$, $\eta_i = \eta_e = \infty$.

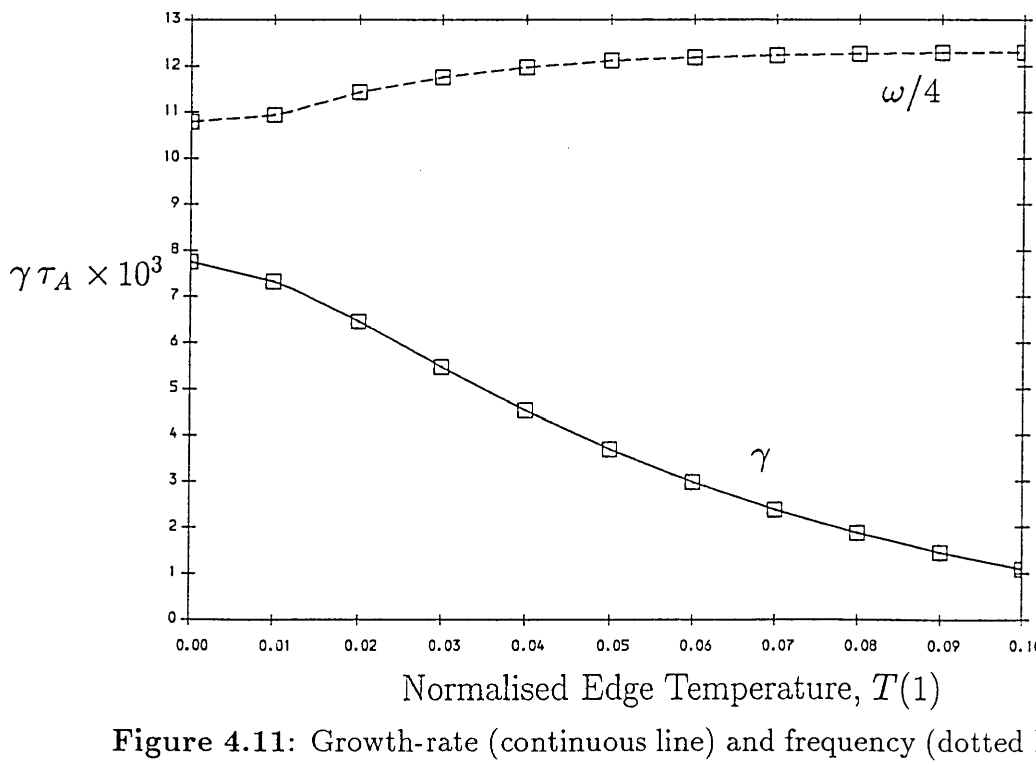

Figure 4.11: Growth-rate (continuous line) and frequency (dotted line) of branch (4) versus edge temperature, $T(1)$. $S = 7.266 \times 10^5$, $C_\nu = 1.0$, $C_{\kappa_e} = (1,1,1)$, $\eta_i = \eta_e = \infty$.

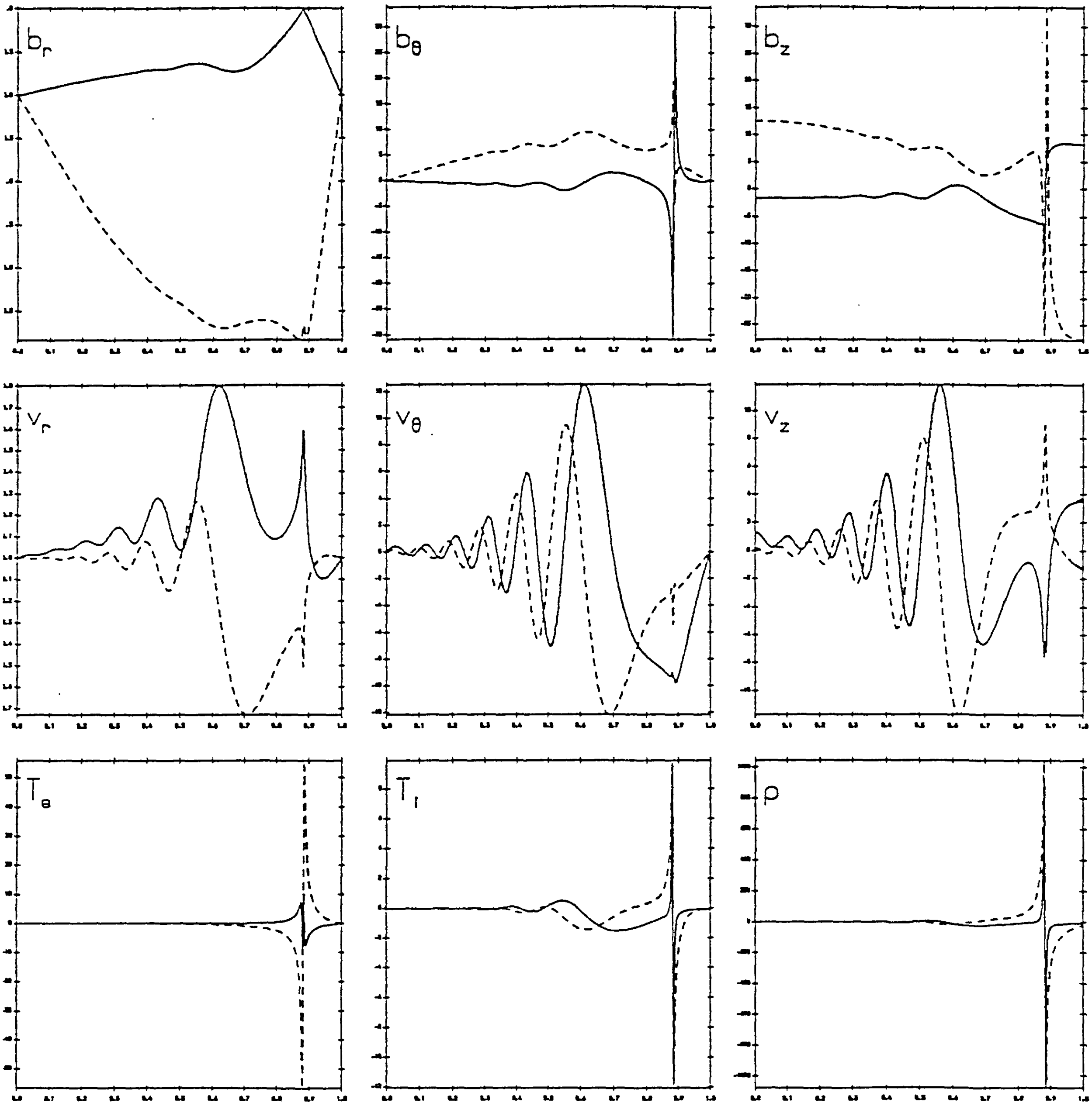

Figure 4.12: Profiles of perturbed variables for branch (4). $S = 7.266 \times 10^5$, $T(1) = 0.01$, $C_\nu = 1.0$, $C_{\kappa_e} = (1,1,1)$, $\eta_i = \eta_e = \infty$; $\gamma\, \tau_A = (7.332 + i\, 43.760) \times 10^{-3}$.

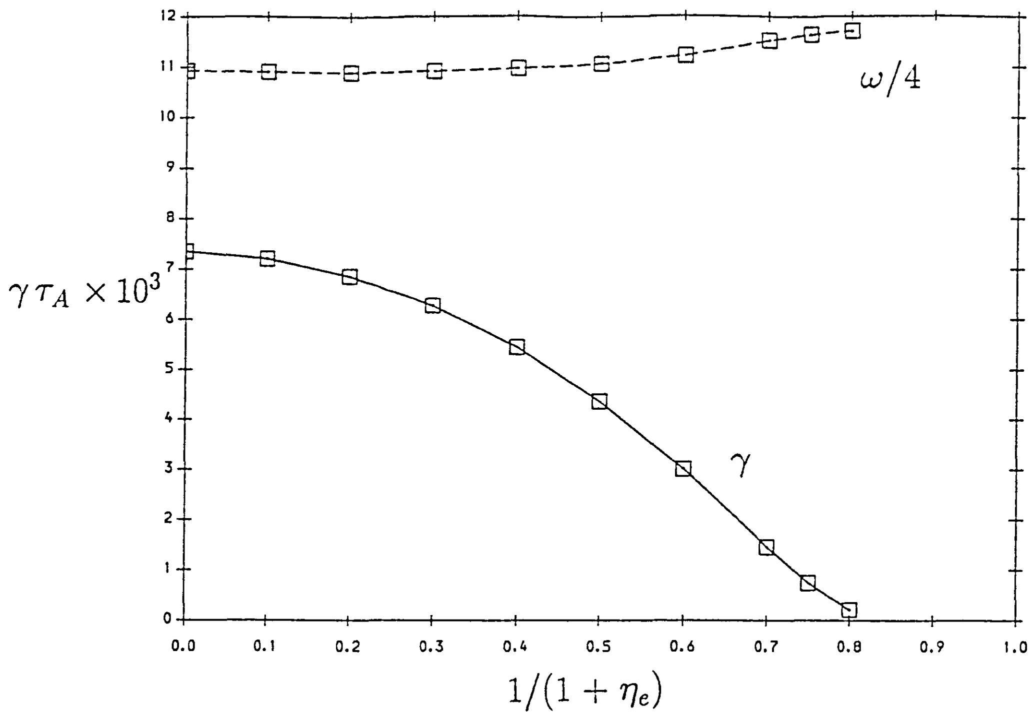

Figure 4.13: Growth-rate and frequency of branch (4) versus $1/(1+\eta_e)$. $S = 7.266 \times 10^5$, $T(1) = 0.01$, $C_\nu = 1.0$, $C_{\kappa_e} = (1,1,1)$, $\eta_i = \eta_e$.

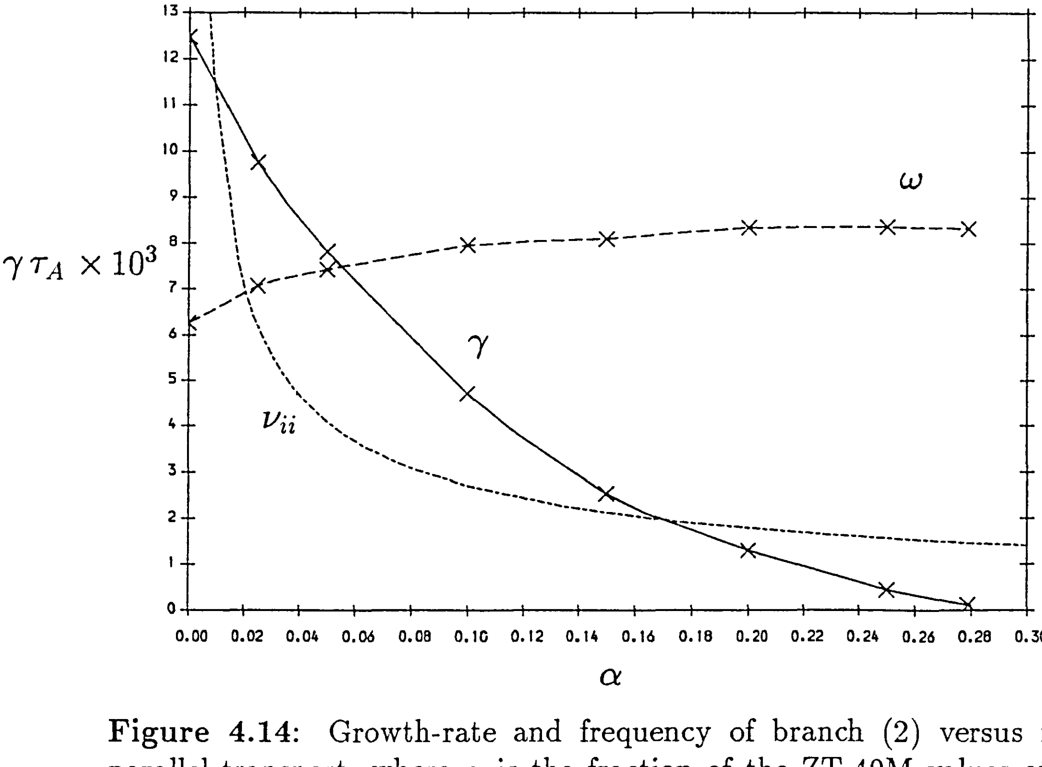

Figure 4.14: Growth-rate and frequency of branch (2) versus ion-parallel transport, where α is the fraction of the ZT-40M values of $\mu_{||}$ and $\kappa_{i||}$. Also shown as a dot-dash line, is the ion-ion collision frequency. $S = 7.266 \times 10^5$, $T(1) = 0.01$, $C_\nu = 1.0$, $C_{\kappa_e} = (1,1,1)$, $C_\mu = (\alpha,0,0,0,0)$, $C_{\kappa_i} = (\alpha,0,0)$, $\eta_i = \eta_e = \infty$.

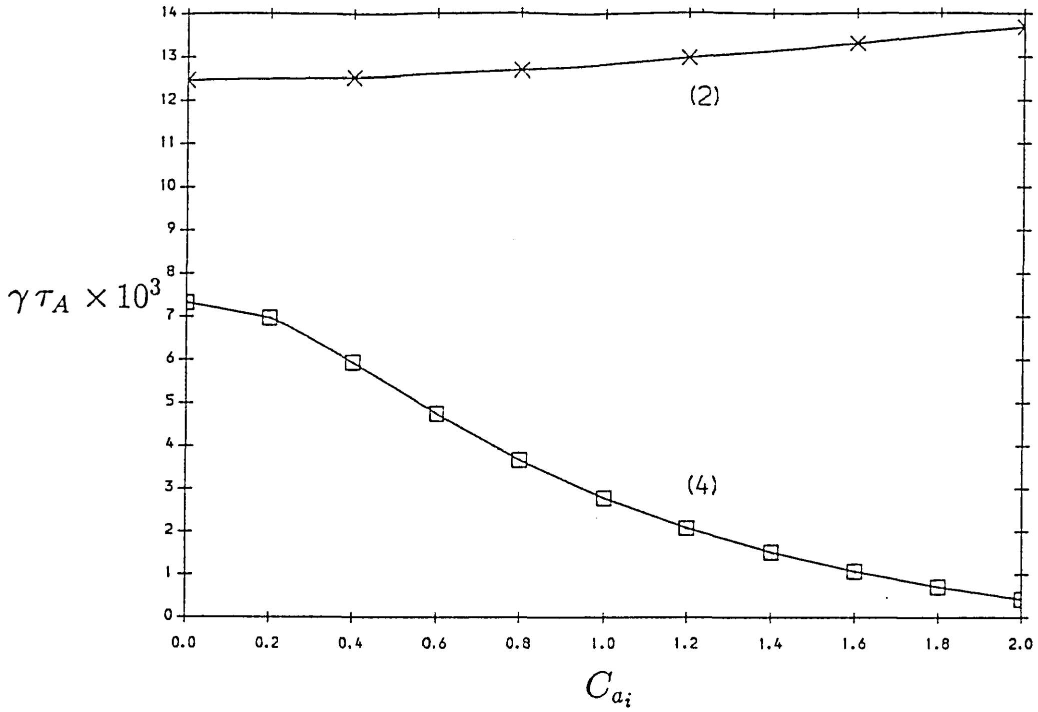

Figure 4.15: Growth-rates of branches (2) and (4) versus ion Larmor radius, ($a_i/a = 0.044 \times C_{a_i}$). $S = 7.266 \times 10^5$, $T(1) = 0.01$, $C_\nu = 1.0$, $C_{\kappa_e} = (1,1,1)$, $C_\mu = (0, C_{a_i}^2, C_{a_i}^2, C_{a_i}, C_{a_i})$, $C_{\kappa_i} = (0, C_{a_i}^2, C_{a_i})$, $\eta_i = \eta_e = \infty$.

4.7 Local Stability Parameters

In this section some important local stability parameters are calculated for the TMS equilibrium. The radial profiles of these parameters summarise the local stability properties of this equilibrium according to the various layer theories and allow comparison with the numerical work presented above. Also, since the numerical and analytical results are in good qualitative agreement, one may reasonably assume that the parameters embody the conclusions that would be derived from an extensive numerical study (i.e. one that examined all modes rather than just $m = 0$, $ka = 1.0$).

Figure 4.16 is a stability diagram for the twisting parity resistive mode (section 4.3). The ordinate is related to the normalised growth-rate derived by Finn and Mannheimer for compressible resistive MHD [4.11]:

$$\Omega^{3/2} = (\gamma\tau_A\, S^{1/3}\,(ka)^{-2/3})^{3/2} = \frac{\Gamma\beta B_\theta|P'|}{2r_s}\left(\frac{2D}{\Gamma\beta} - s - 1\right)$$

Thus wherever $\Omega^{3/2} > 0$ the equilibrium is unstable to an twisting parity resistive mode. For comparison note that the $m = 0$ mode is resonant at $r/a = 0.883$, so that for T(1)=0.1 this mode is stable, as stated in section 4.3. Figure 4.16 demonstrates the stabilising effect of finite beta. Although the twisting parity mode is unstable for $r/a \geq 0.75$ when T(1)=0.0, at T(1)=0.1 (higher beta) the mode is stable at every radial location.

Next, we summarise the stability of the resistive-g mode according to the theory of Hahm and Chen [4.18] (section 3.4). Recall that Hahm and Chen considered a model amounting to compressible resistive MHD plus the Hall terms in Ohm's Law. They found both twisting and tearing parity instabilities were suppressed with increasing electron drift frequency, ω_{*e}, so that for $\Delta' = 0$ both modes were stable for drift frequencies greater than some critical value. Since the drift frequency is proportional to the axial wavenumber, k, this defines a critical axial wavenumber:

$$k_c\, a = 4\,\sqrt{2}\,\pi^2 \frac{(\omega_{ci}\,\tau_A)^3}{S}\frac{r_s}{a}\frac{\bar{B}}{B_\theta}\frac{\sqrt{s}D}{\Gamma\beta^2}$$

Modes with $k > k_c$ are stable. Figure 4.17 shows the corresponding critical toroidal mode number ($n_c = k_c/R_0$) for the TMS equilibrium using the reference ZT-40M parameters. Since this equilibrium has $\Delta' < 0$ everywhere this figure may be considered a pessimistic estimate of the stability of tearing parity resistive modes. Note also that integer values of n_c are the only ones with any physical significance (integer n_k being the requirement for single- valuedness in a toroidal device). Thus for T(1)=0.1, all modes with $n_k > 0$ are stable everywhere except close to the axis. The situation is similar for T(1)=0.0, although the vanishing of β at the wall leads to an additional unstable region. Above all else, figure 4.17 demonstrates the strong stabilising effect of Hall terms on resistive-g modes, and suggests that instabilities of this type should be far less prevalent in current RFP's than is implied by simple resistive MHD. However, as was made clear in section 4.5 this conclusion only applies when the electrons obey an adiabatic equation of state.

When the model is extended to include finite electron thermal conductivity the g-mode no longer stabilises with increasing ω_{*e}, instead it evolves into the Magnetic Curvature Drift (MCD) mode [4.16]. Figures 4.18 and 4.19 show the important parameters for the MCD mode [4.16]. Recall that this mode can be driven unstable by either curvature or cross-field transport. In the former case an instability exists for a range of ω_c/ω_{*e} (see figure 3.3) values. The ratio ω_c/ω_{*e} is shown in figure 4.18. The regime of instability shrinks with decreasing η_e, but always lies in the domain $0.05 < \omega_c/\omega_{*e} < 2.9$ (for positive values of η_e). Thus we conclude from figure 4.18, that the TMS equilibrium will be unstable to a MCD mode that is resonant at large radii, with the unstable region considerably diminished at large T(1). Figure 4.19 shows the parameter that determines the destabilising effect of cross-field transport:

$$\zeta_* = \frac{L_s}{2L_p}$$

where

$$L_s = \left| \frac{P}{P'} \frac{B^2}{B_z B_\theta} \right|$$

is the shear length and

$$L_p = \left| \frac{p}{p'} \right|$$

is the length-scale associated with the pressure. The reader is referred to reference [4.16] for further details. Here we need only point out that the MCD mode can be driven by the perpendicular transport even in the absence of curvature, and that under these conditions the mode is maximally unstable (i.e. has largest growth-rate) at $\zeta_* \approx 0.4$.

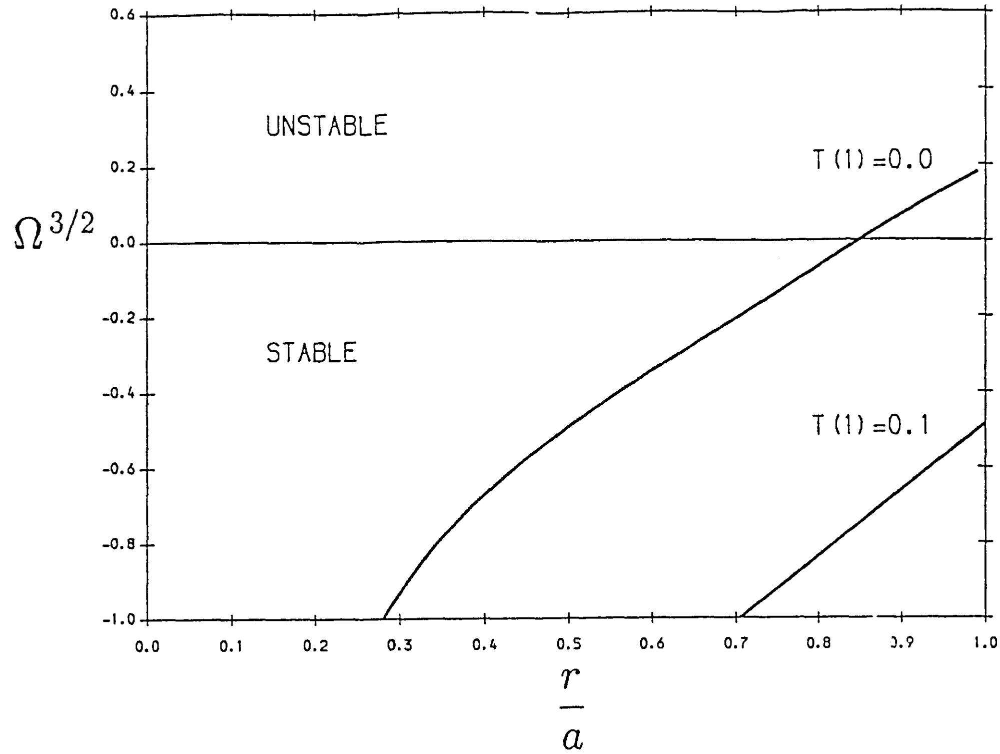

Figure 4.16: Stability diagram for the even parity resistive mode in the TMS equilibrium with $D = 0.2$ and $\Gamma = 5/3$. Here Ω is a normalised growth-rate: $\Omega = \gamma\tau_A\, S^{1/3}\,(ka)^{-2/3}$.

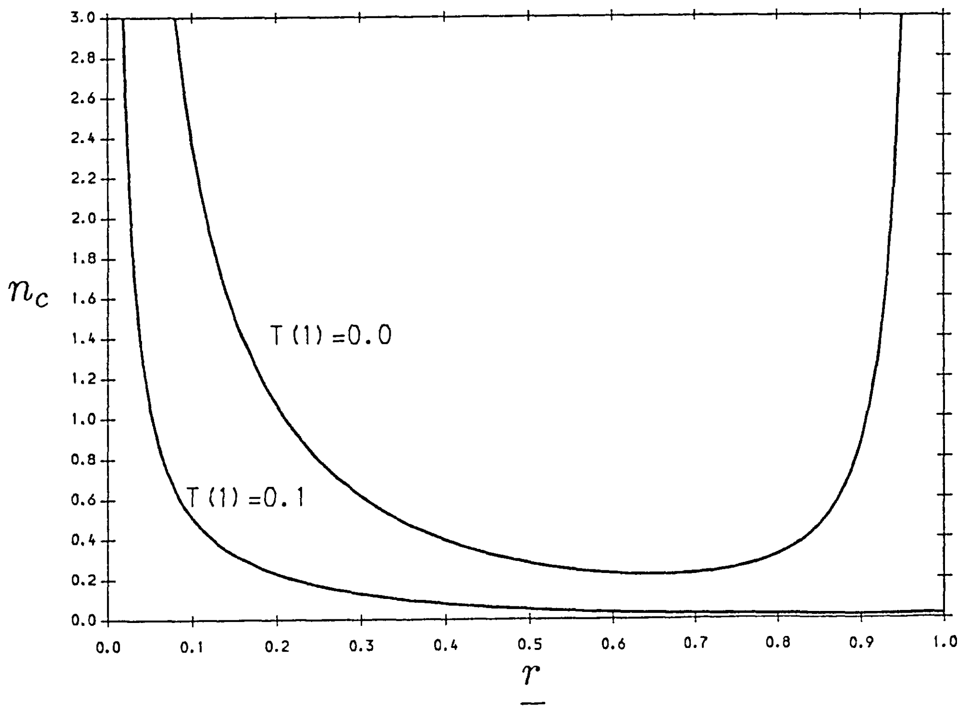

Figure 4.17: Critical toroidal mode number, n_c, for the resistive-g mode in the TMS equilibrium with $D = 0.2$ and for ZT-40M parameters. Modes with $n > n_c$ are stabilised by the Hall terms.

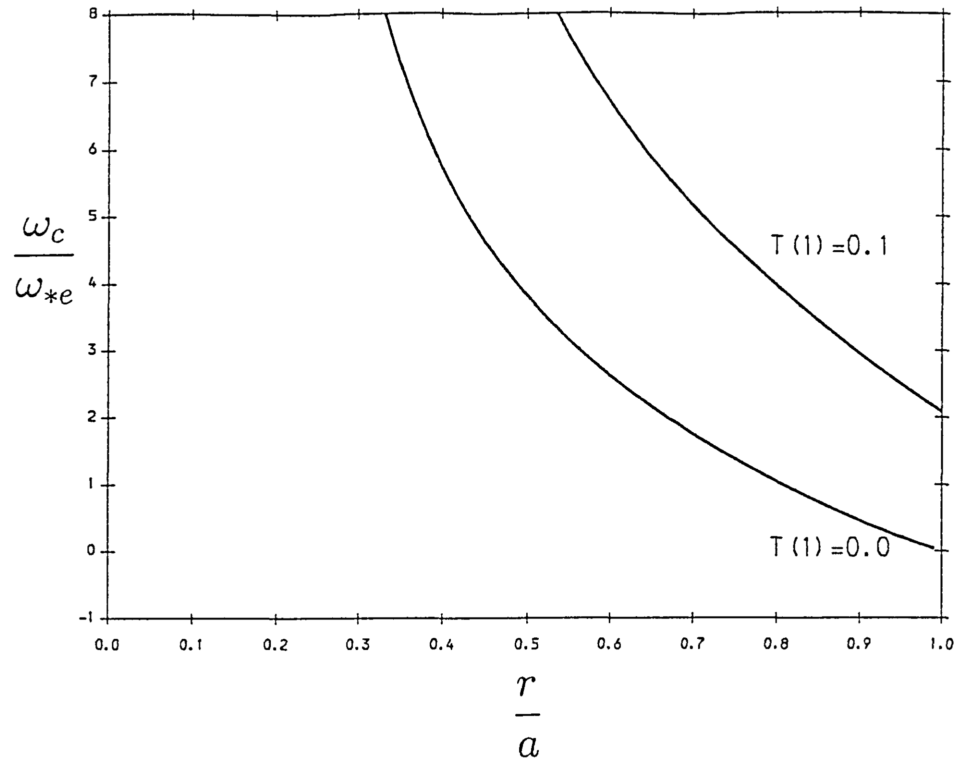

Figure 4.18: ω_c/ω_{*e} for the TMS equilibrium with $D = 0.2$ and $T_e = T_i$. For $\eta_e = \infty$ the MCD mode is unstable for $0.05 \leq \omega_c/\omega_{*e} \leq 2.9$.

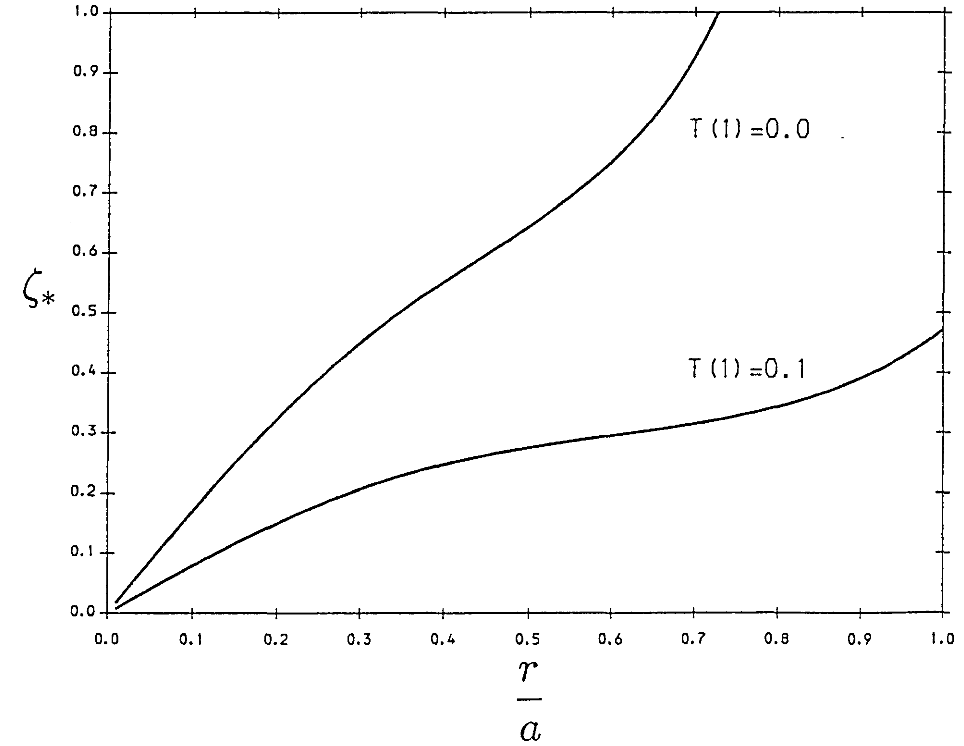

Figure 4.19: ζ_* for the TMS equilibrium with $D = 0.2$ and $T_e = T_i$. For finite ζ_* the MCD mode can be destabilised by cross-field transport even in the absence of curvature, with a maximum growth-rate at $\zeta_* \approx 0.4$ (see reference [4.9]).

4.8 Conclusion

The paper by MOKBE [4.5] was the prime motivation for this chapter. In that work the ODRIC linear stability code was used to examine the effect of additional transport on resistive instabilities in a tearing mode stable Reversed field pinch equilibrium. Surprisingly, MOKBE reported total stability when all available terms were included. This appears to be in contradiction with some of the existing analytical work.

This chapter contains new results obtained using the modified version of ODRIC (see chapter 2). The equations solved are those of the version used by MOKBE but now including the equilibrium density gradient terms. The remaining modifications are all associated with more effective convergence, so that in the flat density limit the code is identical to the original. However, this chapter has been primarily concerned with a more careful comparison of the numerical results with the predictions from various layer theories, in the attempt to resolve some of the questions raised by reference [4.5].

In general, the layer theories have been demonstrated to be qualitatively correct. Thus:

(i) In compressible resistive MHD the twisting parity mode has been observed to be stabilised by finite $\Gamma\beta$ in agreement with reference [4.17]. This has required convergence to a mode other than the fastest growing mode, and would not have been possible in a conventional initial value code. It is therefore a demonstration of the considerable benefit that "tuning" of the timestep can yield (see section 2.3).

(ii) The inclusion of the Hall terms in Ohm's law leads to a coupling of the resistive-g mode with the electron drift wave. In agreement with references [4.11] and [4.18], the mode can be completely stabilised for typical experimental RFP parameters. However, a new instability (plus harmonics) emerges and has a growth rate increasing with ω_{*e}. This mode is the 'even' parity instability reported by MOKBE. The inclusion of the equilibrium density gradient terms has allowed a scaling of growth-rate with η_i to be determined. The mode has been shown to be stable for $\eta_i < 2/3$ and thus identified as the fluid limit of the η_i mode.

(iii) The extension of the model to include finite electron thermal conductivity leads to a different scaling of the resistive-g mode branch with ω_{*e}. At low ω_{*e} the mode is suppressed much as for the adiabatic electron model, but with increasing ω_{*e} (or equivalently ν) it is no longer completely stabilised. Instead it reaches a finite minimum growth-rate before evolving into a semicollisional tearing mode that is driven by the electron temperature gradient. The behaviour of this mode is in agreement with the work of Finn and Drake [4.16], who dubbed this limit of the branch the "Magnetic Curvature Drift Mode". The η_i mode has been observed independently and appears largely unaffected by the electron thermal conductivity.

Thus in the cold ion limit there are two important instabilities:

- the η_i mode
- the MCD mode.

(iv) The ion parallel transport appears to have a strong stabilising effect on the η_i mode, suggesting the source of the total stability observed by MOKBE. However, a comparison of the mode frequency with the ion-ion collision frequency shows the ions to be insufficiently collisional to be described by fluid equations. Thus in this regime ($\omega > \nu_{ii}$) the ion parallel transport can only be described by kinetic theory, and the effect of the parallel ion viscosity and parallel ion thermal conductivity must be discounted.

Inclusion of the finite Larmor radius terms alone shows the MCD mode can be suppressed by these but that the η_i mode has a growth-rate increasing with ion Larmor radius. However, both $m = 0$, $ka = 1.0$ modes remain unstable for the ZT-40 reference parameters.

Thus we conclude that there are (at least) two important confinement degrading (i.e. finescale) instabilities in RFP's:

- the η_i mode for $\eta_i > 2/3$.
- the MCD mode for $\omega_c/\omega_{*e} \lesssim 3$.

The performance of current and future RFP's is likely to be dependent on the non-linear dynamics of these modes. There have been numerous attempts to calculate the anomalous transport due to η_i modes, but only reference [4.19] has been specifically concerned with energy confinement in RFP's. There appears to be a good case for further studies, especially since the heating of the ions by dynamo fluctuations [4.20] suggests that ion thermal transport will be an important limiting factor for RFP confinement. As far as the author is aware, there are no publications dealing specifically with the transport due to MCD modes in RFP geometry. Here we will merely point out that the dominant transport mechanism is likely to be opposite for the two modes. The η_i mode is basically an electrostatic instability and so the anomalous transport to be expected from it will be largely due to the fluctuating $\tilde{\vec{E}} \times \vec{B}$ drifts, where $\tilde{\vec{E}}$ is the fluctuating electric field. In contrast the MCD mode is a tearing parity instability and therefore leads to the formation of magnetic islands. The resulting transport will presumably be of the "magnetic flutter" type.

References

[4.1] Furth, H.P., Killeen, J., Rosenbluth, M.N., Phys. Fl. **6**, 459 (1963).

[4.2] Mirin, A.J., Bonugli, R.J., O'Neill, N.J., Killeen, J., Comp. Phys. Comm. **41**, 85 (1986).

[4.3] Braginskii, S.I., Sov. Phys. J.E.T.P. **6**, 358 (1958).

[4.4] Dibiase, J.A., Killeen, J., Jour. Comp. Phys. **24**, 158 (1977).

[4.5] Mirin, A.J., O'Neill, N.J., Killeen, J., Bonugli, R.J., Ellis, M.J., Phys. Fl. **29**, 512 (1986).

[4.6] Robinson, D.C., Nucl. Fus. **18**, 939 (1978).

[4.7] Coppi, B., Greene, J.M., Johnson, J.L., Nucl. Fus. **6**, 101 (1966).

[4.8] Robinson, D.C., Dibiase, J.A., Furzer, A.S., Killeen, J., Nunn-Price, J.E., The Growth of Resistive Instabilities in a Diffuse Pinch, Internal Rep. CLM-P710, Culham Laboratory (1983).

[4.9] Hosking, R.J., Robinson, D.C., in Controlled Fusion and Plasma Physics (Proc. 9^{th} Eur. Conf. Oxford, 1979), Vol.1, European Physical Society (1979) 61.

[4.10] Hender, T.C., Robinson, D.C., Com. Phys. Comm. **24**, 413 (1981).

[4.11] Finn, J.M., Mannheimer, W.M., Antonsen, T.M., Phys. Fl. **26**, 962 (1983).

[4.12] Suydam, B.R., in Peaceful Uses of Atomic Energy (Proc. 2^{nd} United Nations Int. Conf. Geneva, 1958) (United Nations, 1958), Vol.31, 157.

[4.13] Baker, D.A., Buchenauer, C.J., Burkhardt, L.C., et al., in Plasma Physics and Controlled Nuclear Fusion Research 1984 (Proc. 12^{th} Int. Conf. London, 1984), Vol.II, IAEA, Vienna (1985) 439.

[4.14] Coppi, B., Rosenbluth, M.N., Sagdeev, R.Z. , Phys. Fl. **10**, 582 (1967).

[4.15] Antonsen, T., Coppi, B., Englade, R., Nucl. Fus. **19**, 641 (1979).

[4.16] Finn, J.M., Drake, J.K., Phys. Fl. **29**, 3672 (1986).

[4.17] Finn, J.M., Mannheimer, W.M., Phys. Fl. **25**, 697 (1982).

[4.18] Hahm, T.S., Liu Chen, Phys. Fl. **28**, 2432 (1985).

[4.19] An Z.G., Lee G.S., Diamond P.H., Energy Confinement in a High-Current Reversed Field Pinch, Internal Rep. IFSR #96, Institute of Fusion Studies, Univ. of Texas (1985).

[4.20] Carolan, P.G., Field, A.R., Lazaros, A., Rusbridge, M.G., Tsui, H.Y.W., Bevir, M.K., in Controlled Fusion and Plasma Physics (Proc. 14^{th} Eur. Conf. Madrid, 1987) Vol.2, Part I, European Physical Society (1987) 469.

[4.21] Gibson, R.D., Whiteman, K.J., Plas. Phys. **10**, 1101 (1968).

[4.22] Hastie, R.J., private communication (1987).

Appendix 4A : Tearing Mode Growth-Rates in the BFM

In order to test the accuracy of ODRIC, all transport except resistivity was "switched off" and the growth-rates of tearing modes in the Bessel Function Model (BFM) were determined. The BFM equilibrium takes the simple form:

$$
\begin{aligned}
B_\theta &= B_0\, J_1(\mu r) \\
B_z &= B_0\, J_0(\mu r)
\end{aligned}
$$

and this allows an exact analytic calculation of Δ', where:

$$
\Delta' = \left.\frac{b_r'}{b_r}\right|_+ - \left.\frac{b_r'}{b_r}\right|_-
$$

The required functional form of b_r can be obtained by solving the linearised version of $\nabla \times \vec{B} \times \vec{B} = 0$. The solution yields the following expression for Δ':

$$
\begin{aligned}
\Delta' &= \left[\frac{\frac{m\mu(\mu^2-k^2)^{1/2}}{\mu-k} Z_{m-1}(x_s) - \left(\frac{kr_s^2(\mu+k)+m^2}{r_s}\right) Z_m(x_s)}{kr_s\frac{(\mu^2-k^2)^{1/2}}{\mu-k} Z_{m-1}(x_s) + mZ_m(x_s)}\right] \\
&- \left[\frac{\frac{m\mu(\mu^2-k^2)^{1/2}}{\mu-k} J_{m-1}(x_s) - \left(\frac{kr_s^2(\mu+k)+m^2}{r_s}\right) J_m(x_s)}{kr_s\frac{(\mu^2-k^2)^{1/2}}{\mu-k} J_{m-1}(x_s) + mJ_m(x_s)}\right] \qquad (4A.1)
\end{aligned}
$$

where:

$$
\begin{aligned}
Z_m(x_s) &= J_m(x_s) - C\,Y_m(x_s) \\
x_s &= r(\mu^2 - k^2)^{1/2} \\
C &= \frac{mJ_m(x_w) + \frac{(\mu^2-k^2)^{1/2}}{\mu-k} kr_w J_{m-1}(x_w)}{mY_m(x_w) + \frac{(\mu^2-k^2)^{1/2}}{\mu-k} kr_w Y_{m-1}(x_w)}
\end{aligned}
$$

with r_w the wall radius, J_m the m^{th} order bessel function of the first type and Y_m the m^{th} order bessel function of the second type.

For $m = 0$ this reduces to the expression given by Gibson and Whiteman [4.21]:

$$\Delta' = \frac{-2\,J_1(x_w)}{\pi r_s J_1(x_s)[Y_1(x_w)\,J_1(x_s) - J_1(x_w)\,Y_1(x_s)]} \tag{4A.2}$$

Resistive layer theory yields the growth-rate as a function of Δ':

$$\gamma\tau_A = 0.547\left(\frac{ka\,\hat{B}_\theta\hat{P}'}{\hat{r}_s}\right)^{2/5} S^{-3/5}\Delta'^{4/5} \tag{4A.3}$$

where all variables have been normalised so that $\hat{B}_\theta = B_\theta/\bar{B}$, $\hat{r}_s = r_s/a$ etc.

Figure 4.20 is a log-log plot of growth-rate versus Lundquist parameter for $m = 0$, $ka = 1.65$, and $\mu = 5.5$. The two solid lines correspond respectively to growth-rates from ODRIC and from an incompressible code. The latter were supplied by Peter Kirby at Culham Laboratory. The dotted line represents the analytic result. Notice that the numerical results only approach the analytic theory in the $S \to \infty$ limit. This is a good illustration of the limitations of the layer theory, which includes resistivity only in a narrow region about the resonant point. As such it captures the fundamental effect of resistivity, i.e. reconnection, but neglects the damping effect of the resistivity outside the resonant layer. A proper treatment of the latter requires retaining resistivity throughout the plasma, and generally demands a numerical treatment. At low S values the resistive damping can in fact dominate so that the growth-rate increases with increasing S, ($\gamma \propto S$), rather than following the $S^{-3/5}$ tearing-mode scaling. However, at large S the resistive damping is negligible and the numerical and analytic results are in good agreement.

The slight discrepency between the incompressible results of P.Kirby and the compressible results of ODRIC is attributable to the small stabilising effect that arises from allowing only incompressible motions [4.22].

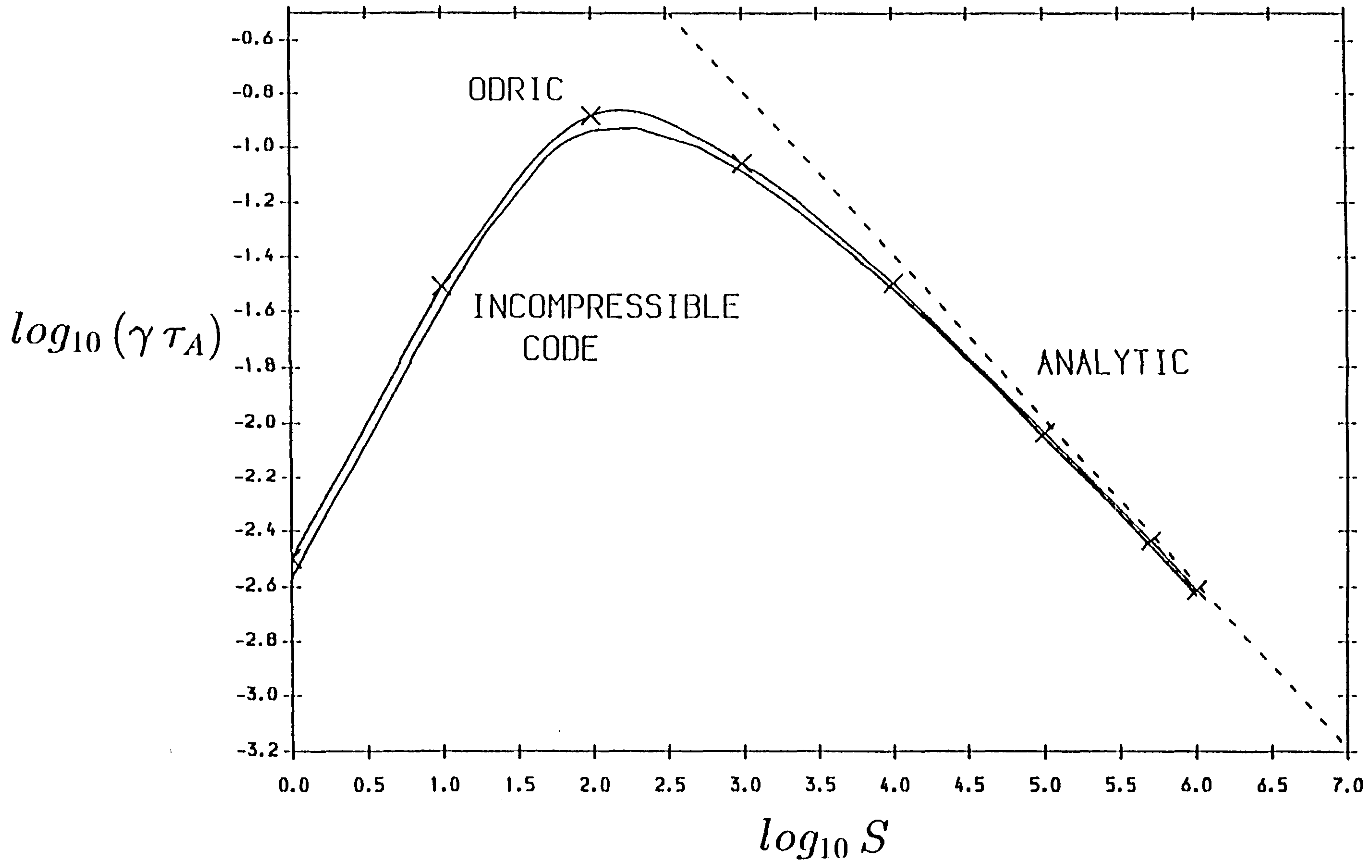

Figure 4.20: Normalised growth-rate versus Lundquist parameter for the $m = 0$, $ka = 1.65$ tearing mode in the BFM with $\mu = 5.5$.

Chapter 5

Resistive and Viscous Effects on Z-Pinch Stability

5.1 Introduction

The theoretical description of the Z-pinch in terms of Ideal MHD suggests that it is strongly unstable to large-scale instabilities growing on the Alfvén timescale [5.1]. However, Z-pinch experiments often achieve discharges lasting for many Alfvén times [5.2], [5.3]. Much of the work of Z-pinch theorists is directed towards finding an explanation for this anomalous stability.

Papers by Culverwell and Coppins [5.4] and Cochran and Robson [5.5], have shown that the evolution of the equilibrium is of importance for resistive Z-pinches. They find that the time-dependence of the equilibrium can have a stabilising influence on global $m = 0$ and $m = 1$ modes for sufficiently small Lundquist parameter, S. This is seen to be of particular relevance to the results from deuterium fibre pinches [5.6].

Spies [5.7] has looked at the combined effect of resistivity and collisional viscosity on the stability of static equilibria. Since reference [5.7] was the primary motivation for this chapter it is briefly reviewed in the next section.

5.2 Review of Work by Spies

Spies studied the effect of a scalar viscosity and resistivity on the modes of an incompressible plasma. His starting point was the following set of linearised equations for a mode of frequency, ω:

$$\left(i\omega - \frac{1}{R}\nabla^2\right)\vec{v} + \nabla\chi - (\vec{B}.\nabla)\vec{b} - (\vec{b}.\nabla)\vec{B} = 0 \tag{5.1}$$

$$\left(i\omega - \frac{1}{S}\nabla^2\right)\vec{b} + (\vec{v}.\nabla)\vec{B} - (\vec{B}.\nabla)\vec{v} = 0 \tag{5.2}$$

$$\nabla.\vec{b} = 0 \tag{5.3}$$

$$\nabla.\vec{v} = 0 \tag{5.4}$$

where χ is the total perturbed pressure (thermal+magnetic). The variables in these equations have been normalised to the pinch radius, a, the Alfvén velocity,

v_A, and the magnetic field at $r = a$. The resistivity and viscosity are contained respectively in the Lundquist parameter, S, and the viscous Reynold's number, R:

$$S = \frac{\tau_R}{\tau_A} = \frac{4\pi a^2}{\eta c^2}\frac{1}{\tau_A}$$

$$R = \frac{\tau_v}{\tau_A} = \frac{\rho a^2}{\mu_{||}\tau_A}$$

To make progress analytically Spies specifically considered modes with short axial wavelengths in a weakly dissipative plasma, i.e. $k^2 \sim S \sim R \ll 1$. Under this ordering the model yields the following tenth order differential equation:

$$\left\{\left[\left(i\omega + \frac{k^2}{R}D^2\right)\left(i\omega + \frac{k^2}{S}D^2\right) + \frac{m^2B^2}{r^2}\right]^2 D^2 - \frac{4m^2B^4}{r^4}\right.$$

$$\left. -2B\left(\frac{B}{r}\right)'\left[\left(i\omega + \frac{k^2}{R}D^2\right)\left(i\omega + \frac{k^2}{S}D^2\right) + \frac{m^2B^2}{r^2}\right]\right\} v_r = 0 \qquad (5.5)$$

where

$$D^2 = 1 + \frac{1}{k^2}\frac{d^2}{dr^2}$$

Interestingly, this equation is invariant under the interchange of S and R. Thus any stability conditions derived from it must contain viscosity and resistivity on an equal footing.

Ideally one would like to solve equation 5.5 and obtain eigenfrequencies as a function of S and R, but in general this is not straightforward. However, for the special case of the constant current density equilibrium:

$$\frac{B}{r} = \frac{J_z}{2} = 1$$

$$\left(\frac{B}{r}\right)' = 0$$

equation 5.5 reduces to one with constant coefficients and has a solution:

$$v_r \sim \exp\{in_r\pi r\}$$

where n_r counts the radial nodes of the eigenfunction. The dispersion relation that results is a quartic in ω, but it may be factorised into two quadratics, which may be compactly written in the form:

$$\omega^2 - i\left\{\frac{k^2}{S} + \frac{k^2}{R}\right\} p^2\omega - \frac{k^4}{RS}p^4 - m^2 \pm \frac{2m}{p} = 0 \tag{5.6}$$

where:

$$p^2 = 1 + \frac{n_r^2\pi^2}{k^2}$$

The positive and negative signs correspond to the two separate quadratics. Equation 5.6 differs from the dispersion relation for Alfvèn waves in a uniform field [5.8] only by the additional $\pm 2m/p$ term. We are primarily interested in the unstable roots of equation 5.6, i.e. ones which have $Im\{\omega\} < 0$. Since this model yields purely imaginary unstable eigenvalues, the most unstable root is the one with the largest positive value of $i\omega$:

$$i\omega = \gamma = \left[\frac{k^4p^4}{4}\left\{\frac{1}{S} + \frac{1}{R}\right\}^2 + \frac{2m}{p} - m^2\right]^{1/2} - \left(\frac{1}{S} + \frac{1}{R}\right)\frac{k^2p^2}{2}$$

The maximally unstable mode of this root has $m = 1$ and $p = 1$ (no radial nodes):

$$\gamma_{max} = \left[\frac{k^4}{4}\left\{\frac{1}{S} + \frac{1}{R}\right\}^2 + 1\right]^{1/2} - \left(\frac{1}{S} + \frac{1}{R}\right)\frac{k^2}{2}$$

Thus for total stability we require $\gamma_{max} < 0$, which leads to a condition on the axial wavenumber, k:

$$k > k_c = (SR)^{1/4} \tag{5.7}$$

Equation 5.7 is the primary result of Spies' paper [5.7]. It states that short wavelength modes (i.e. ones with $k > k_c$) can be stabilised by the combined effect of resistivity and viscosity. Indeed, in this ordering the stabilisation is due to the product of R and S, so if either the viscosity or resistivity is excluded the effect disappears.

Spies also considered general Z-pinch current profiles. He was able to show that a similar stabilising effect occurs, and for $m = 1$ he ascertained the range in which the critical wavenumber, k_c, lies:

$$SRJ_0^2 \leq 4k_c^4 \leq SRJ_{max}^2 \tag{5.8}$$

where J_0 is the current density on axis, and J_{max} is the maximum current density (both normalised so that $B(a) = 1$).

Equations 5.7 and 5.8 offer the intriguing possibility of explaining some of the reports of anomalous Z-pinch stability. However, the model used by Spies' to derive these conditions is unrealistic in two ways:

(i) The assumption of incompressibility.
In particular this makes it impossible to describe the $m = 0$ sausage modes. Thus the dispersion relation (equation 5.6) yields no unstable $m = 0$ modes, whereas there are growing $m = 0$ modes in a compressible plasma.

(ii) The use of a scalar viscosity.
This means that the results are only strictly applicable in the $\omega_{ci}\tau_i \rightarrow 0$ limit. Otherwise the viscosity should be described by the Braginskii ion stress tensor (see appendix 1B and [5.9]).

In this chapter both of these shortcomings are eliminated, so that a more experimentally relevant picture of visco-resistive stabilisation can be formed. The results have been obtained numerically using the ODRIC initial value code [5.10]. Since the equations are solved computationally, no ordering assumptions are required and it is possible to determine the effects of viscosity and resistivity across the entire range of k (recall that Spies' specialised to $k \gg 1$).

5.3 The Model

The following set of equations have been solved for linear $m = 0$ and $m = 1$ modes:

$$\begin{aligned}
\frac{\partial\rho}{\partial t} + \nabla.(\rho\vec{v}) &= 0 \\
\rho\frac{D\vec{v}}{Dt} &= \vec{J}\times\vec{B} - \nabla p - \nabla.\mathbf{\Pi}_i \\
\vec{E} + \vec{v}\times\vec{B} &= \eta\vec{J} \\
\frac{D}{Dt}\left(\frac{p}{\rho^{5/3}}\right) &= 0
\end{aligned}$$

where $\mathbf{\Pi}_i$ is the ion Braginskii stress-tensor [5.9] (see appendices to chapter 1), and D/Dt is the convective derivative. The system is closed by Maxwell's equations.

For total consistency the transport coefficients should be calculated at each radial location from the equilibrium parameters at that point. However, this is likely to make the results very dependent on the choice of equilibrium, which is rather arbitrary. In particular, the density and temperature profiles are constrained only by the requirement to produce the equilibrium pressure gradient, but must otherwise be determined by experimental measurements (which are not currently available). For this reason it is not considered worthwhile to introduce the additional complexity of radially varying transport coefficients, and instead the resistivity and viscosity coefficients are taken to be constants across the radius with values determined by the plasma parameters on axis.

The equations above constitute compressible resistive MHD plus the ion-stress tensor. It should be noted that they include neither heat flux terms nor Ohmic heating, so that the pinch is assumed to be adiabatic. A more complete set of Braginskii equations is available in ODRIC, but here we assume the model above in order to clarify the effects of resistivity and viscosity only. Despite this, the model can be considered as an extension of that used by Spies [5.7], since:

(i) the plasma is compressible, whereas Spies imposed incompressibility.

(ii) the viscosity can be anisotropic, (since the full Braginskii stress tensor is included), whereas Spies assumed a scalar viscosity.

The boundary conditions are those appropriate to a perfect wall surrounding the plasma, so that only internal modes are considered. Coppins [5.1] has shown that the most significant effect of the wall is to stabilise long wavelength $m = 1$ modes, that would otherwise be unstable in a free-boundary plasma. However, aside from this, the effects of viscosity and resistivity are expected to be largely independent of the plasma boundary condition.

The equilibrium used corresponds to a pinch of constant radius, which is sustained by a current rising as $I \propto t^{\frac{1}{3}}$ [5.11]. For a uniform temperature the profiles are:

$$\left.\begin{aligned} B_\theta(r) &= \frac{I_1(qr)}{I_1(q)} \quad ; \quad J_z(r) = q\frac{I_0(qr)}{I_1(q)} \\ \rho(r) &= \frac{I_0^2(q) - I_0^2(qr)}{I_0^2(q) - 1} \quad ; \quad T(r) = \frac{I_0^2(q) - 1}{2I_1^2(q)} \end{aligned}\right\} \tag{5.9}$$

where I_0, I_1 are modified Bessel functions, $q = 1.656$, B_θ has been normalised to its value at the plasma edge ($r = 1$) and ρ has been normalised to its on axis value.

This equilibrium has been chosen to allow comparison with the results of Culverwell and Coppins [5.4]. However, in contrast to that work, we neglect the time-variation of the equilibrium and instead opt to consider a more complete stability model. As such, the results presented below are only applicable to a weakly resistive Z-pinch, i.e. one in which the equilibrium changes negligibly over a typical mode growth-time. Strictly this corresponds to the equilibrium of equation 5.9 at late times (since $S \propto t^{4/3}$).

The major reason for assuming a static equilibrium, is one of simplicity. It allows an obvious comparison with the analytical work of Spies [5.7], without the additional complication of equilibrium evolution. Also, the non-viscous results compliment the work of Culverwell and Coppins [5.4], in that they demonstrate

	I(kA)	n(cm^{-3})	T(eV)	a(cm)	S	R	$\omega_{ci}\tau_i$
I.C. Comp. pinch	150	7×10^{17}	150	0.5	1053	4.3	1.9
Extrap Z1	25	5×10^{16}	60	1.0	160	2.0	0.5
Los Alamos DZP	250	2×10^{21}	150		44	212	

Table 5.1: Experimental Z-pinch parameters for the Imperial College compressional Z-pinch [5.2], Extrap Z1 [5.12], and the Los Alamos DZP [5.3].

the effect of resistivity on a static equilibrium. Thus the contribution to their results from equilibrium evolution, can be isolated.

Although the neglect of equilibrium variation is at best an approximation, it is a good approximation for a number of existing Z-pinches. Table 5.1 shows experimental Z-pinch parameters for three different machines. Extrap Z1 is not a simple Z-pinch, but has been included because its stability has often been studied using Z-pinch geometry [5.7], [5.12]. The deuterium-fibre Los Alamos DZP has a very high density and correspondingly resistive nature. Consequently it would seem to require an evolving equilibrium treatment. However, both the Imperial College compressional pinch and Extrap Z1 can be adequately studied with a static equilibrium. In both cases the plasmas are quite viscous, ($R \approx 4$ for the I.C. pinch and $R \approx 2$ for Extrap Z1), and so they are candidates for visco-resistive stabilisation as described by Spies.

The remainder of this chapter is devoted to the presentation and discussion of the results from ODRIC. Section 5.4 shows the effect of resistivity alone. In section 5.5 the zero-field limit ($\omega_{ci}\tau_i \to 0$) of $\mathbf{\Pi}_i$ is included in accordance with the work of Spies. Finally section 5.6 examines the effect of using the full anisotropic stress-tensor.

	$\gamma\tau_A$	
ka	Shooting code	ODRIC
0.1	0.069	0.067
1.0	0.657	0.643
10.0	3.249	3.138

Table 5.2: Comparison of $m = 0$ ideal growth-rates.

5.4 Resistive Spectra

The resistivity is parameterised in terms of the Lundquist parameter, S, which is defined by:

$$S = \frac{\tau_R}{\tau_A} \tag{5.10}$$

where $\tau_A = a/v_A$ is the Alfvén time, and $\tau_R = 4\pi a^2/\eta_\perp c^2$ is the resistive diffusion time (in C.G.S. units). Here v_A is the Alfvén velocity, a is the plasma radius and $\eta_\perp$ is the perpendicular resistivity.

In the $S \to \infty$ limit the system of equations reduce to compressible ideal MHD. Thus by taking large S it is possible to test ODRIC against ideal results. Table 5.2 shows the comparison of ODRIC $m = 0$ growth-rates for $S = 10^6$, against results from a shooting code [5.13]. Here and throughout growth-rates are normalised to the inverse of the Alfvén time. The growth-rates are within 3% across the entire spectrum and the eigenfunctions are also satisfactorily similar.

Figures 5.1 and 5.2 show $m = 0$ and $m = 1$ spectra respectively, for various values of S. It is apparent from figure 5.1 that resistivity has a stabilising influence on $m = 0$. However, low values of S are required before significant reduction in the growth-rate occurs. The $m = 1$ behaviour is rather more complicated but generally a similar conclusion may be drawn. Notice also that $m = 1$ modes with $ka \lesssim 1.7$ are stable. This is presumably due to the stabilising influence of the wall and is similar to that observed by Coppins [5.1].

In both cases the effect is insignificant at values of S for which the time evolution of the equilibrium may be neglected. This is in contrast to the results of Culverwell and Coppins [5.4], who include equilibrium time-dependence and find that perturbations are stable for $S < S_c$, where:

$$\left.\begin{aligned} S_c &\approx 50(ka)^{-0.86} \qquad && \text{for} \quad m = 0 \\ S_c &\approx 40(ka)^{-0.75} \qquad && \text{for} \quad m = 1 \end{aligned}\right\} \tag{5.11}$$

These empirical formulae yield complete stability of $ka = 10.0$, $m = 0$ for $S_c \approx 7$, whereas in the static equilibrium treatment, similar parameters result in a mode growth-rate that is still more than 1/2 of the ideal growth-rate. Two conclusions may be drawn from this:

(i) the static equilibrium treatment that is presented here, is only valid for $S \gg S_c$.

(ii) the resistive stabilisation observed by both Culverwell and Coppins [5.4] and Cochran and Robson [5.5], cannot be attributed to the effect of resistivity on a static equilibrium, i.e. the stabilisation is dependent on the resistive evolution of the pinch.

5.5 Visco-Resistive Spectra

The dimensionless parameter that characterises the viscosity is the Reynold's number, R:

$$R = \frac{\rho a^2}{\mu_{\|}\tau_A} \tag{5.12}$$

where $\mu_{\|}$ is the parallel viscosity coefficient (see appendix 1B). To make contact with Spies [5.7] the viscosity is taken to be scalar i.e. $\nabla.\mathbf{\Pi}_i \rightarrow \mu_{\|}\nabla^2\vec{v}$. This is the $\omega_{ci}\tau_i \rightarrow 0$ limit of $\mathbf{\Pi}_i$.

The effect of viscosity on a slightly resistive plasma is demonstrated in figures 5.3 and 5.4. At the $S = 1000$ value chosen, the resistive stabilisation is totally negligible and in the non-viscous limit the growth-rates are essentially those of ideal MHD. At finite values of R the stabilisation is obvious. When $R \approx 10$ the $m = 0$ growth-rates are down by factors of between 10 and 80 across the spectrum. For $m = 1$ the shorter wavelengths seem to be preferentially damped, but even the least affected modes are 4 times less slowly growing than their ideal counterparts.

Equation 5.8 embodies Spies' claim that short-wavelength modes can be totally stabilised by a sufficiently small SR product. Figures 5.5 and 5.6 show the visco-resistive stabilisation of $ka = 10.0$ for $m = 0$ and $m = 1$ respectively. On each graph $S = 100$ and $S = 1000$ lines are plotted. It is noticeable that the SR product for stabilisation is approximately the same for both values of S.

$$\left.\begin{array}{lll} SR|_{crit} \approx 5000 & \text{for} & m = 0 \\ & & \\ SR|_{crit} \approx 7500 & \text{for} & m = 1 \end{array}\right\} \tag{5.13}$$

The $m = 1$ value falls within the ranges defined by equation 5.8 for this equilibrium:

$$6000 \leq SR|_{crit} \leq 19000 \tag{5.14}$$

However, contrary to the incompressible model that Spies analysed, stability of $m = 1$ kinks is not the most stringent requirement. In this case $m = 0$ modes need a smaller SR product for stability (i.e. the plasma must depart further from being "ideal").

5.6 The Effect of an Anisotropic Stress Tensor

The assumption of scalar viscosity is only valid for $\omega_{ci}\tau_i \ll 1$. However, as shown in table 5.1, Z-pinches do not generally obey this inequality.

Thus to accurately assess visco-resistive effects on Z-pinch stability, the full ion stress-tensor must be included. This is possible with ODRIC which contains all five viscosity coefficients (see appendix 1B).

Figure 5.7 shows the full stress-tensor effect on $m = 0$ for $S = 1000$, $R = 10$ and a range of $\omega_{ci}\tau_i$ values. The $\omega_{ci}\tau_i = 0$ curve is the $R = 10$ curve of figure 5.3. It is noticeable that as $\mathbf{\Pi}_i$ becomes more anisotropic the stabilising effect becomes weaker. When $\omega_{ci}\tau_i \rightarrow \infty$ the effect is quite insignificant.

In order to isolate the effect of the finite-larmor radius (FLR) terms in the stress-tensor, $m = 0$ spectra are presented in figure 5.8 for finite $\omega_{ci}\tau_i$, both with and without these terms. The FLR terms are seen to have only a small stabilising influence at $\omega_{ci}\tau_i$ values relevant to Z-pinch experiments.

Table 5.3 lists the fastest growing $m = 0$ and $m = 1$ modes for the I.C. Compressional pinch, using the parameters shown in table 5.1 and the full stress-tensor.

m	ka	$\gamma\tau_A$
0	6.0	0.339+i0.249
1	3.0	0.310+i0.338

Table 5.3: Most unstable modes for the I.C. Compressional pinch, using the parameters of Table 5.1.

It is noticeable that the FLR terms introduce a strong oscillatory component to the instabilities. However, of greater relevance is the growth-time of the fastest growing mode, because this gives some indication of the expected lifetime of the pinch (lifetime $\sim 1/\gamma$). Thus, this model predicts that the I.C. pinch should last at least 3 Alfvén times. Although this prediction is an improvement on ideal MHD, which yields arbitrarily fast growing modes for arbitrarily large wavenumber, it is still short of explaining the stability that is claimed for this experiment:

I.C. pinch stable for $\sim 10\, \tau_A$ [5.2].

Thus, for the I.C. pinch we conclude that one or both of the following are true:

(i) some of the physics omitted from this model has a significant effect on linear stability, e.g.:

- other magnetohydrodynamic terms such as the Hall term and the ion and electron heat flux vectors.
- kinetic effects such as singular or resonant particle orbits.

(ii) non-linear effects are important, possibly leading to mode growth much slower than exponential.

If the latter is true, then the growth-time of the fastest growing mode is merely a lower estimate of the pinch lifetime.

For Extrap Z1, its small SR product would surely lead to greater visco-resistive stabilisation, and this could perhaps explain its extended lifetime. However, confirmation of this requires using a magnetic geometry more appropriate to this experiment, rather than the simple Z-pinch model used here.

5.7 Discussion

In the last section $\omega_{ci}\tau_i$ was varied for fixed S and R values, in order to demonstrate the effect of an increasingly anisotropic stress tensor. In particular this suggested that visco-resistive stabilisation would be small in tokamaks and RFP's, where $\omega_{ci}\tau_i$ is large, although it could still be significant in Z-pinches, which often have small $\omega_{ci}\tau_i$.

However, there is an inconsistency in this procedure for Z-pinches, since choosing S and R actually fixes $\omega_{ci}\tau_i$ [5.14]. This is because Z-pinches in equilibrium must obey the Bennett relation:

$$\beta_\theta I^2 = 200 N k_B (T_e + T_i)$$

where $k_B = 1.6 \times 10^{-12} erg\, eV^{-1}$, N is the line density in cm^{-1}, T_e and T_i are the electron and ion temperatures in eV, and I is the current in A. For a Z-pinch $\beta_\theta \approx 1$, so that the mean temperature is determined by the current and the line-density. Similarly, the magnetic-field (at the pinch edge) is derivable from Ampére's Law and is a function of the current and the pinch radius:

$$B_\theta(a) = 0.2\frac{I}{a}$$

where a is the pinch radius in cm and $B_\theta(a)$ is the magnetic field at the edge in G. Also the mean volume number density can be written in terms of the line density and the pinch radius:

$$\bar{n} = \frac{N}{\pi a^2}$$

Thus the temperature, density and magnetic field strength can all be written in terms of a, N and I, and so the transport coefficients are also dependent only on these three parameters. It is straightforward to derive expressions for the relevant stability parameters:

$$S = 2.06 \times 10^{18} \frac{I^4 a}{\ln \Lambda} \frac{1}{N^2}$$

$$
\begin{aligned}
R &= 9.39 \times 10^{-33} \frac{\ln \Lambda}{I^4 a} N^3 \\
\omega_{ci}\tau_i &= 1.95 \times 10^{24} \frac{I^4 a}{\ln \Lambda} \frac{1}{N^{5/2}} \\
SR &= 1.94 \times 10^{-14} N
\end{aligned}
$$

where $\ln \Lambda$ is the Coulomb logarithm. These expressions are valid for deuterium plasmas and have been calculated using the mean density, $\bar{n}$, the Bennett temperature, $\bar{T} = T_e = T_i$, and taking $\bar{B} = B_\theta(a)/2$ as the mean magnetic field [5.14]. Notice that each of these parameters is actually a function of $I^4 a/\ln \Lambda$ and N, only. Indeed, in reference [5.14] it has been shown that other important stability parameters can be written in terms of $I^4 a$ and N. This means that (for given $\ln \Lambda$) the stability properties of any Z-pinch discharges can be expressed as a point in a two dimensional space (of $I^4 a$ vs. N). Of greater relevance here is the conclusion that selecting any two of S, R and $\omega_{ci}\tau_i$ determines the third. This is a direct result of the fact that all Z-pinch discharges have $\beta_\theta \approx 1$. For RFP's and tokamaks this is not true, and therefore these machines inhabit a three dimensional space, with the third dimension corresponding to discharges with different β values.

In this section, the visco-resistive stabilisation of Z-pinches is re-examined using this requirement of self-consistency. The SR product is fixed and $\omega_{ci}\tau_i$ is varied. These two parameters determine the individual values of S and R by the relations above:

$$
\begin{aligned}
S &= 7.58\,(SR)^{1/2}\omega_{ci}\tau_i && (5.15) \\
R &= 0.132\,(SR)^{1/2}(\omega_{ci}\tau_i)^{-1} && (5.16)
\end{aligned}
$$

Table 5.4 shows the critical axial wavenumber, k_c, above which $m = 0$ modes are stable for $SR = 1000$ and various values of $\omega_{ci}\tau_i$.

This value of SR corresponds to a line density of $N = 5.15 \times 10^{16}\, cm^{-1}$, which is close to the value used by Haines in his zero-dimensional model of Z-pinch

$\omega_{ci}\tau_i$	0.01	0.10	0.30	0.50	0.70	1.00	2.00	5.00
k_c	4.83	4.95	5.02	6.34	7.44	8.84	12.49	20.40

Table 5.4: Critical axial wavenumber, k_c versus $\omega_{ci}\tau_i$ for $m = 0$ modes with $SR = 1000$.

radiative collapse [5.15]. Since the line density remains constant throughout, the SR product is also a constant which is set by the initial conditions. The evolution of the collapsing pinch leads to a time varying value of $\omega_{ci}\tau_i$ and therefore a time-dependent value of k_c. Given $\omega_{ci}\tau_i$ as a function of time, table 5.4 indicates how the critical wavenumber varies and thus how the visco-resistive stabilisation varies during the discharge.

Table 5.4 confirms the conclusion of the last section - that effective visco-resistive stabilisation requires small $\omega_{ci}\tau_i$ values. The result at $\omega_{ci}\tau_i = 0.01$ corresponds approximately to the scalar viscosity case studied by Spies. However as $\omega_{ci}\tau_i$ is increased the critical wavenumber increases slowly for $\omega_{ci}\tau_i \lesssim 0.3$, but quite rapidly thereafter. The slow increase for low $\omega_{ci}\tau_i$ may be due to the FLR terms (μ_3 and μ_4), which vary like $\omega_{ci}\tau_i$ for $\omega_{ci}\tau_i \ll 1$. For $\omega_{ci}\tau_i \gg 1$ the five viscosity coefficients vary like:

$$\begin{aligned}
\mu_{\|} &\sim 1 \\
\mu_1, \mu_2 &\sim (\omega_{ci}\tau_i)^{-2} \\
\mu_3, \mu_4 &\sim (\omega_{ci}\tau_i)^{-1}
\end{aligned}$$

and thus the stabilisation that is derived from the FLR terms and the perpendicular collisional viscosity (μ_1 and μ_2) quickly diminishes with increasing $\omega_{ci}\tau_i$. From equation 5.15 we conclude that the most effective visco-resistive stabilisation occurs at low S (i.e. low $\omega_{ci}\tau_i$). Unfortunately this is precisely the regime in which the time variation of the equilibrium should be included [5.4, 5.5]. Thus for a rapidly evolving pinch there is only a short fraction of the duration of the discharge for which the visco-resistive stabilisation is significant and yet the evolution of the equilibrium can be neglected. We quantify this requirement as $S > S_c$ (see section 5.4) and $\omega_{ci}\tau_i < 1$, which determines a range for $I^4 a$:

$$5.13 \times 10^{-25} N^{5/2} > \frac{I^4 a}{\ln \Lambda} > 4.85 \times 10^{-19} N^2 S_c$$

For very small line densities this range vanishes, implying that the visco-resistive stabilisation of a static equilibrium is not relevant. Conversely, we require:

$$N > 8.94 \times 10^{11} S_c^2$$

for an appreciable effect. This condition is easily met in the I.C. pinch and Extrap. It is also satisfied in the model of reference [5.15], which implies that for some finite duration the discharge will be significantly stabilised by viscosity and resistivity. However, a glance at table 3 of that reference immediately shows that $\omega_{ci}\tau_i$ is less than unity only very early in the lifetime of the pinch ($t \lesssim 5 \times 10^{-9} sec.$) and that the visco-resistive stabilisation is negligible for the remaining time.

One would obviously like to increase the stabilising effect. Spies' theory offers a simple recipe - merely decrease the SR product by having low line densities. The more realistic study presented here yields a less clear cut recommendation, since a lower line density implies larger $\omega_{ci}\tau_i$ (for given $I^4 a / \ln \Lambda$), and a reduced stabilising effect. We still need to minimise SR but without making the stress tensor anisotropic. Table 5.4 suggests that $\omega_{ci}\tau_i$ can be as large as 0.3 before the anisotropy of the stress tensor has a serious detrimental effect. Thus this empirical result suggests an optimum line density:

$$N_{opt} = 8.4 \times 10^9 \left(\frac{I^4 a}{\ln \Lambda}\right)^{2/5}$$

5.8 Conclusions

(i) Resistive stabilisation of $m = 0$ and $m = 1$ modes is insignificant at S values for which the time-dependence of the equilibrium may be neglected (figures 5.1 and 5.2).

(ii) The combined effect of a scalar viscosity and resistivity can strongly damp both $m = 0$ and $m = 1$ modes at realistic S and R values (figures 5.3 and 5.4).

(iii) Short wavelength modes can be entirely stabilised by a sufficiently small SR product (figures 5.5 and 5.6), in agreement with Spies [5.7]. Of relevance to this is the fact that for a Z-pinch in pressure balance (i.e. obeying the Bennett relation), the SR product is dependent only on the line density:

$$SR = 2.74 \times 10^{-14}\, N\, (\frac{1}{A})^{1/2}$$

where N is the line density in cm^{-1}, A is the mass of the ions in units of the proton mass. Thus stability is improved for low line densities.

(iv) Although the viscosity and resistivity are equally important in this respect, figures 5.5 and 5.6 also show that for the remaining instabilities the viscosity has the larger damping effect. (Note that the $S = 1000$ curves lie below the $S = 100$ curves).

(v) Assuming a scalar viscosity over-estimates the visco-resistive damping. When the full stress-tensor is included the effect is seen to decrease with increasing anisotropy of the stress-tensor (figure 5.7 and table 5.4). Although it remains significant for typical Z-pinch parameters ($\omega_{ci}\tau_i \sim 0(1)$), the stabilising influence is negligible at $\omega_{ci}\tau_i$ values relevant to RFP's and tokamaks ($\omega_{ci}\tau_i \geq 1000$).

(vi) The FLR terms in the stress-tensor contribute only a minor damping effect at realistic values of S, R and $\omega_{ci}\tau_i$ (figure 5.8).

These conclusions only apply rigorously to the self-similar equilibrium studied. However, this equilibrium does not possess any unique stability properties, (it is for example very like the constant-current density equilibrium), and so the conclusions almost certainly apply to a wider class of Z-pinch equilibria.

It should be noted that only the FLR terms in the stress-tensor have been included. A full appraisal of FLR effects requires the inclusion of the Hall terms in Ohm's Law and the FLR terms in the heat-fluxes. However this chapter has been concerned specifically with visco-resistive effects and so the full effect of FLR on Z-pinch stability remains a topic for future work.

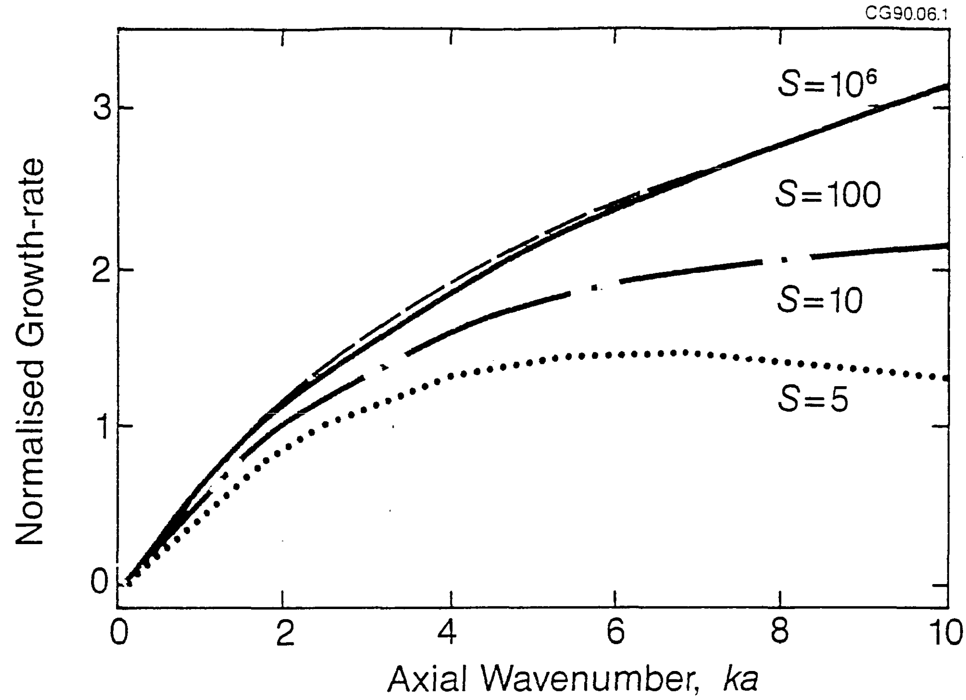

Figure 5.1: The $m = 0$ resistive spectrum ($R = \infty$) for various values of Lundquist parameters, S. The growth-rate is normalised to the inverse of the Alfvén time.

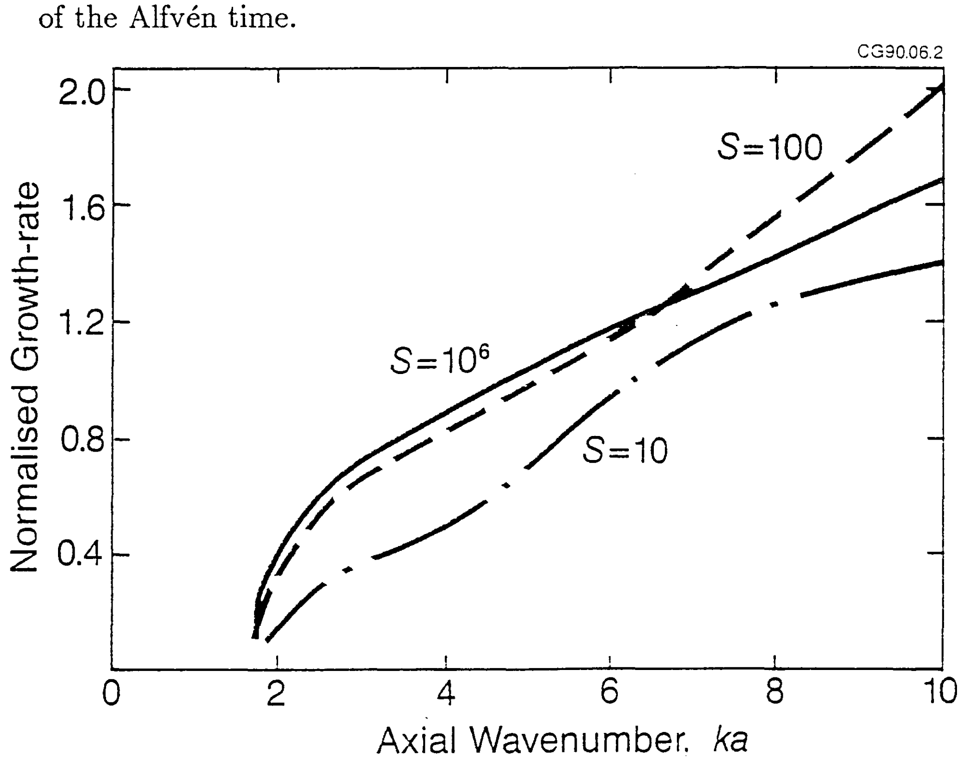

Figure 5.2: The $m = 1$ resistive spectrum ($R = \infty$) for various values of Lundquist parameters, S.

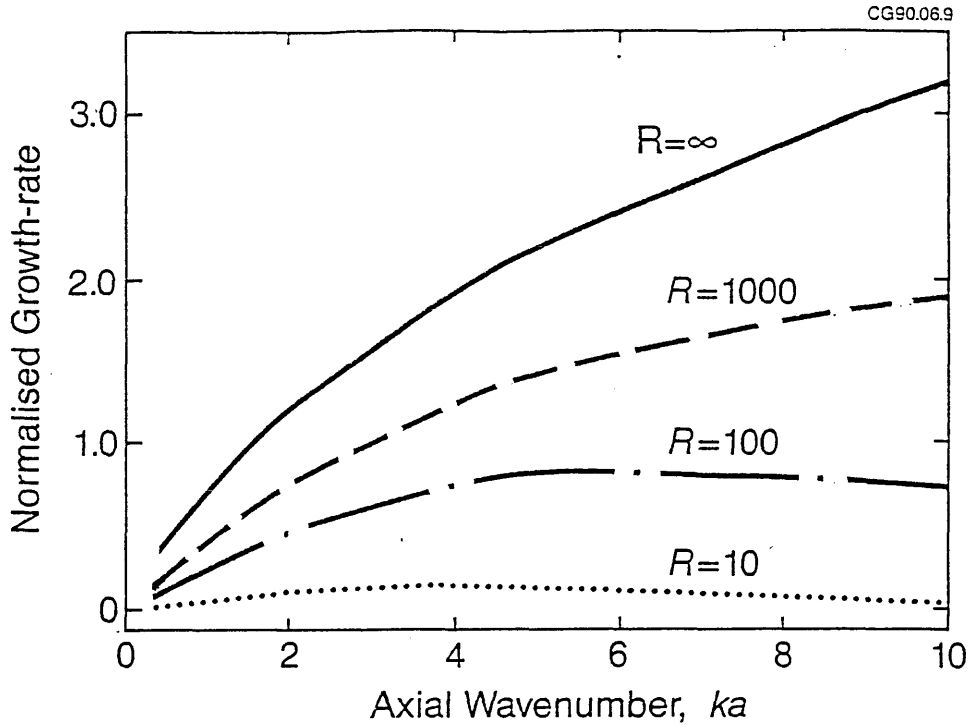

Figure 5.3: The $m = 0$ visco-resistive spectrum for $S = 1000$ and various values of scalar viscosity. R is the Reynold's number.

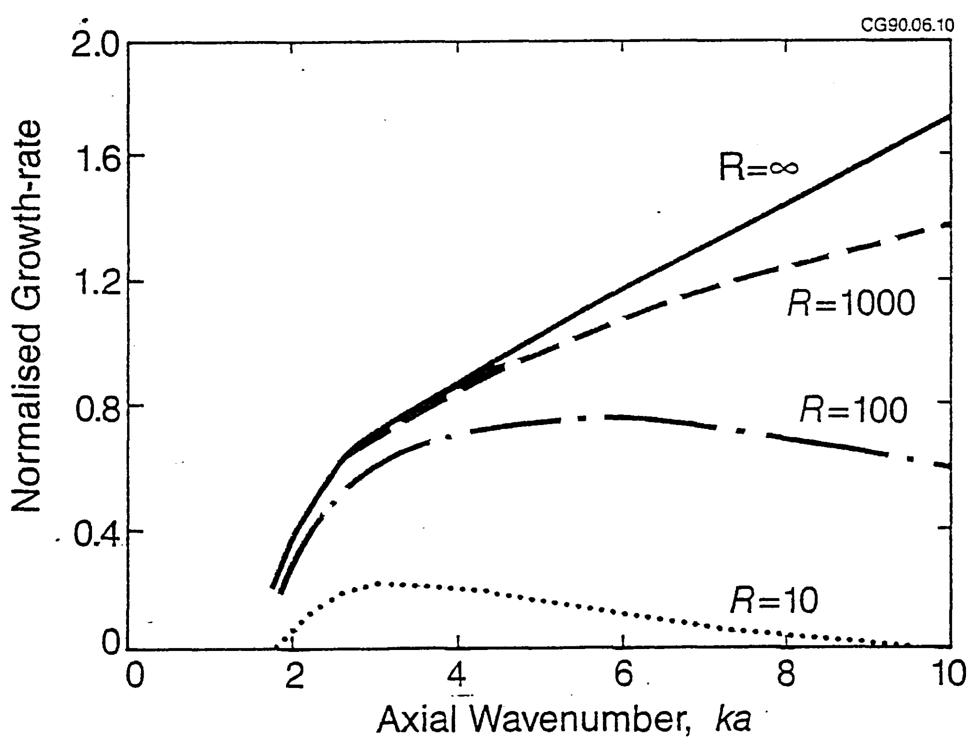

Figure 5.4: The $m = 1$ visco-resistive spectrum for $S = 1000$ and various values of scalar viscosity.

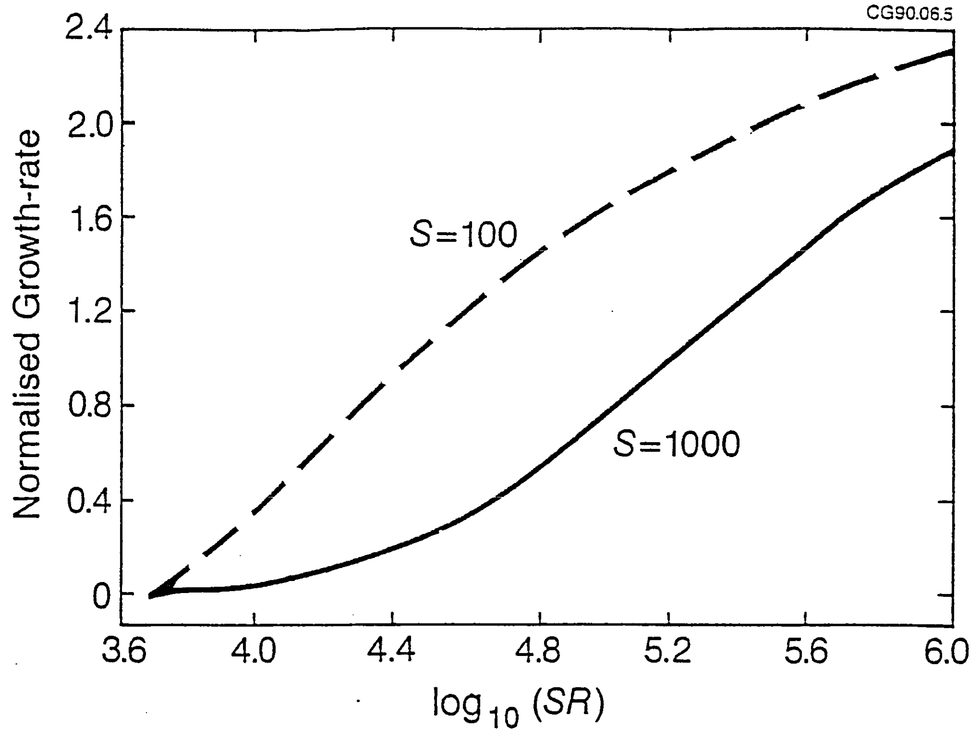

Figure 5.5: The visco-resistive stabilisation of $m = 0$, $ka = 10.0$ for $S = 1000, 100$.

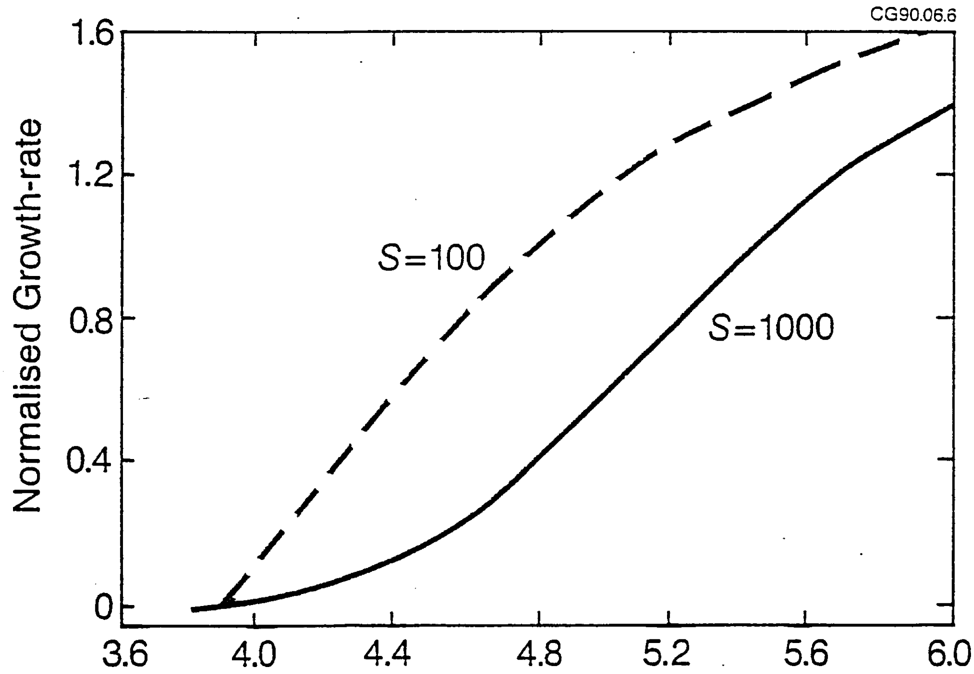

Figure 5.6: The visco-resistive stabilisation of $m = 1$, $ka = 10.0$ for $S = 1000, 100$.

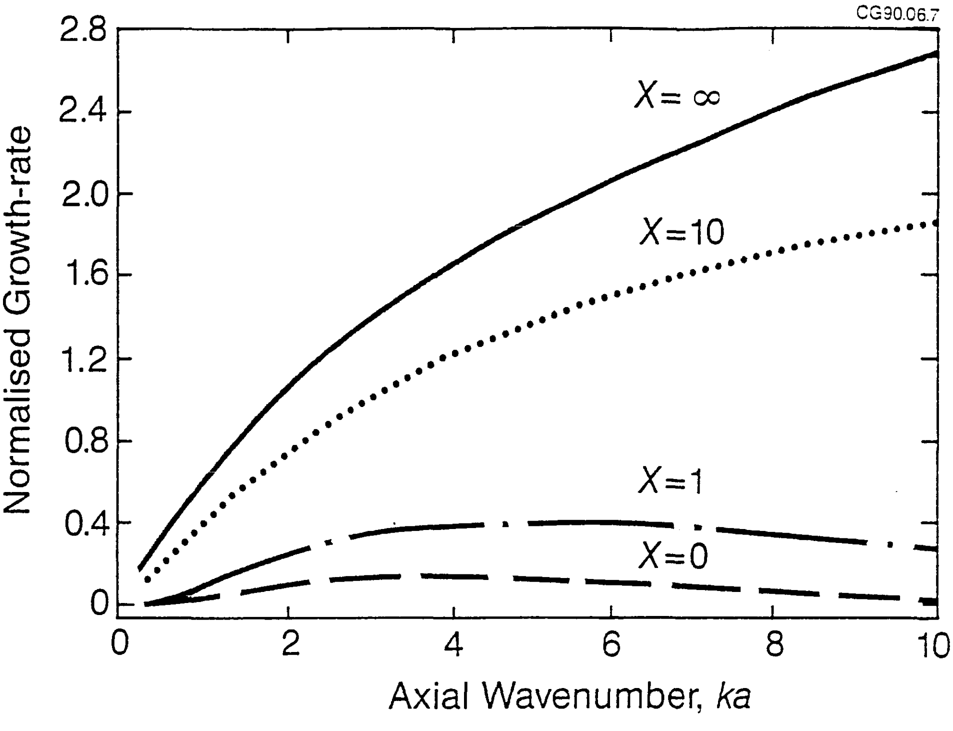

Figure 5.7: The $m = 0$ visco-resistive spectrum for $S = 1000$, $R = 10$, using the full stress-tensor for various values of $\omega_{ci}\tau_i$. Here $X = \omega_{ci}\tau_i$, so that $X = 0$ corresponds to a scalar viscosity.

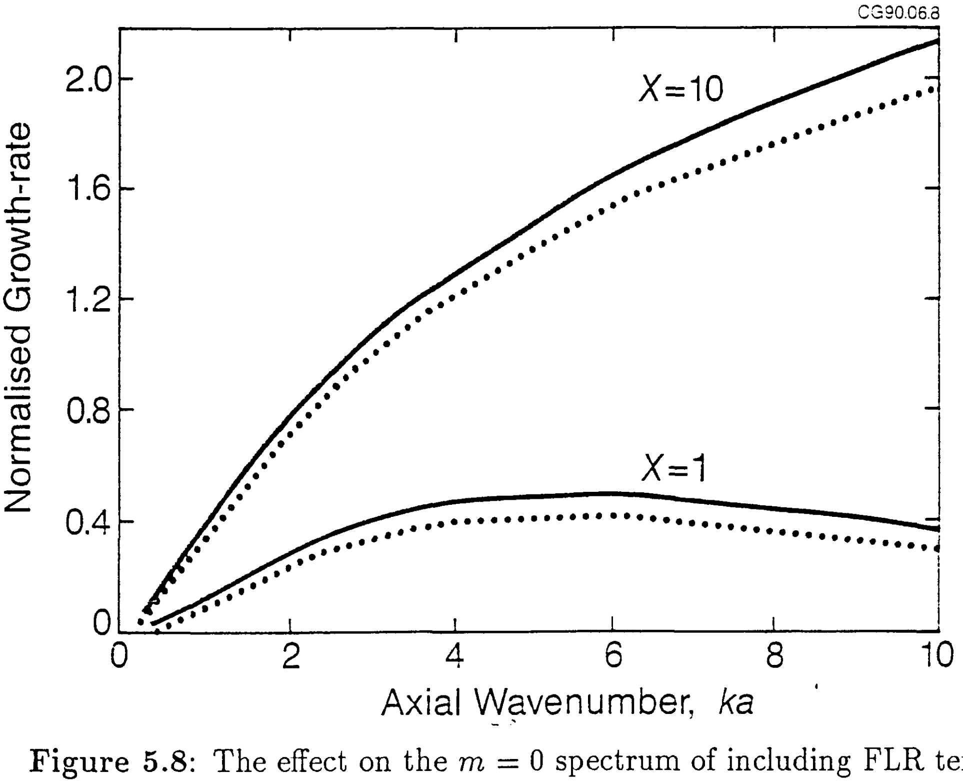

Figure 5.8: The effect on the $m = 0$ spectrum of including FLR terms in the stress-tensor. The broken lines include FLR, the continuous lines do not.

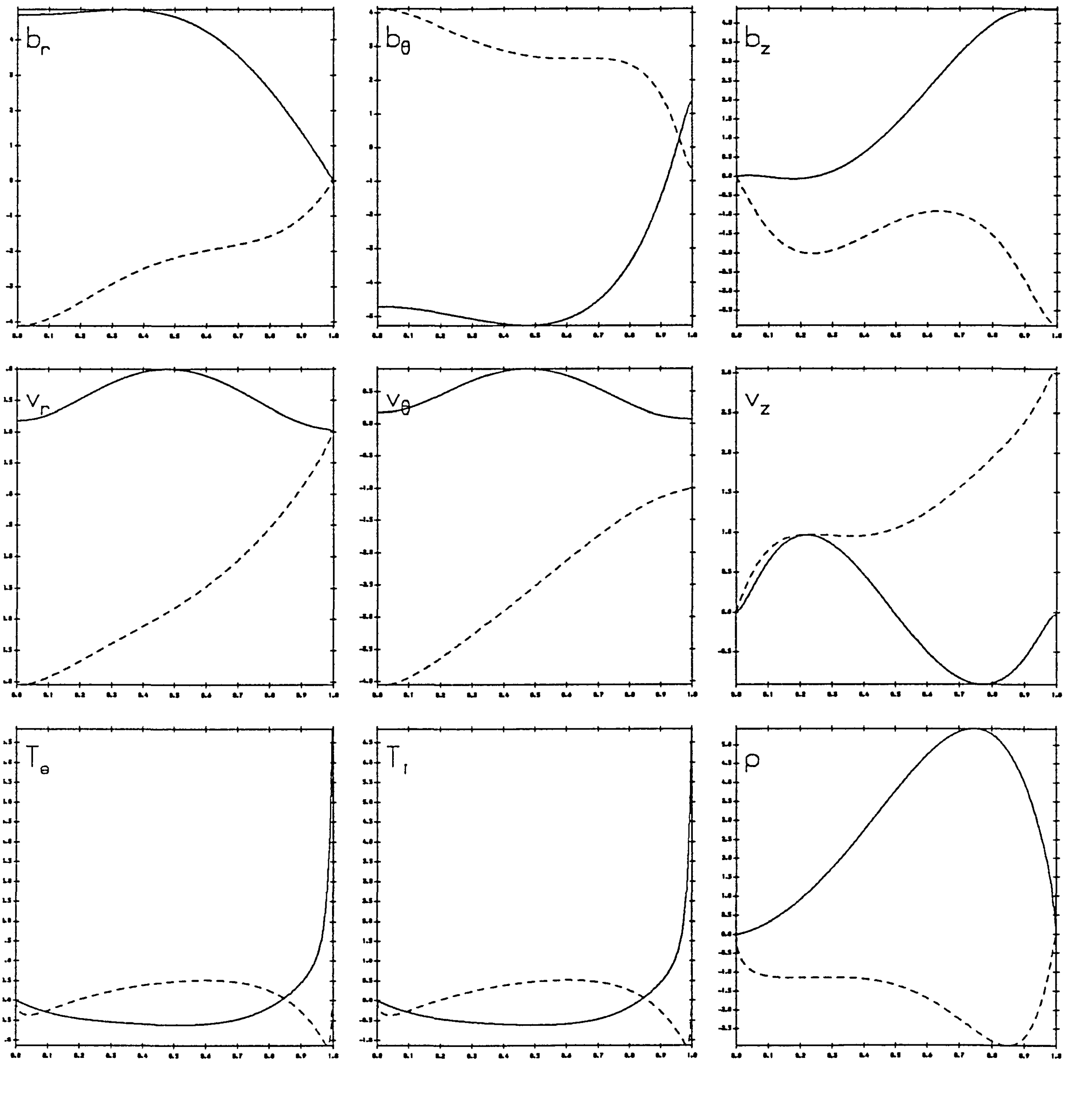

Figure 5.9: Radial profiles of the $m = 0$, $ka = 3.0$ perturbation for the full stress tensor and I.C. pinch parameters. The dotted line represent the imaginary part of the perturbation.

References

[5.1] Coppins, M., Plasma Phys. and Contr. Fusion **30**, 201 (1988).

[5.2] Haines, M.G., Bayley, J., Baldock, P., Chittenden, J., Choi, P., Coppins, M., Culverwell, I.D., Dangor, A.E., Figura, E.S., McCall, G., Twelfth International Conf. on Plasma Phys. and Contr. Nucl. Fusion Res., paper **C-IV-4.2** (1988).

[5.3] Glasser, A.H., Hammel, J., Lewis, H.R., Lindemuth, I.R., McCall, G.H., Nebel, R.A., Scudder, D., Schlachter, J., Twelfth International Conf. on Plasma Phys. and Contr. Nucl. Fusion Res., paper **C-IV-4.1** (1988).

[5.4] Culverwell, I.D., Coppins, M., Phys. Fluids **B2**, 129 (1990).

[5.5] Cochran, F.L., Robson, A.E., Phys. Fluids **B2**, 123 (1990).

[5.6] Sethian, J.D., Robson, A.E., Gerber, K.A., De Silva, A.W., Phys. Rev. Lett. **59**, 892 (1987).

[5.7] Spies, G.O., Plasma Phys. and Contr. Fusion **30**, 1025 (1988).

[5.8] Haines, M.G., Private Communication (1990).

[5.9] Braginskii, S.I., Sov. Phys. J.E.T.P. **6**, 358 (1958).

[5.10] Mirin, A.A., O'Neill, N.J., Killeen, J., Bonugli, R.J., Ellis, M.J., Phys. Fluids **29**, 512 (1986).

[5.11] Coppins, M., Culverwell, I.D., Haines, M.G., Phys. Fluids **31**, 2688 (1988).

[5.12] Scheffel, J., Faghihi, M., J. Plasma Phys. **41**, no.3, 427 (1988).

[5.13] Culverwell, I.D., Private Communication (1989).

[5.14] Haines, M.G., Coppins, M., Culverwell, I.D., in "Dense Z-Pinches" (Proc. of the 2^{nd} Int. Conf. on Dense Z-Pinches Laguna Beach, 1989), (AIP, 1989) p203.

[5.15] Haines, M.G., Plasma Phys. and Contr. Fusion **31**, 759 (1989).

Chapter 6

Pressure-Driven Thin-Shell Instabilities in RFP's

6.1 Introduction

Until recently Reversed-Field Pinch (RFP) experiments have operated with an effectively ideal wall (resistive time-constant of the wall, $\tau_w \gg$ pulse-length of the discharge, τ_d). However, as RFP's approach reactor conditions, (and τ_d increases), the magnetic field has time to diffuse through the wall and the plasma is expected to display different behaviour. Consequently it is important to determine the effects on the RFP configuration of replacing the usual ideal wall with a resistive one.

The stability analysis has been simplified by Gimblett [6.1], who recognised that most experiments operate with a "thin-shell" (i.e electromagnetic skin-depth $\gg$ wall thickness, δ_w). This allows the diffusion equation for the magnetic field in the wall, to be replaced by:

$$\frac{\partial b_r}{\partial t} = \frac{\eta_w}{a\delta_w}\Delta'_w b_r \tag{6.1}$$

where Δ'_w is the normalised jump in the logarithmic derivative of the radial magnetic field across the wall:

$$\Delta'_w = \left(\left.\frac{\partial b_r}{\partial r}\right|_{out} - \left.\frac{\partial b_r}{\partial r}\right|_{in} \right) \frac{1}{b_r} = \Delta_{out} - \Delta_{in} \tag{6.2}$$

η_w is the wall resistivity , δ_w is the wall thickness.

For modes growing exponentially with growth rate γ, equation 6.1 yields:

$$\gamma \tau_w = \Delta'_w \tag{6.3}$$

where τ_w is the long time constant of the wall:

$$\tau_w = \frac{a\delta_w}{\eta_w}$$

The linear theory of current-driven thin-shell instabilities has shown good agreement with the HBTXIC experiment [6.2], satisfactorily predicting the dominant $m = 1$ instabilities that are observed in the ranges $n_k = (-5, -6, -7)$ and

$n_k = (2,3)$. However, a mode grouping at $n_k = (9,10,11)$ has also been detected, and these are unaccounted for by the theory. In this chapter the ideal stability analysis is extended to finite-beta equilibria in an attempt to explain these modes.

In section 6.2 asymptotic solutions of the marginal ideal MHD equation are used to derive local stability criteria for modes resonant close to both sides of the resistive wall. Section 6.3 presents the thin-wall, non-resonant, $m = 1$ spectrum for a finite-beta equilibrium. This is derived from the numerical integration of the marginal MHD equation. The equilibrium used is a variable-μ profile that has been inflated to uniform Suydam-parameter across the radius. In section 6.4 inertia is included in the treatment of modes that are resonant within an inertial layer width of the wall. This leads to an amended thin-shell dispersion relation that yields instabilities growing at a rate dependent on both the Alfvén and wall times. Section 6.5 contains a discussion of the relevance of the results to thin-shell RFP's and section 6.6 lists the conclusions to drawn from this work.

6.2 Local Stability Conditions

Consider the linear-growth of a perturbation in a cylindrically symmetric plasma. The perturbation is fourier-transformed in both axial (z) and poloidal (θ) directions, so that the perturbed radial magnetic-field, b_r, is written as:

$$b_r(\vec{r}) = b_r(r)\exp(im\theta + ikz + \gamma t)$$

Away from resistive and inertial layers b_r obeys the equation below, as given in reference [6.3]:

$$\frac{d^2\Psi}{dr^2} + A\Psi = 0 \tag{6.4}$$

where

$$\Psi = \frac{r^{3/2}b_r(r)}{(m^2 + k^2r^2)^{1/2}}$$

and

$$
\begin{aligned}
A &= -K^2+\mu^2-\frac{d\mu}{dr}\frac{(mB_z-krB_\theta)}{Fr}+\frac{2\mu mk}{K^2r^2} \\
&+ \frac{(m^4+10m^2k^2r^2-3k^4r^4)}{4K^4r^6}-\frac{2k^2}{F^2r}\frac{dp}{dr} \\
&+ \frac{d}{dr}(\frac{1}{B^2}\frac{dp}{dr})-(\frac{1}{B^2}\frac{dp}{dr})^2+\frac{(m^2-k^2r^2)}{K^2r^2}\frac{1}{rB^2}\frac{dp}{dr} \\
&+ \frac{2}{B^2}\frac{dp}{dr}\frac{1}{Fr}[\mu(mB_z-krB_\theta)+kB_z-\frac{mB_\theta}{r}]
\end{aligned}
$$

Here $\mu = \vec{J}.\vec{B}/B^2$, $F = mB_\theta/r + kB_z$ and $K^2 = m^2/r^2 + k^2$. Equation 6.4 may be simplified close to the resonant point, $r = r_s$, where $F(r_s) = 0$.
Writing:

$$F(r) = F'(r_s)(r-r_s) = F'(r_s)x$$

then for small x, equation 6.4 reduces to:

$$\frac{d^2\Psi}{dx^2}+(\frac{C_1}{x}+\frac{C_2}{x^2})\Psi = 0 \tag{6.5}$$

where

$$
\begin{aligned}
C_1 &= 2k^2\frac{F''}{F'^3r}\frac{dp}{dr}-\frac{1}{F'r}\{\frac{d\mu}{dr}(mB_z-krB_\theta) \\
&- \frac{2}{B^2}\frac{dp}{dr}[\mu(mB_z-krB_\theta)+kB_z-\frac{m}{r}B_\theta]\}
\end{aligned}
$$

and

$$C_2 = -\frac{2k^2}{F'^2r}\frac{dp}{dr} = D_s$$

Equation 6.5 has a series solution:

$$
\begin{aligned}
\Psi &= A_I|x|^{\nu+1}(1-\frac{C_1}{2(\nu+1)}|x|+\cdots) \\
&+ B_I|x|^{-\nu}(1+\frac{C_1}{2\nu}|x|+\cdots) \qquad \text{for } r \geq r_s
\end{aligned} \tag{6.6}
$$

and

$$\Psi = A_{II}|x|^{\nu+1}(1 + \frac{C_1}{2(\nu+1)}|x| + \cdots)$$

$$+ B_{II}|x|^{-\nu}(1 - \frac{C_1}{2\nu}|x| + \cdots) \qquad \text{for } r \leq r_s \tag{6.7}$$

Here A_I, B_I, A_{II} and B_{II} are undetermined constants and
$\nu = -\frac{1}{2} + \frac{1}{2}(1 - 4D_s)^{1/2}$.

Equations 6.6 and 6.7 can be used to study the stability of modes that have singular points close to the plasma edge. The two cases of the resonance just inside, or just outside the plasma, must be considered separately.

(i) Resonant Modes

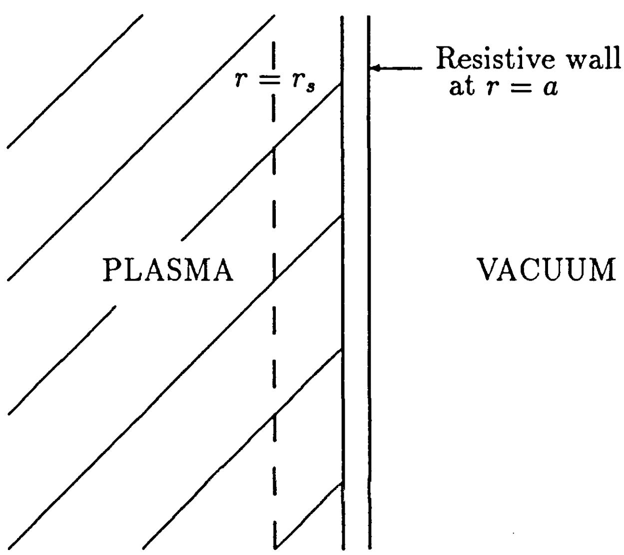

We are interested in calculating $b_r'/b_r|_{r=a}$ so that equation 6.3 may be used to determine stability conditions. Thus we require $\Psi(x_w)$ where $x_w = a - r_s \geq 0$. Equation 6.6 yields the required relationship for small x_w :

$$\left.\frac{b_r'}{b_r}\right|_{in} = \frac{(\nu+1)A_I|x_w|^{\nu} - \nu B_I|x_w|^{-\nu-1}\{1 - (1-\nu)b|x_w|\}}{A_I|x_w|^{\nu+1} + B_I|x_w|^{-\nu}\{1 + \nu b|x_w|\}} \tag{6.8}$$

where $b = C_1/2\nu^2$. The ratio A_I/B_I is equilibrium dependent and its calculation requires the numerical integration of equation 6.4, such as is carried out in section 6.3. However, the work of Newcomb [6.4] indicates that ideal stability is determined solely by the small solution at the singular point. So confining ourselves for the time being to determining stability criteria, (i.e. not growth-rates), we set $B_I = 0$. Then:

$$\left.\frac{b_r'}{b_r}\right|_{in} = \frac{\nu + 1}{|x_w|} \tag{6.9}$$

(ii) **Non-Resonant Modes**

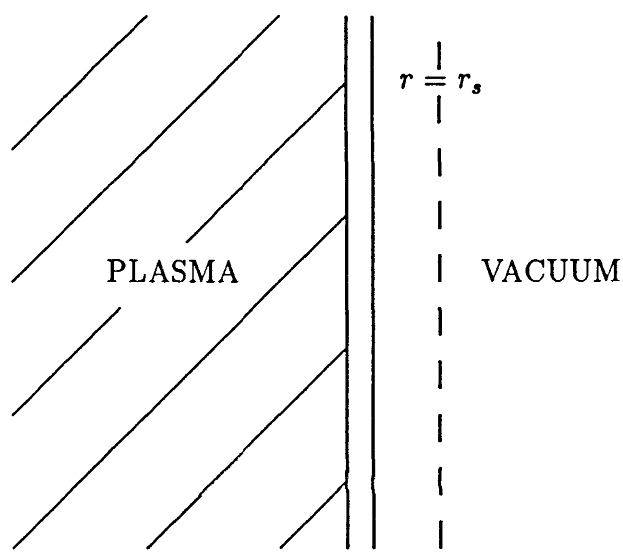

In this case $x_w = a - r_s \leq 0$ so that $\partial/\partial r = -\partial/\partial|x|$, and equation 6.8 is replaced by:

$$\left.\frac{b_r'}{b_r}\right|_{in} = \frac{-(\nu+1)A_{II}|x_w|^{\nu} + \nu B_{II}|x_w|^{-\nu-1}\{1 + (1-\nu)b|x_w|\}}{A_{II}|x_w|^{\nu+1} + B_{II}|x_w|^{-\nu}\{1 - \nu b|x_w|\}} \tag{6.10}$$

Once again we are faced with the undetermined ratio A_{II}/B_{II}. We require a sufficient stability condition and so consider the most unstable case of $x_w \to 0$. Thus for small but finite ν equation 6.10 is reduced to:

$$\left.\frac{b_r'}{b_r}\right|_{in} = \frac{\nu}{|x_w|} \tag{6.11}$$

In both the resonant and non-resonant cases the choice of solution is in agreement with the work of Hastie (see Wesson [6.5]). In that treatment, stability conditions were derived from an energy principle, and the solutions were chosen on the basis that the energy integral should remain finite.

Using equations 6.3, 6.9 and 6.11 we can now derive stability criteria. The contribution from the vacuum, $b_r'/b_r|_{out}$, is only dependent on the perturbation (m, k), and so for small enough x_w the plasma terms dominate. The stability condition is simply that the growth-rate, γ, should be negative, implying stability if:

$$\nu + 1 \geq 0 \qquad \text{for resonant modes} \tag{6.12}$$

$$\nu \geq 0 \qquad \text{for non-resonant modes} \tag{6.13}$$

For Suydam-stable plasmas $-1/2 \leq \nu \leq 0$, where the upper limit corresponds to zero pressure-gradient and the lower limit corresponds to the Suydam condition. Thus equation 6.12 implies that resonant-modes are always stable, whilst equation 6.13 implies that non-resonant modes are destabilised by any (negative) pressure-gradient at the plasma-edge.

This result is in conflict with Hastie (Wesson [6.5]), but the discrepancy may be traced to the inclusion of a vacuum region surrounding the plasma in that treatment. Thus far in this chapter the plasma has been denied the freedom to deform its boundary and expend energy in doing so. Not surprisingly this has repercussions for the stability conditions.

Now we include a vacuum region between the plasma and the wall, and calculate the Δ' associated with it. We begin with the MHD momentum equation:

$$\rho \frac{d\vec{v}}{dt} = \vec{J} \times \vec{B} - \nabla p$$

Once again inertial terms are neglected so that the linearised version of this equation yields:

$$\vec{J}_1 \times \vec{B} + \vec{J}_0 \times \vec{b} = \nabla p_1$$

where $\vec{J_1}$, $\vec{b}$ and p_1 are perturbed current density, magnetic-field and pressure respectively. Taking the scalar product with the wavevector, $\vec{k}$, leads to:

$$\vec{k}.(\vec{J_1} \times \vec{B}) + \vec{k}.(\vec{J_0} \times \vec{b}) = iK^2 p_1$$

Writing the first term on the left-hand side in terms of scalar products and using $\nabla.\vec{b} = 0$ to eliminate $\vec{k}.\vec{b}$:

$$\frac{F}{r}\frac{\partial(rb_r)}{\partial r} = \vec{k}.(\vec{J_0} \times \vec{b}) - iK^2[\vec{B}.\vec{b} + p_1] \tag{6.14}$$

This equation applies to both the plasma and the vacuum region between the plasma and the wall. In order to calculate a Δ' we subtract equation 6.14 for the plasma from equation 6.14 for the vacuum:

$$F\left[\frac{1}{r}\frac{\partial(rb_r)}{\partial r}\right]_-^+ = [\vec{k}.(\vec{J_0} \times \vec{b})]_-^+ - iK^2[\vec{B}.\vec{b} + p_1]_-^+ \tag{6.15}$$

where $[\ ]_-^+$ denotes the discontinuity in the enclosed term across the interface. Continuity of total perturbed pressure means that the second term on the right-hand side of equation 6.15 is zero. In addition, for modes resonant close to the edge $F \sim F'x$ and F' may be written in terms of the parallel current, $J_{||} = \vec{J}.\vec{B}/B$. Thus the Δ' across the interface reduces to:

$$\Delta'_v = \frac{1}{x_w}\frac{BrJ_{||}}{(2B_zB_\theta - BrJ_{||})} \tag{6.16}$$

where $B = (B_z^2 + B_\theta^2)^{1/2}$.

Equation 6.3 remains valid even for the free-boundary case, but now equations 6.9 and 6.10 must be re-interpreted as $b'_r/b_r|_{plasma}$, where

$$\left.\frac{b'_r}{b_r}\right|_{in} = \left.\frac{b'_r}{b_r}\right|_{plasma} + \Delta'_v$$

Consequently the stability conditions, equations 6.12 and 6.13, are replaced by:

$$\nu + 1 + \frac{BrJ_{||}}{(2B_zB_\theta - BrJ_{||})} \geq 0 \qquad \text{for resonant modes} \tag{6.17}$$

$$\nu - \frac{BrJ_{||}}{(2B_zB_\theta - BrJ_{||})} \geq 0 \qquad \text{for non-resonant modes} \tag{6.18}$$

These criteria are the same as those of Hastie. Notice that in the absence of any parallel current at the plasma edge they reduce to the fixed boundary conditions, equations 6.12 and 6.13.

Reversed-field pinches (RFP's) are believed to have zero, or at most small parallel current at the edge, and so the conclusions derived from equations 6.12 and 6.13 remain valid. Thus we expect RFP's to be unstable to modes that are just non-resonant (i.e. have small F at the plasma edge). The $n_k = (9, 10, 11)$, $m = 1$ grouping observed in HBTX1C appear to be non-resonant [6.2], and if this is the case they fit the description of the pressure driven thin-shell instabilities of equation 6.13.

6.3 The m=1 Finite-Beta Thin-Wall Spectrum

Although the local stability conditions indicate where instabilities will arise, they do not give the strength of the instabilities nor the overall effect of finite-beta on the spectrum. In this section we find the finite-beta, non-resonant $m = 1$ spectrum by the numerical integration of equation 6.4. The restriction to non-resonant modes is made for two reasons. Firstly the local stability analysis suggests that any new instabilities will be non-resonant and secondly the treatment of resonant modes requires integration through the singular point at $r = r_s$, which is a far more difficult numerical problem.

The integration is carried out from the origin to the wall by a leap-frog method. The requirement of regularity leads to the boundary condition at the origin: $\Psi \propto r^{m+1/2}$ [6.3]. The solution at the wall is used to calculate $b_r'/b_r|_{in}$, while $b_r'/b_r|_{out}$ is given by the vacuum solution:

$$\left.\frac{b_r'}{b_r}\right|_{out} = \left(\frac{m^2}{a^2} + k^2\right) \frac{K_m(|k|a)}{K_m'(|k|a)}$$

where K_m is the m^{th} order modified Bessel function of the second kind. Then equations 6.2 and 6.3 yield the linear growth-rates.

In order to make contact with previous work [6.2], the equilibrium studied is a "variable-μ" profile [6.6] where:

$$\mu = \frac{J_{\|}}{B} = \frac{2\Theta_0}{a}\left[1 - \left(\frac{r}{a}\right)^{\alpha}\right] \tag{6.19}$$

and Θ_0 and α parameterise the equilibrium. At zero-beta equation 6.19 is enough to define the B_θ and B_z profiles. However, we require a finite-beta equilibrium and so must additionally specify the pressure-profile. This is done by inflating the equilibrium to uniform Suydam parameter, D_s, where:

$$D_s = -\frac{2k^2}{F'^2 r}\frac{dp}{dr}$$

The parameters Θ_0, α and D_s totally determine the equilibrium via the pressure balance equation. If we choose $D_s \leq 0.25$ local ideal stability is guaranteed, which we require to study specifically thin-shell instabilities (i.e. instabilities that do not exist when an ideal wall surrounds the plasma). Note that inflating with a power-law pressure profile often leads to a violation of Suydam's criterion at the edge.

A comparison of B_θ and B_z profiles at $D_s = 0.0$ (zero-beta) and $D_s = 0.2$ is shown in figure 6.1. The magnetic-field profiles are only slightly affected by the pressure, which amounts to a central beta, $\beta_0 = 8.2\%$, at $\Theta_0 = 1.65$ and $\alpha = 4.0$.

Figures 6.2 and 6.3 show the $m = 1$ spectra for HBTX1C like profiles ($\Theta_0 = 1.65$, $\alpha = 4.0$). Here $ka = n_k a/R_0$ where R_0 is the major radius. For HBTX1C $a = 0.26m$ and $R_0 = 0.8m$ so that $n_k \sim 3.1ka$. Figure 6.2 shows the effect of finite pressure on the current-driven thin-shell instabilities. The $D_s = 0$ spectrum is in good agreement with Alper et al. [6.2], while $D_s = 0.2$ demonstrates the additional destabilising influence of finite pressure. The unstable part of the spectrum is only slightly broadened. Figure 6.3 shows specifically the modes that are just non-resonant at the wall. Modes with $ka \geq 4.125$ are resonant, but here only non-resonant modes are considered. Notice that the finite beta equilibrium has instabilities where there were none for zero beta. More precisely, Δ'_w tends to infinity as x_w tends to zero, as expected from equation 6.11. However, the spectrum does not take the simple $1/x_w$ form except at very small values of x_w. The numerical solution is equivalent to calculating $b_r'/b_r|_{in}$ from equation 6.7 to all orders, with the ratio A_{II}/B_{II} determined by the boundary condition at the origin. Its departure from $1/x_w$ implies that higher-order terms are not negligible and that they must be included in the growth-rate calculation. This is not surprising for modes of a global nature such as $m = 1$ kinks. However, for very small x_w the $1/x_w$ term in $b_r'/b_r|_{in}$ dominates and equation 6.11 is valid. The numerical solution shows this limit is the most unstable and so the stability criterion derived from equation 6.11, (equation 6.13), remains a sufficient condition.

Figure 6.4 shows a similar plot for $\Theta_0 = 1.9$ and $\alpha = 3.2$. In this case modes with $ka \geq 1.57$ are resonant. Once again the current-driven external kinks are further destabilised, but now the unstable region is broadened to such a degree that it merges with the purely pressure-driven instabilities which are represented by the line that asymptotes to $ka = 1.57$. Thus the entire positive n_k non-resonant spectrum is unstable.

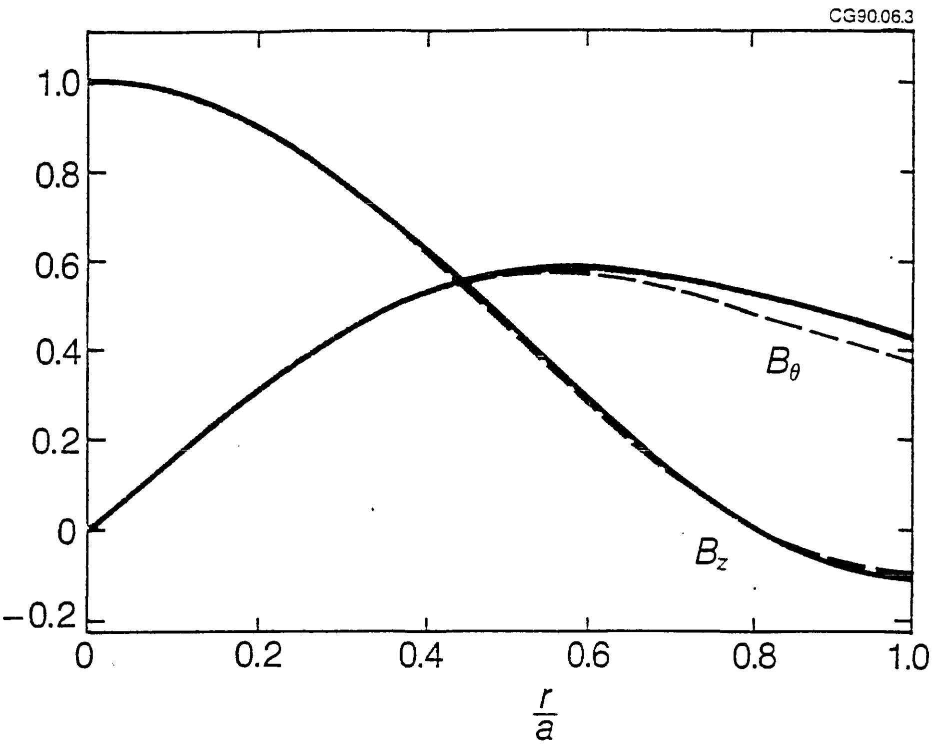

Figure 6.1: The equilibrium magnetic-field for a variable-μ profile with $\Theta_0 = 1.65$ and $\alpha = 4.0$. The broken lines are for $D_s = 0.0$ and the continuous lines for $D_s = 0.2$.

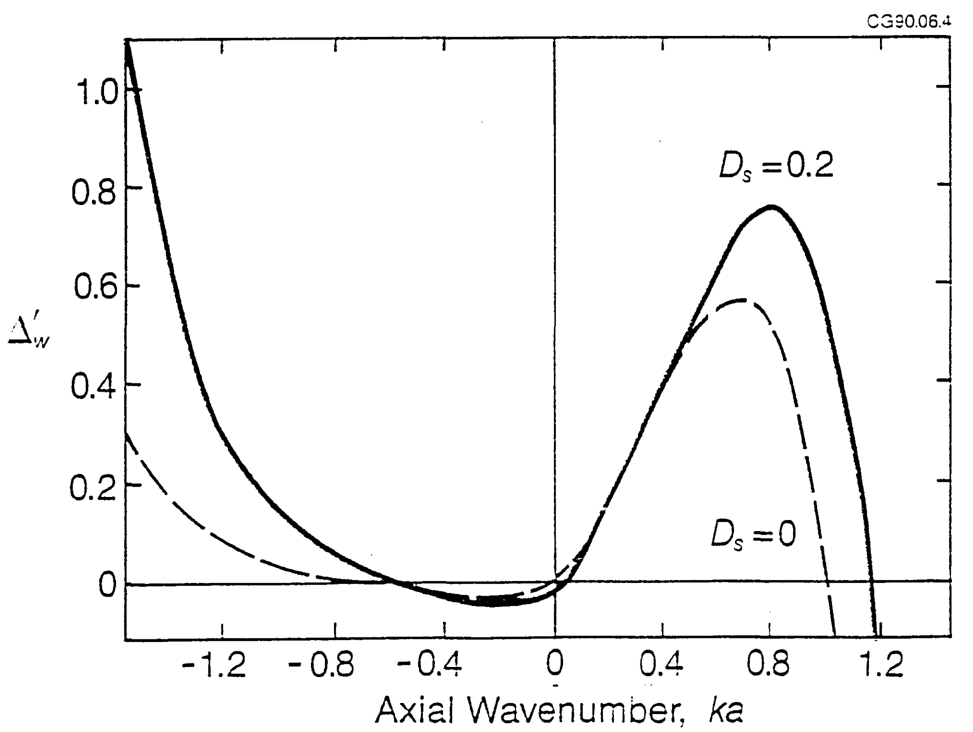

Figure 6.2: The $m = 1$ thin-wall spectrum for the equilibria of figure 6.1. For HBTX1C the wavenumber range corresponds to $-4.6 \le n \le 4.6$.

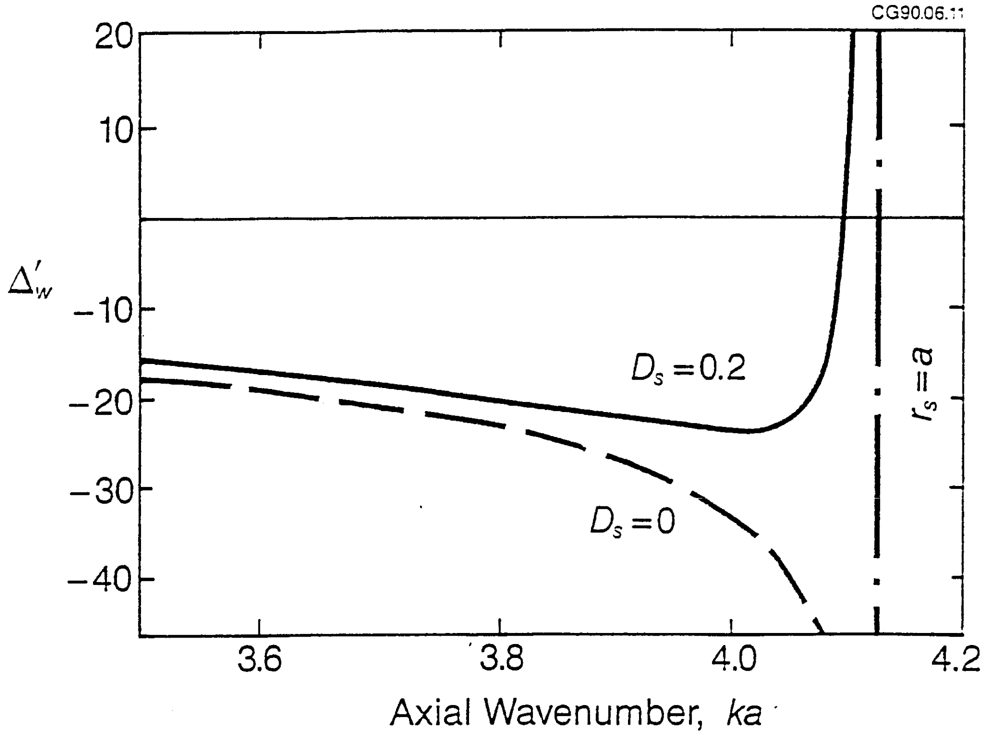

Figure 6.3: The $m = 1$, just non-resonant modes for the equilibria of figure 6.1.

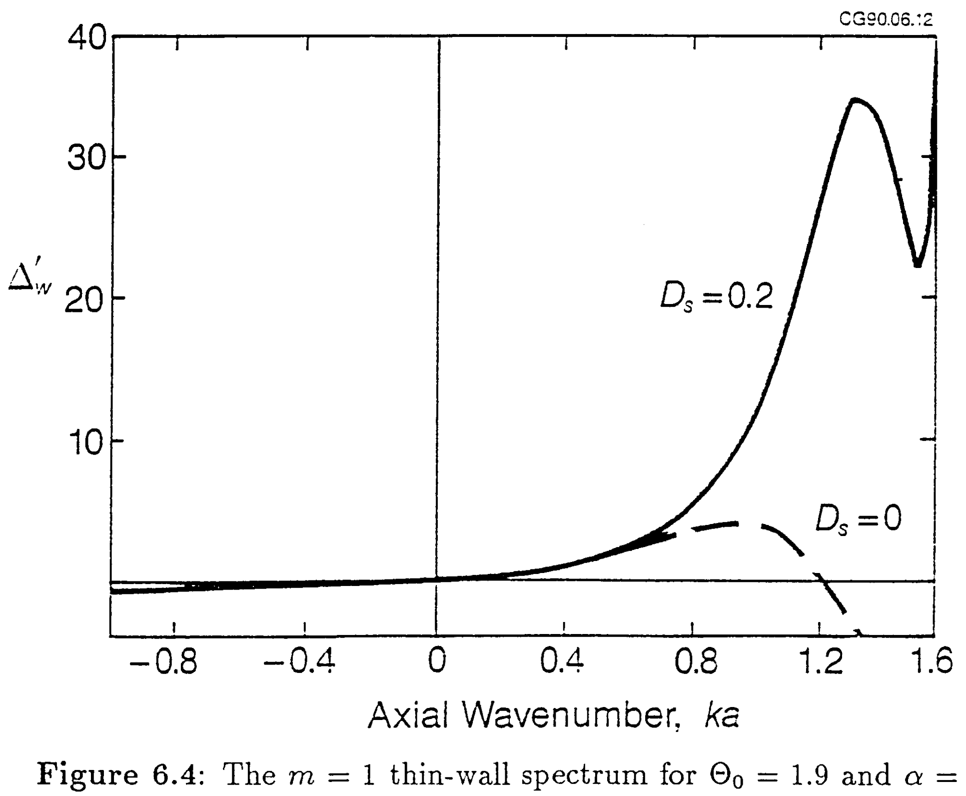

Figure 6.4: The $m = 1$ thin-wall spectrum for $\Theta_0 = 1.9$ and $\alpha = 3.2$. Marginally resonant modes, $(r_s = a)$, occur at $ka \sim 1.57$.

6.4 The Effect of Inertia

In a real plasma the growth-rate cannot increase without limit as $x_w \to 0$. Eventually inertial or resistive effects will become important and the analysis used above breaks down. In this section the inertial layer equation is solved and the solution is used to calculate the growth-rate of pressure-driven thin-shell modes in the small x_w limit.

Close to the resonant surface of an ideal plasma the radial displacement, ξ is described by [6.7]:

$$\frac{d}{dz}(1-z^2)\frac{d}{dz}\xi - \left[D_s - \frac{4/P'^2}{1-z^2+B^2/\Gamma p}\right]\xi = 0 \tag{6.20}$$

where Γ is the ratio of specific heats, $P = rB_z/B_\theta$ is the pitch of the magnetic field (with the prime denoting it's derivative) and

$$z^2 = -\left(\frac{r-r_s}{a}\right)^2\left(\frac{k^4a^4}{m^2+k^2r_s^2}P'^2\right)\frac{1}{(\gamma\tau_A)^2} = -x^2\left(\frac{\alpha}{\gamma\tau_A}\right)^2$$

with τ_A the Alfvèn time defined at $r = r_s$. For simplicity we consider the incompressible limit, $\Gamma \to \infty$. In this limit equation 6.20 becomes Legendre's equation, and has a corresponding solution in terms of Legendre functions [6.8]:

$$\xi = EP_\nu^\sigma(z) + FQ_\nu^\sigma(z) \tag{6.21}$$

where E and F are constants, and σ and ν are defined by:

$$\nu(\nu+1) = -D_s$$

$$\sigma^2 = -\frac{4}{P'^2}$$

In general E and F can only be determined by matching to a solution of the marginal (inertial-less) equation. This solution in turn requires a numerical integration such as that reported in section 6.3. For the purposes of illustration we shall specialise the treatment here to localised instabilities, i.e. set either E or F to zero. Specifically we choose to retain only the solution with the $z^{-\nu-1}$ dependence in the large z limit, since this makes the non-resonant modes maximally unstable (see section 6.2). The Legendre functions have the following behaviour for large z:

$$P_\nu^\sigma \quad \rightarrow \quad 2^{-\nu-1}\pi^{-1/2}\frac{\Gamma(-1/2-\nu)}{\Gamma(-\nu-\sigma)}z^{-\nu-1} + 2^\nu \pi^{-1/2}\frac{\Gamma(1/2+\nu)}{\Gamma(1+\nu-\sigma)}z^\nu$$

$$e^{-i\sigma\pi}Q_\nu^\sigma \quad \rightarrow \quad 2^{-\nu-1}\pi^{1/2}\frac{\Gamma(1+\nu+\sigma)}{\Gamma(\nu+3/2)}z^{-\nu-1}$$

Thus retaining only the $z^{-\nu-1}$ solution requires setting E=0, so that:

$$\xi = Q_\nu^\sigma(z)$$

Now, $b_r = F'x\xi$, so the corresponding contribution to the thin wall dispersion relation is:

$$\Delta_{in} = \frac{1}{x} + \frac{z}{x}\frac{\partial Q_\nu^\sigma}{\partial z}\frac{1}{Q_\nu^\sigma}$$

The derivative can be evaluated in terms of Q_ν^σ and $Q_\nu^{\sigma-1}$. Writing these functions in terms of hypergeometric series [6.8], yields:

$$\frac{\partial Q_\nu^\sigma}{\partial z}\frac{1}{Q_\nu^\sigma} = \frac{-\sigma z}{(z^2-1)} - (\nu-\sigma+1)\frac{z}{(z^2-1)}\frac{G(\nu,\sigma-1,z^2)}{G(\nu,\sigma,z^2)}$$

where $G(\nu,\sigma,z^2)$ represents the following hypergeometric function:

$$G(\nu,\sigma,z^2) = F(1+\frac{\nu}{2}+\frac{\sigma}{2},\frac{1}{2}+\frac{\nu}{2}+\frac{\sigma}{2},\nu+\frac{3}{2};\frac{1}{z^2})$$

Now, for $z^2 \gg 1$:

$$\frac{G(\nu,\sigma-1,z^2)}{G(\nu,\sigma,z^2)} \approx 1 - \frac{(1+\nu+\sigma)}{(2\nu+3)}\frac{1}{z^2}$$

and so we have the simpler form:

$$\frac{\partial Q_\nu^\sigma}{\partial z}\frac{1}{Q_\nu^\sigma} = -(\nu+1)\frac{z}{(z^2-1)} + \frac{((\nu+1)^2-\sigma^2)}{(2\nu+3)}\frac{1}{z(z^2-1)}$$

Thus for $|z^2| \gg 1$, the plasma contribution to the thin-shell dispersion relation is :

$$\Delta_{in} = -\frac{1}{x}\left(\nu + \frac{\kappa}{z^2}\right) \tag{6.22}$$

where

$$\kappa = 1 - \left\{\frac{(\nu+1)^2 - \sigma^2}{2\nu+3}\right\}$$

For $|z^2| \gg |\kappa/\nu|$ equation 6.22 reduces to the previous result for non-resonant modes i.e. $\Delta_{in} = -\nu/x_w$. Otherwise the κ/z^2 inertial term is significant and should be included in the analysis. For $1 \ll |z^2| \ll |\kappa/\nu|$ the inertial term dominates.

The thin-shell dispersion relation that results from equation 6.22 is:

$$\gamma\tau_w = \Delta_{out} + \frac{1}{x_w}\left(\nu - \frac{(\gamma\tau_A)^2}{x_w^2}\frac{\kappa}{\alpha^2}\right) \tag{6.23}$$

There are two roots to this equation. The thin-shell mode corresponds to the root which has a vanishing growth-rate as $S_w \to \infty$:

$$\gamma\tau_w = -\frac{x_w^3 S_w^2}{2\hat{\kappa}}\left[1 - \left\{1 + \left(\frac{\nu}{x_w} + \Delta_{out}\right)\frac{4\hat{\kappa}}{x_w^3 S_w^2}\right\}^{1/2}\right] \tag{6.24}$$

where $S_w = \tau_w/\tau_A$ and $\hat{\kappa} = \kappa/\alpha^2$. The two opposite limits of equation 6.24 yield very different scaling of $\gamma\tau_w$ with x_w. For large x_w:

$$\gamma\tau_w = \frac{\nu}{x_w} + \Delta_{out}$$

which corresponds to the inertia-free limit.

In the small x_w limit the scaling depends on the sign of $\hat{\kappa}$. We shall just consider $\hat{\kappa} < 0$ since this is the case relevant to the equilibria used in section 6.3. For negative $\hat{\kappa}$ the argument of the square root in equation 6.24 is positive for all x_w, so that γ is real. Thus in the $x_w \to 0$ limit we have:

$$\gamma\tau_w = -x_w S_w \left(\frac{\nu}{\hat{\kappa}}\right)^{1/2}$$

Thus the mode actually becomes more stable as $x_w \to 0$. For finite x_w there is a competition between these two scalings and this leads to a maximally unstable value of x_w.

We can calculate the maximum growth-rate by differentiating the dispersion relation (equation 6.23) with respect to x_w and setting $d\gamma/dx_w = 0$. We find turning points of γ at:

$$x_w^2 = 3(\gamma\tau_A)^2\left(\frac{\hat{\kappa}}{\nu}\right)$$

with a maximum at:

$$x_w = x_m = -\gamma\tau_A\left(\frac{3\hat{\kappa}}{\nu}\right)^{1/2} \tag{6.25}$$

Substituting equation 6.25 into equation 6.23 yields an equation for the maximum growth-rate, γ_m, which can easily be solved to give:

$$\gamma_m\tau_w = \frac{\Delta_{out}}{2} + \left\{\frac{\Delta_{out}^2}{4} - \frac{2}{3}S_w\nu\left(\frac{\nu}{3\hat{\kappa}}\right)^{1/2}\right\}^{1/2} \tag{6.26}$$

For a weakly resistive wall (large S_w) we have $\gamma_m\tau_w \sim S_w^{1/2}$ which implies a growth rate scaling:

$$\gamma_m \sim \frac{1}{(\tau_w\tau_A)^{1/2}}$$

Thus the most unstable mode grows on a hybrid timescale of the Alfvén and wall times.

Figure 6.5 shows $\gamma\tau_w$ as a function of x_w, according to equation 6.24 with parameters similar to those expected in HBTX1C equilibria, i.e. $\hat{\kappa} = -1.0$, $\Delta_{out} = -3.8$, $D_s = 0.2$ and $S_w = 1000$. Also shown as dotted lines are the $\gamma \propto 1/x_w$ scaling for large x_w and the $\gamma \propto x_w$ scaling for small x_w.

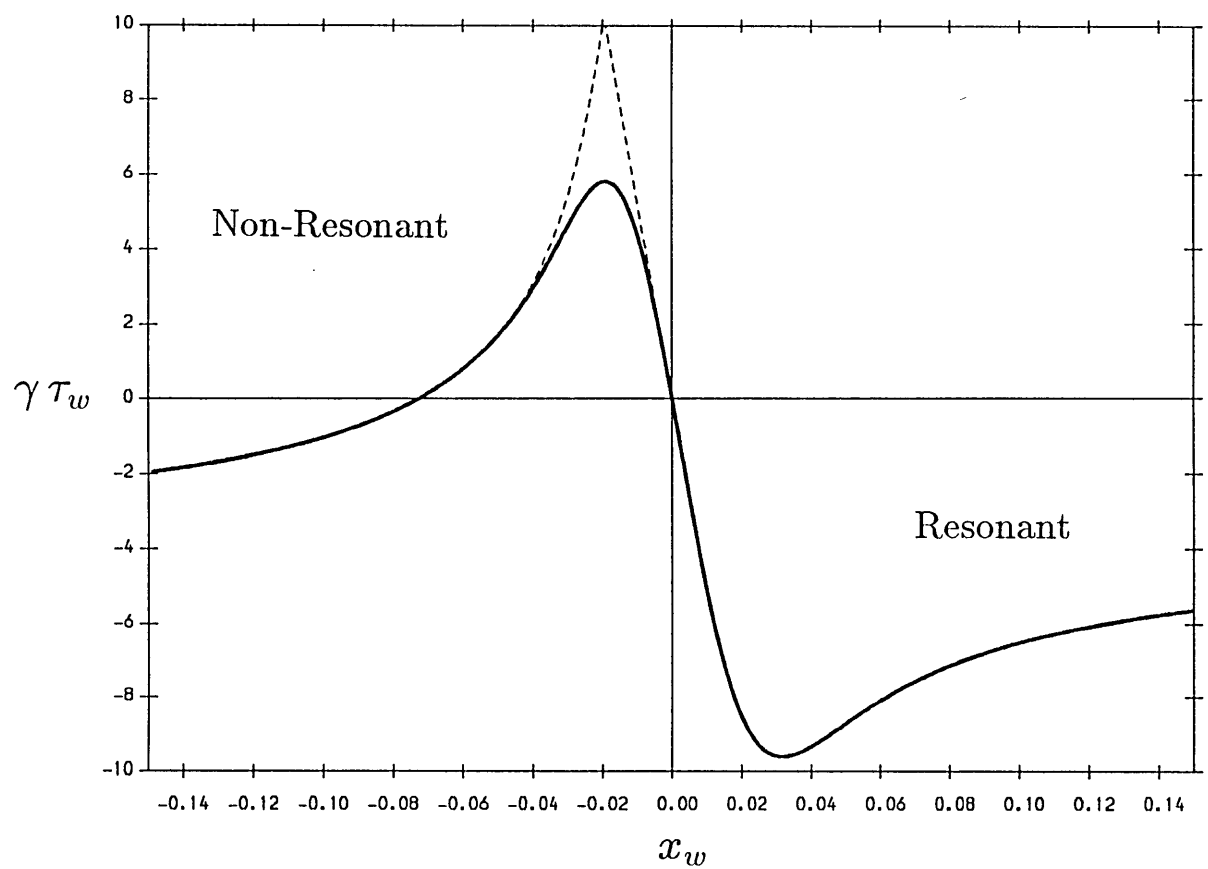

Figure 6.5: $\gamma\tau_w$ as a function of x_w from eqn.24 with $\kappa = -1.0$, $\Delta_{out} = -3.8$, $D_s = 0.2$ and $S_w = 1000$.

6.5 Discussion

This chapter has been concerned with the effect of finite pressure gradient on ideal modes resonant close to either side of a resistive wall. Indeed the analyses of sections 6.2 and 6.4 rely on the proximity of the resonance to the wall to allow the governing equations to be expanded about the wall. The resulting stability conditions are only applicable when this expansion is valid.

In section 6.3 we integrated the marginal MHD equation to calculate Δ'_w for a finite beta RFP equilibrium. Only non-resonant modes can be treated in this way, since a resonance would imply an inertial layer within the plasma and therefore require the inclusion of inertia within the equations. More complex models that include inertia and resistivity, are routinely solved using initial-value or shooting codes, to yield the entire (resonant and non-resonant) spectrum. Merlin and co-workers [6.9] have studied a similar finite beta equilibrium using a resistive MHD model with perfect wall boundary conditions. The introduction of pressure is seen in this reference to have a destabilising influence on both resonant and non-resonant modes. The range of non-resonant instabilities is broadened while the resonant perturbations are unstable to the resistive-g mode. In this chapter, the absence of resistivity and the specialisation to non-resonant modes (in section 6.3) means that resistive-g modes have not been treated. However, the expectation is that resistive-g modes would be similarly (and almost certainly more) unstable in a plasma bounded by a resistive rather than a perfect wall.

Instead of attempting a complete treatment of the effects of pressure gradients on thin shell instabilities, we have concentrated here on modes that are marginally resonant or marginally non-resonant close to the resistive wall. We have demonstrated that there are a novel class of instabilities that arise from modes which are just non-resonant at the wall and which require both a finite pressure-gradient and a non-perfect wall in order to be unstable. These modes appear to be unstable in RFP equilibria, and so they should be unstable in thin-shell RFP's such as HBTX1C.

The motivation for this work are the observations made on HBTX1C [6.2]. Thin-shell instabilities were seen in the $m = 1$ spectrum in the toroidal mode number ranges $n_k = (-5, -6, -7)$, $(2, 3)$ and $(9, 10, 11)$, all of which appeared to be growing exponentially with the same growth-rate: $\gamma\tau_w \sim 0.3$. The existence of the first two mode groupings has been satisfactorily explained by the zero beta thin shell theory [6.1], although the growth-rates are predicted to have a mode number dependence which is not observed. The last mode grouping at $n_k = (9, 10, 11)$ appear to be just non-resonant and could therefore be destabilised in the manner considered in this chapter. For the profile fit to HBTX1C equilibrium measurements (i.e. $\Theta_0 = 1.65$, $\alpha = 4.0$), the theory of section 6.4 predicts that $m = 1$ instabilities should be maximally unstable for $x_w \sim 0.02$ with a maximum growth-rate : $\gamma\tau_w \sim 6$. This corresponds to fastest growing modes at $n_k = (12, 13)$, in contrast to the observed modes at $n_k = (9, 10, 11)$. However, only a small change in the model equilibrium (i.e. error in the fit) is required for the theoretically predicted range to coincide with the range of unstable modes observed. More troublesome is the magnitude of the calculated growth-rate, which far exceeds that observed. However, this should perhaps not be surprising since by the time instabilities are experimentally observable they are almost certainly in a non-linear regime. As such the linear growth-rates calculated here are not applicable, they merely express the degree of linear instability, and suggest the important mode numbers. Also, the observation of very similar growth-rates for each of the unstable modes suggests that different toroidal mode numbers are coupled. Once again this can not be treated in the linear cylindrical model considered here.

In summary, the work presented in this chapter indicates that modes which are just non-resonant will be linearly unstable in a thin-shell RFP. The observation of $m = 1$, $n_k = (9, 10, 11)$ instabilities in HBTX1C, is in qualitative agreement with this prediction.

6.6 Conclusions

(i) Local ideal stability criteria have been derived for pressure-driven instabilities that are resonant close to a resistive shell. If a vacuum is included between the plasma and the wall, the stability conditions coincide with previous results derived from the energy principle (Hastie in Wesson [6.5]).

(ii) In the case where the parallel current at the edge vanishes, the free-boundary and fixed-boundary criteria coincide. Both predict that pressure gradients destabilise modes that are just non-resonant at the edge.

(iii) The numerical calculation of the non-resonant $m = 1$ thin-wall spectrum shows the general destabilising influence of pressure gradient, but additionally introduces new purely pressure-driven instabilities, which are identifiable with the modes derived from the local analysis.

(iv) As $F = \vec{k}.\vec{B}$ at the edge goes to zero, inertial effects become important and must be included in the dispersion relation. For localised non-resonant modes the inclusion of inertia leads to a maximally unstable value of $x_w = F/F'$. The corresponding instability grows on a timescale which is determined by both the Alfvén and wall times:

$$\gamma \sim \frac{1}{(\tau_w \tau_A)^{1/2}}$$

(v) The previously unexplained $n_k = (9, 10, 11)$, $m = 1$ instabilities in the HBTX1C experiment appear to be non-resonant and have small $F = \vec{k}.\vec{B}$ at the wall. Thus they could conceivably correspond to the class of pressure-driven thin-shell instabilities described here.

References

[6.1] Gimblett, C.G., Nuc. Fus. **26**, 617 (1986).

[6.2] Alper, B., Bevir, M.K., Bodin, H.A.B., Bunting, C.A., Carolan, P.G., Cunnane, J., Evans, D.E., Gimblett, C.G., Hayden, R.J., Hender, T.C., Lazaros, A., Moses, R.W., Newton, A.A., Noonan, P.G., Paccagnella, R., Patel, A., Tsui, H.Y.W., Wilcock, P.D., Plasma Phys. and Contr. Fusion **31**, 205 (1989).

[6.3] Robinson, D.C., Nuc. Fus. **18**, 939 (1978).

[6.4] Newcomb, W.A., Annals of Physics **10**, 232 (1960).

[6.5] Wesson, J.A., Nuc. Fus. **18**, 87 (1978).

[6.6] Antoni, V., Merlin, D., Ortolani, S., Paccagnella, R., Nuc. Fus. **26**, 1711 (1986).

[6.7] Chance, M.S., Greene, J.M., Grimm, R.C.,Johnson, J.L., Nuc. Fus. **17**, 65 (1977).

[6.8] Erdèlyi, A., Magnus, W., Oberhettinger, F., Tricomi, F.G., Higher Transcendental Functions, Vol.1, McGraw Hill (1953).

[6.9] Merlin, D., Ortolani, S., Paccagnelli, R., Scapin, M., Nuc. Fus. **29**, 1153 (1989).

Chapter 7

Concluding Remarks and Further Work

7.1 Final Remarks

The general conclusion of this research is that the simplest Ideal and Resistive MHD models often inadequately describe the stability of magnetically confined plasmas.

The results presented in chapters 4, 5 and 6 are concerned with the effect of relaxing one or more of the assumptions which are implicit in the use of these simpler models. In each case the stability properties of the plasma have been shown to be significantly altered. When additional physics was included in the study of resonant modes in the RFP (Chapter 4), the existing pressure driven resistive modes were stabilised but new branches of instability emerged. Thus the more complete plasma models give a different (and more accurate) description of the instabilities that are likely to lead to confinement degrading fluctuations in the RFP.

In Chapter 5 resistive and viscous effects were shown to have a stabilising effect on kink and sausage modes in Z-pinches. However, in this case the simplest scalar viscosity model led to an over-estimation of this effect. Once again a more complete full stress tensor model was required to formulate conclusions on many current Z-pinch experiments.

Finally in Chapter 6, using the simplest boundary conditions was shown to give an optimistic picture of RFP stability. Clearly, there are many instances when the simpler ideal and resistive MHD models fail to give quantitative predictions about magnetic confinement experiments.

7.2 Further Work

Each of Chapters 4, 5 and 6 have suggested possible areas of further work, these are summarised below:

(i) A study of the effect of collisionless ion dynamics on instabilities with $\omega > \nu_{ii}$.

(ii) The development of non-linear turbulence theories of η_i-modes and MCD modes in RFP's.

(iii) A study of the effect of resistivity and viscosity on the stability of an evolving Z-pinch equilibrium.

(iv) A study of the non-linear coupling of the thin-shell instabilities in the RFP.

Acknowledgements

During the course of this research I have had help and encouragement from people within the Plasma Physics Group at Imperial College and the Theory Division at Culham Laboratory. I would particularly like to thank Professor Malcolm Haines, who was my supervisor at Imperial and Jim Hastie at Culham Laboratory who was always available to offer insight and guidance. The completion of this thesis has largely been made possible by the encouragement (or nagging) of my good friends at Culham, Oddly and Pigsy, both of whom took the role of the "thesis ghost" at sometime or other. Most of all though, I would like to thank my girlfriend, Julie, who has patiently tolerated my moods during writing up and my parents for supporting me during undergraduate studies.

Published Papers

[1] "Resistive and Viscous Effects on Z-Pinch Stability", P.M. Cox
Plasma Physics and Controlled Fusion **32**, 553 (1990).

[2] "Pressure-Driven Thin-Shell Instabilities in HBTX1C", P.M. Cox
accepted for publication in Plasma Physics and Controlled Fusion.